Controls on the diversity of the fault slip styles at the brittle-ductile transition:

Examples from the Cape Fold Belt, Nuy Valley, South Africa

Antónia de Carvalho

Dissertation presented for the degree of

Master of Science

Department of Geological Sciences, University of Cape Town
South Africa

February 2019

Supervisors
Johann Diener and Åke Fagereng

Acknowledgements

First and foremost, I thank my supervisors: Johann Diener and Äke Fagereng, for all the support in the field and for supervising, funding and giving life to this project.

I would like to acknowledge Conradie and Leipzig Farms for granting access to their property and allowing us to come back many times over to collect data for this project.

Processing of samples would not have been possible without UCT Geology Department staff: Chris Harris, Sherrisa Roopnarain and Phil Janey responsible for the XRF data and oxygen isotope laboratory.

Shout out to Leslie Huang for all the field work assistance and endless entertainment in the field under the scalding summer sun, going over and through canals; and to my dear friends and office mates, Bogdana Radu, Simon Schorn and Benjamin Whitehead, whose support was priceless.

Lastly, I would like to thank BP (Angola) for funding most of my academic career at UCT. I will forever be grateful for the opportunity.

Declaration

1. I know that plagiarism is wrong. Plagiarism is to use another's work and pretend that it is one's own.

2. I have used the South African Journal of Geology convention for citation and referencing. Each contribution to, and quotation in, this project from the work(s) of other people has been attributed and has been cited and referenced.

3. This project is my own work.

4. I have not allowed, and will not allow, anyone to copy my work with the intention of passing it off as his or her own work.

Signature Signed by candidate

Date: 11.02.2019

Abstract

Crustal deformation models have a first-order rheological division, with pressure-dependent brittle deformation predominating at shallow depths, and temperature-dependent viscous deformation occurring in the deeper levels of the crust. The brittle-ductile transition zone separates these two regimes, it occurs at approximately 350°C for quartz and it is characterised by mixed-mode brittle and viscous deformation.

Complex fault zones exhumed to the surface may preserve evidence that can explain the mechanics and the complex slip behaviour of faults. Fault rocks response to applied shear stress is affected by environmental conditions during deformation (such as temperature and pressure), composition of fault zone, fluid presence and strain rate. Thus, the interplay of these factors determines the slip style of a specific fault and may lead to multiple slip styles that overprint each other.

The Nuy Valley area in Worcester, Western Cape, South Africa, exposes a section through the deeper parts of the Cape Fold Belt, where the Malmesbury Group schists experienced thrust faulting in response to crustal shortening. Individual thrust faults are manifested in different ways, with quartz-cemented breccias, limestone mylonites, abundant quartz veining and cataclasites attesting to faulting occurring by a diversity of slip style, which allows investigating how the interplay of the controlling factors lead to the observed diversity of fault rock. Through mineral equilibria modelling, the pressure-temperature conditions under which faulting occurred was determined to lie between 5 – 8 KPa and 250 – 420°C, with fluid content lines indicating low amounts of dehydration during peak metamorphism. The exhumed fault being analysed in this study was active at 10 – 15 km deep at 25°C.km^{-1} geothermal gradient. The temperature over this transition is relatively constant and short ranged throughout geological evolution of Worcester and the cyclic superposition of ductile and brittle deformation and change in slip styles along fault zones as found in Nuy Valley cannot be justified by ambient temperature and pressure oscillations. Lithotype and competency of wallrocks play an essential role in deformation partitioning by being crucial determinants of rheological properties, and accounts for the coexistence of brittle and ductile fabrics but not for cyclic overprint of slip styles. Fluid presence is evidenced by an intense network of quartz veins and hydraulic breccias and contributes to the weakening and strengthening of wallrock during deformation. Slip style diversity in the study area is considered to the result of the interplay of compositional variabilities, fluid flow and strain rate variations associated with the seismic cycle.

Contents

1. Introduction

The general view of the Earth as we see it today revolves around the broad concept of plate tectonics, and in particular on mechanisms such as rifting, subduction and collision of lithospheric plates. At a smaller and more discrete scale, the processes that have shaped our planet are deformation, faulting, melting and recrystallisation, seen individually or as an ensemble of subsequent stages. Whereas some of these transformations occur on a geological timescale and have had little or no direct observable influence on humanity, more rapid processes such as seismic ruptures, are among the main factors affecting the distribution of earthquakes, volcanoes and landslides. The study of diverse fault slip systems is therefore of great consequence for the improvement of our knowledge of such complex processes.

Fault slip styles are categorized into seismic slip (earthquakes) as a result of sudden frictional instabilities, aseismic creep by continuous frictional sliding and creep (e.g. Scholz, 1998) and, more recently, into mixed-mode fault slip behaviour whereby aseismic creep is interspersed with seismicity (Fagereng and Sibson, 2010; Collettini *et al.*, 2011). Previous studies reiterate the relevance of identifying the parameters and mechanisms behind seismic slip and the factors governing the seismic-aseismic deformation partitioning (Hickman et al., 1995; Fagereng and Toy, 2011). To accomplish this, carrying out geological studies in exhumed complex fault zones is key as these faults may preserve evidence that can explain the mechanics and the complex slip behaviour of faults (Tesei et al., 2014).

Fault rocks response to applied shear stress is affected by environmental conditions during deformation (such as temperature and pressure), composition of fault zone, fluid presence and pressure, strain rate, and orientation of the stress field and pre-existing fabrics (Passchier and Trouw, 1996, 2005; Tesei *et al.*, 2014 and others). However, the factors controlling the development of different types of fault rock assemblages are still not fully understood. This is partly due to the difficulty associated with direct observations and inference of the physical properties and deformation mechanisms along natural faults in the middle and lower crust (Hickman et al., 1995); and partly because, in practice, seismic slip is based on depth-distribution of microseismic activity and seismic–postseismic sequences, whereas many crustal fault zones have not experienced significant earthquakes since seismometers have been available (Fagereng and Toy, 2011).

Crustal deformation and fault rock models have a first-order rheological division, with pressure-dependent brittle deformation predominating at shallow depths, and temperature-dependent viscous deformation occurring in the deeper levels of the crust. The brittle-ductile transition zone separates these two regimes and it is characterised by mixed-mode brittle and viscous deformation (Scholz, 1989; Kohlstedt et al., 1995; Fagereng and Toy, 2011). The brittle-ductile transition zone is associated with the seismic-aseismic transition zone and is ideal to study the combination of deformation styles and the factors that contributed to their diversity.

In general terms, rheology of rocks is primarily determined by the physical properties of their mineral constituents and vary dependent on pressure and temperature. For quartz, the transition of dominantly brittle to dominantly ductile occurs at approximately 350°C (Kohlstedt et al., 1995; Scholz, 1998), whereas micas can deform viscously from much lower temperatures (Tullis, 2002). Thus, a fault rock assemblage defined by different rheological properties cause variations in shear strength, viscosity, shear strain rate and faulting styles (Fagereng and Sibson, 2010). Furthermore, the presence of fluid is likely to affect rheology by altering the composition and cohesion of the fault rock, shifting its rheological

properties towards those of the fluid material, post precipitation and cementation. The rate at which a material absorbs stress, strain rate, also plays an essential role in determining under which mechanisms deformation takes place, where slow strain rates favour viscous deformation and high rates favour brittle deformation. Thus, it is likely that the fault slip behaviour of heterogeneous natural faults is a complex interplay of all these parameters.

In practice, the extent of overprinting deformation mechanisms can be challenging to establish, and deformation in rocks is commonly partitioned (Passchier and Trouw, 2005). Nevertheless, attempting to constrain the dominant deformation mechanism is relevant in order to understand the factors that control the fault rheology in the brittle-ductile transition and drive the different slip styles in this level of the continental crust. In this project, I consider field, laboratory and microstructural evidence for the deformation mechanisms active during deformation of the lower part of the Cape Fold Belt which exposes the Malmesbury Group; geochemical and isotope analysis to determine the likely pressure and temperature conditions during deformation, amount of fluid present and its source, in order to evaluate the contribution of these parameters to the diversity of fault slip styles.

1.1. Research Aims

The primary objective of this project is to contribute to the current knowledge on upper crustal deformation processes as exemplified in this part of the Cape Fold Belt and to add to the understanding of the contribution of the different deformation factors on the deformation styles and fault rocks in the brittle-viscous transition.

In this pursuit, this project focuses on exhumed thrust faults in the Cape Fold Belt in Nuy Valey, Worcester, South Africa. This area exposes a section through the deeper parts of the Cape Fold Belt, where the Malmesbury Groups schists experienced thrust faulting in response to crustal shortening. Individual thrust faults are manifested in different ways, with quartz-cemented breccias, limestone mylonites, abundant quartz veining and cataclasites attesting to faulting occurring by a diversity of slip styles. Therefore, the Nuy Valley provides a well-constrained natural example for investigating how the interplay of the various controlling factors lead to the observed diversity of fault rock, as well as how changing these factors with time would affect the evolution of an individual shear zone.

This dissertation will:

- Describe deformation of rocks in macro-, micro- and regional level in order to analyse how deformation is accommodated along Nuy thrust fault zone and determine distribution of fault rock types and their properties contribution to deformation styles;
- Explain slip mechanisms and the controls on the change of slip mechanisms along the thrust;
- Determine the fluid-rock interaction in wall rock and mineral composition in silicified and veined fault rock surrounding the fault plane to study fluid contribution;
- Determine kinematic movement of the rocks in this part of the Nuy, CFB, under which tectonic and metamorphic conditions deformation occurred to determine fault orientation with regards to compressive stress and
- Narrow down pressure and temperature conditions and depth during active deformation.

Ultimately, this project aims to investigate how the interplay of the various controlling factors lead to the observed diversity of fault rock, as well as how the variability and interplay of these factors with time would affect the evolution of an individual fault.

2. Fault slip styles, factors and deformation mechanisms

Faults slip at a range of speeds, from slow creep at plate tectonic rates, also referred to aseismic creep (~ 1–10 cm. year^{-1}), to rapid frictional sliding (~ 1 m.s^{-1}) during seismic ruptures (earthquakes). Seismic slip is considered to result from 'stick-slip' frictional instability, as elastic strain is stored in the wallrock surrounding developing or existing planes of weakness until the shear stress along this surface overcomes its frictional strength and fracture occurs (Scholz, 1998; Fagereng and Toy, 2011).

The shear stress at failure, τ_f, is approximated by the empirical Amontons' law:

$$\tau_f = C_0 + \mu_s(\sigma_n - P_f) \qquad (1)$$

where C_0 is cohesive strength, μ_s is the static coefficient of friction, σ_n is normal stress, and P_f is fluid pressure. Equation (1) indicates the shear stress conditions at which a fault will slip.

Equation (1) does not account for the rate at which fault slips occur. For this, there is a commonly used description of the time and velocity dependence of friction, rate-and-state friction law, based on experiments in homogenous rock samples, the Dieterich–Ruina law (Fagereng and Toy, 2011):

$$\mu = \mu_0 + a \ln(v/v_0) + b \ln(v_0\theta/D) ; \qquad (2)$$

$$d\theta/dt = 1 - \theta v/D$$

where μ_0 is the coefficient of friction at a reference slip velocity (v_0), D is the critical slip distance, θ is a state variable that evolves over time, and a and b are empirical material constants. Other controlling factors such as rock composition and structure, fluid pressure, dominant deformation mechanism, temperature and pressure are part of the empirical material constants a, b, D and θ. Equation 2 does not account for the effect of a present fluid-phase and ongoing chemical reactions, but fluid-pressure driven fluctuations in effective normal stress contributed to the value of shear stress at failure (τ_f) (Fagereng and Toy, 2011).

Frictional stability depends on the empirical constants a, b and D; where, if the difference (a - b) is positive, the material is said to be 'velocity strengthening' and friction (μ) increases with slip. On the other hand, if (a - b) is negative, friction decreases with slip and the material is 'velocity weakening' (Scholz, 1998; Fagereng and Toy, 2011). Scholz (1998) describes three possible stability regimes for crustal faults: a stable zone where seismic slip cannot occur, an unstable zone where episodic seismic slip occurs, and a conditionally stable zone (Bilek and Lay, 2002). Seismic slip may happen where the wallrock has as an unstable or conditional frictional stability, but it can only nucleate within the unstable regime and then spread into conditionally unstable regions (Scholz, 1998; Fagereng and Toy, 2011). The seismic/aseismic transition zone lies below the unstable, seismogenic, zone and it is associated with the Brittle-Ductile Transition (Figure 3.2).

2.1. Fault-Rock Deformation Mechanisms

Shear stress and strain (change in shape resultant from stress applied) are accommodated in fault rocks through deformation mechanisms. These mechanisms that lead to rock deformation can be inferred from the rock structures and microstructures created and preserved in the rocks (Knipe, 1989; Fagereng and Toy, 2011) which form in response to tectonic stresses and vary depending on physical and environmental factors such as temperature and pressure, composition and grain size, fluid presence and fluid pressure and strain rate.

Mineral deformation mechanisms are classified into three categories (Passchier and Trouw, 2005):

(1) Cataclastic flow: involves grain fragmentation and rotation, microcracking, fracturing and frictional sliding (Sibson, 1977).

(2) Intracrystalline plasticity: crystals are deformed internally through the movement of lattice line defects and twinning; this includes dislocation creep and dislocation glide processes (Tullis, 2002).

(3) Diffusive mass transfer (Knipe, 1989): material is redistributed along stress-induced chemical potential gradients and occurs through solid-state diffusion or fluid-assisted diffusion, also referred to as dissolution-precipitation creep. Solid-state diffusion associated mechanisms are further classified based on the mode of material transfer: Nabarro-Herring Creep if diffusion occurs through mineral grains; and Coble Creep, if predominantly on grain boundaries.

2.1.1. Deformation Mechanisms at the Brittle-Ductile Transition

The three main deformation mechanisms dominant around the brittle-ductile transition (Figure 3.2) and their dependence on physical and environmental factors are described below:

1) Frictional Fracturing or Cataclasis:

Cataclasis is associated with grain size reduction through fracturing, fragmentation and rigid body rotation, with grain boundary fictional sliding and rotation (Sibson, 1986). In quartz, formation of some subgrains may be enhanced by brittle fracturing, rotation and annealing via precipitation from fluid (Passchier and Trouw, 2005). Submicroscopic cataclasis may cause fractured grains with blurry grain boundaries and undulose subgrains (Tullis, 1990), thus subgrain-like structures and undulose extinction can form by a dense network of microscopic fractures

Cataclasis is primarily dependent on pressure and hindered by elevated confining pressures, but is possibly enhanced by increasing fluid pressures via reduction of the effective normal stress, which may take place rapidly as result of short-lived and cyclic high velocity events (i.e. seismic slip strain rates) or resultant from low-velocity fracturing of single grains (Sibson, 1986). This process leads to common development of veins in breccias and cataclasites.

2) Dissolution-Precipitation:

Dissolution-precipitation is a mechanism for diffusive mass transfer which occurs via diffusion through a fluid phase and is, therefore, fluid assisted. This mechanism typically works at low strain rates, at low temperatures and low differential stress (Fagereng, 2012). Differences in intergranular stress create a chemical potential, which causes mineral phases to be dissolved and precipitated is such a way as to decrease the intergranular stress. Evidence for dissolution is given by stylolites, truncated mineral grains

and evidence for precipitation is given by veins, pressure shadows and mineral overgrowths (Knipe, 1989). Rock textures associated with diffusive mass transfer are common in low-grade metamorphic rocks in the mid to upper crust, where this mechanism is considered to compete with cataclasis and frictional sliding (Fagereng and Toy, 2011).

Dissolution-precipitation becomes more efficient at small grain sizes, and therefore can be associated by cataclasis during faulting or grain size reduction during viscous flow (Scholz, 2002) Dissolution-precipitation is an important deformation mechanism in fluid-saturated, fractured and fine-grained rocks (Fagereng and Toy, 2011), thus dependent on grain-size and fluid presence.

3) Dislocation Creep:

Dislocation Creep is a grain-scale deformation mechanism intracrystalline plasticity whereby strain occurs by propagation of line defects through a crystal lattice (Tullis, 2002; Passchier and Trouw, 2005); reducing the internal strain energy of a crystal. At low strains, dislocations can form in a crystal resulting in undulose extinction, and as strain accumulates or temperature increases, the formed dislocations migrate, creating deformation bands and dislocation walls. Increasing strain may lead to a greater accumulation of dislocations, resulting in the formation of subgrain boundaries. Subgrains are commonly misorientated. Typical microstructural fabrics associated with dislocation creep in quartz include undulose extinction, deformation lamellae and presence of subgrains (Passchier and Trouw, 2005).

The rate of dislocation creep is affected by differential stress, temperature and mineralogy, in the absence of lithological heterogeneities (Hirth et al., 2001). Dynamic recrystallisation occurs as dislocations migrate into subgrain boundaries, resulting in subgrain rotation and ultimately the segregation of recrystallised grains (Passchier and Trouw, 2005). Dynamic Recrystallization is the process by which new crystal grains form from old grains without significantly altering the composition of the mineral grains during deformation. This process occurs through three mechanisms, which do not necessarily operate independently, and which produce characteristic microstructures (represented in Figure 2.1):

Grain Boundary Bulging (regime 1) is associated with low to moderate strain and is characterised by relatively equant porphyroclasts with deformation bands and strong undulatory extinction, and anastomosing zones of extremely fine, often not resolvable recrystallised grains along their boundaries and progressive reduction of porphyroclasts' size (Figure 2.1). Sheared samples develop an S-C' fabric, with sigmoid porphyroclasts defining the foliation and zones of recrystallised grains defining extensional shear bands (Tullis, 2002).

Subgrain Rotation (SR) (regime 2) is characterised by relatively homogeneously flattened grains containing optically visible subgrains, and recrystallised grains with approximately the same size as that of the subgrains. Other microstructures are 'core and mantle', extremely elongated original grains or entirely replaced by subgrains.

Grain Boundary Migration (GBM) (regime 3) is characterised by highly serrated crystal boundaries as complete recrystallisation occurs at low strain before significant flattening of porphyroclasts can occur. Subgrains rarely accumulate enough misorientation to produce high angle boundaries, but any new grains produced in this way increase their size by boundary migration. The average recrystallised grain size is significantly larger than that in regime 2 and larger than the average co-existing subgrain size.

The transition between the above dislocation creep mechanisms is gradual and mineral dependant (Tullis, 2002). The size of the recrystallised grains increases from regime 1 to 2 to 3 as flow stress decreases with increasing temperature or decreasing strain rate (Hirth and Tullis, 1992; Tullis, 2002). During regime 1, subsequent porphyroclasts and finely recrystallised tails are developed, homogeneously flattened original grains are only developed in regime 2 and complete recrystallisation occurs at low strain in regime 3 (Figure 2.1). Dislocation creep mechanisms are dependent on temperature and strain rates (Tullis, 2002; Fagereng and Toy, 2011) as summarised in Figure 2.1, whereby higher temperatures or low strain rated favours grain boundary migration (regime 1) and lower temperatures or high strain rates favour grain boundary bulging (regime3).

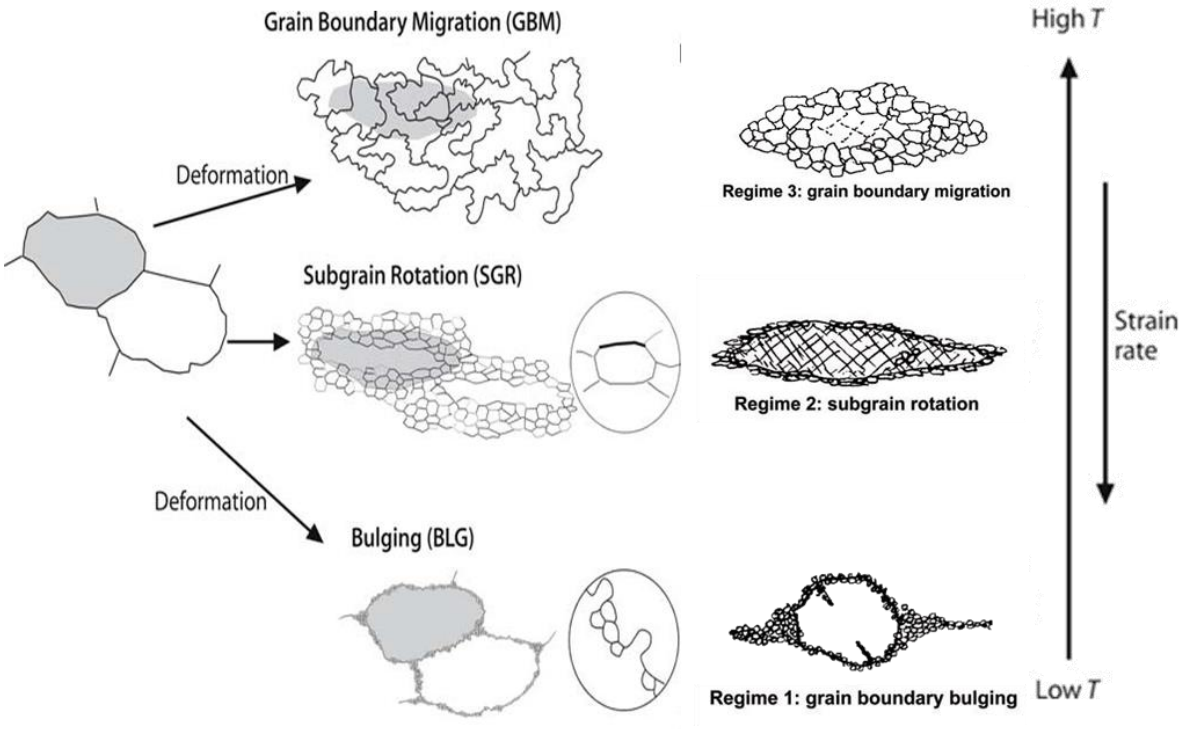

Figure 2.1 Schematic representation of main types of dynamic recrystallisation in polycrystals and relative temperature and strain rate conditions at which they are formed and characteristic optical microstructures developed in quartz aggregates deformed under each mechanism (after Passchier and Trouw, 2005; Tullis, 2002).

In summary, the factors governing deformation partitioning between ductile and brittle structures clearly depend on the mineral deformation mechanism accommodating deformation (Fagereng, 2012). If it occurs by intracrystalline plasticity, then temperature is a critical factor controlling the brittle-ductile transition, whereas in the case of cataclasis and diffusive mass transfer, strain rate and fluid pressure are more important controlling factors of the deformation partitioning (Fagereng, 2012).

3. Deformation and Shear Zones

Shear zones are high strain zones which contain a rotation and a tensile component which displace wall rock segments laterally in relation to each other. Deformation fabric geometry results from the kinematic framework and strain field during deformation, however, deformation fabrics are not necessarily indicative of a particular deformation mechanism (Scholz, 2002). Depending on the temperature, pressure, strain rate and mineralogy, deformation in a shear zone can have a brittle or a ductile component, or both. The terms brittle and ductile describe the rheological behaviour and the resulting fabrics of fault rocks and shear zones.

Discontinuous deformation dominates in the upper crust, at or below lower greenschist facies metamorphism (Fagereng and Toy, 2011) and occurs via the formation of fractures, frictional sliding, mechanical grain rotation and/or grain size reduction when the strength of the rock is exceeded (Sibson, 1977; Twiss and Moores, 1992). Discontinuous deformation propagates with increasing shear, utilising pre-existing structures as far as possible (Faulkner et al., 2010). In the upper crust, discontinuous deformation generally results in the formation of incohesive fault breccias and fault gouges (Sibson, 1977, 1986). At mid-crustal levels, discontinuous deformation in shear zones results in the formation of cataclasites, which are cohesive due to the increased role of fluids and diffusive mass transfer (Knipe, 1989; Passchier and Trouw, 2005). Due to the frictional nature of discontinuous deformation, increasing confining pressure with depth increases the brittle strength of the rock (Sibson, 1977, 1986; Knipe, 1989).

Continuous Viscous deformation is defined as macroscopically continuous deformation at the scale of observation. Continuous deformation plays an important role at or above greenschist facies metamorphism, due to the efficiency of intracrystalline plasticity mechanisms (such as dislocation creep and dynamic recrystallisation) and dissolution-precipitation at temperatures above ~300°C (White et al., 1980; Fagereng and Toy, 2011). In shear zones, ductile deformation mechanisms result in grain size reduction and strain partitioning into mylonites, which often are characterised by anastomosing fabrics, lineations and foliations defined by preferential grain alignment, and occurrence of S-C structures, porphyroclasts and folds within the mylonite (Twiss and Moores, 1992).

Discontinuous deformation is dominant in the upper crust; however, the brittle strength increases linearly with depth due to a gradual increase of confining pressure and temperature. Inversely, continuous deformation is effective in the lower crust, at temperatures above 300°C, but ductile strength increases drastically below 300°C. The zonal depth at which the continuous and discontinuous regimes approach one another is referred to as the **brittle-ductile transition zone**. This transition is not abrupt and the major switch between discontinuous and continuous deformation is likely to occur over a range of pressures and temperatures, typically 350°C to 450°C for quartzofeldspathic crust with a geothermal gradient of ~25°C.km^{-1} (Scholz, 1988, 1989; Fagereng and Toy, 2011). Within this transition zone, both continuous ('ductile') and discontinuous ('brittle') modes of deformation can occur in combination. Cataclastic fabrics give way to mylonitic fabrics over this zone and ductile fabrics are prevalent at high temperatures where crystal plastic deformation mechanisms become dominant over frictional sliding (Sibson, 1977; Scholz, 1988). The brittle-ductile transition is considered a lower limit on seismic faulting, (Sibson, 1982), and it is often referred to as the **seismic-aseismic transition zone**.

The three simplified shear zone or fault models are schematically summarized in Figure 3.1, showing how shear strain rates ($\dot{\gamma}$) and displacement is accommodated across a fault zone before (interseismic phase) and after seismic slip. In Model 1, representing a brittle fault zone, strain accumulates elastically during the interseismic period and is released abruptly along a discrete fault plane, by coseismic slip, the elastic strain in the competent wallrock is recovered, and permanent strain is limited to slip along the fault surface. In Model 2, representing a homogenous, viscous shear zone, finite strain is accumulated and distributed evenly throughout the shear zone during the interseismic period, thus incremental elastic strains accumulated and released during coseismic slip are minimal in comparison. In a heterogeneous shear zone (Model 3), minimal elastic strain accumulates during the interseismic period while permanent finite strain is accommodated by continuous deformation around competent units or on multiple shear surfaces throughout high strain zone. During the seismic event, most strain is taken up by the incompetent layers within the shear zone, where finite strain is concentrated (Fagereng and Sibson, 2010). Shear zones may develop high strain shear bands which wrap around low strain lenses. These dynamics are also observed at microscale as porphyroclasts surrounded by a finer-grained less competent matrix, and on a meso- and regional scale, as anastomosing networks of shear zones separating larger bodies of rock (Sibson, 1977).

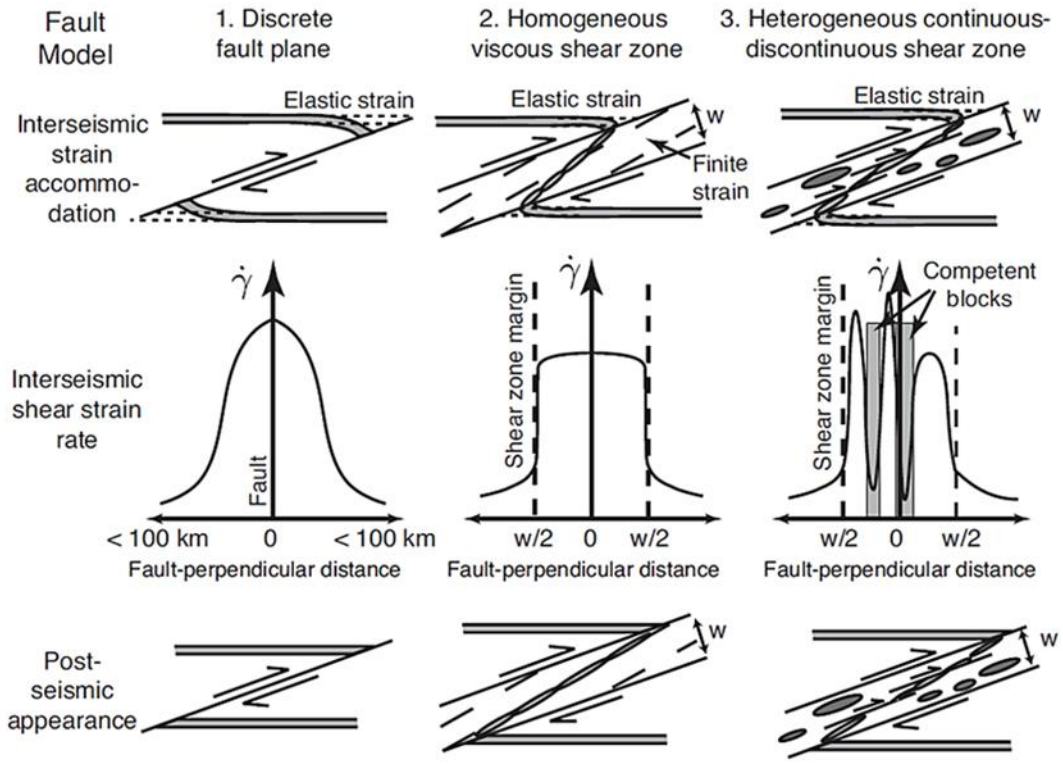

Figure 3.1 Schematic fault zone models (modified from Fagereng and Sibson, 2010) showing accommodation of displacement and interseismic shear strain rate across: (1) a discrete fault plane, (2) a viscous shear zone and a (3) heterogenous shear zone undergoing mixed continuous-discontinuous deformation.

3.1. Crustal Fault Model

The above-mentioned deformation mechanisms, geological features, strain rate and crustal strength, is summarised in a schematic crustal profile in Figure 3.2 (Fagereng and Toy, 2011). The crustal strength increases linearly with depth as the brittle strength increases due to a constant increase of normal pressure. At a temperature of about 300°C, for a geothermal gradient of 25°C.km^{-1}, the brittle strength exceeds the ductile strength, and the rock starts deforming viscously. With increasing temperature, the ductile strength decreases logarithmically. The greatest crustal strength is at the brittle-ductile transition as strain accumulates to the greatest extent. The brittle-ductile transition overlaps with the base of the unstable and seismogenic zones. In the upper crust, discontinuous deformation is favoured, resulting in the formation of fault gouges and cataclasites. In the lower crust, deformation is gradual and continuous and result in mylonites. In between, lies the brittle-ductile transition and a combination of discontinuous and continuous deformation occur, tied up to the seismic/aseismic transition, where both seismic slip and aseismic creep may occur. Complexity in deformation mechanisms and styles is added if the rock is carried through different pressure-temperature conditions and exhumation of the shear or fault zone must be taken into account (Scholz, 2002). This model is of a strike-slip continental fault zone in quartzofeldspathic rock, however, it can be applied to dip-slip (normal and thrust) faults.

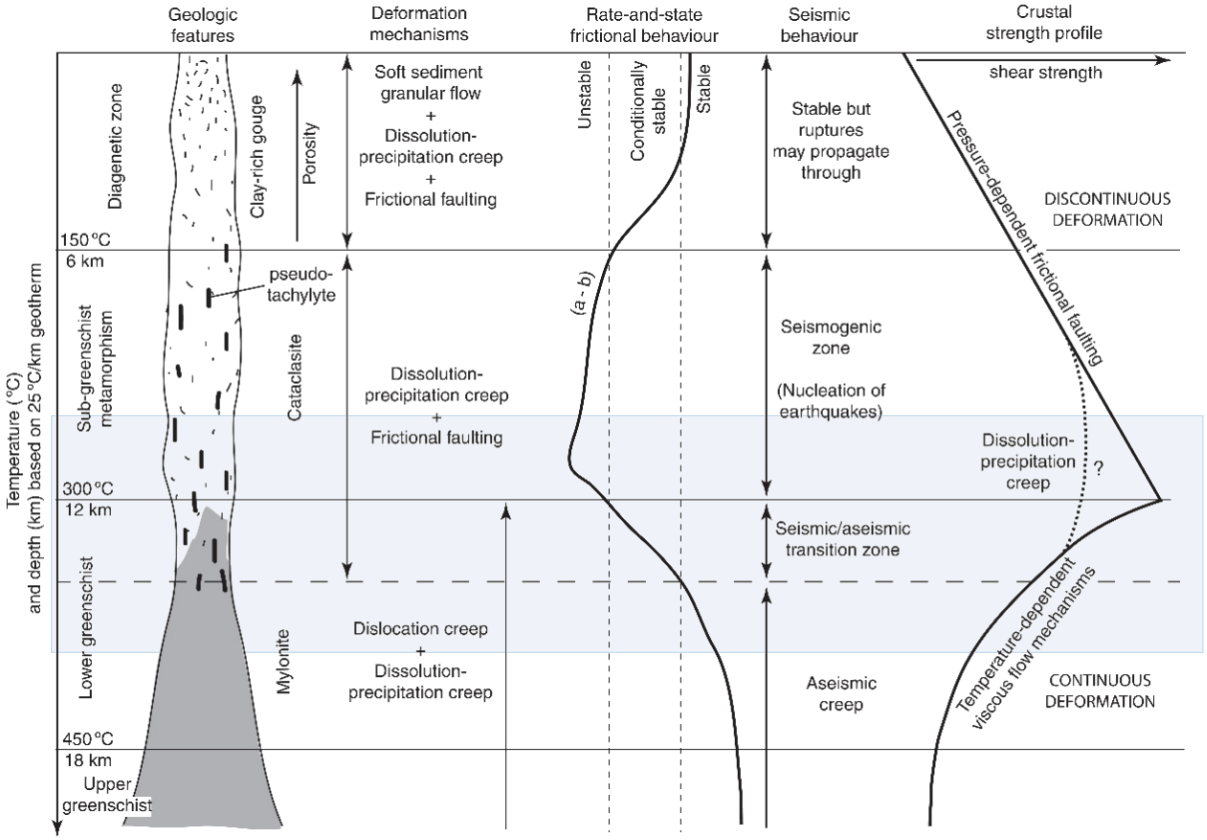

Figure 3.2 Conceptual fault-zone model from Fagereng and Toy (2011), modified from Scholz (2002, 1988); Sibson (1983) showing the changes in geologic features, dominant deformation mechanism, rate and state frictional behaviour, seismic behaviour and deformation regime against temperature and pressure through crustal depth (gradient 25°C.km^{-1}). Blue box shows the temperature range obtained from mineral-equilibrium analysis in Chapter 9.3.

3.2. Fault-Rock Fabrics

Fabrics and fault rocks developed and preserved in shear zones are a result of the mechanical processes which contributed to their development and the physical conditions during deformation (Sibson, 1977, 1986; Knipe, 1989). Sibson (1977) suggests that the main textural division proposed for fault rocks is between random and foliated fabrics in incohesive and cohesive rocks (Table 3.1).

Breccias and fault gouges are incohesive rocks which are distinguished based on grain size, whereas the cohesive rocks are classified by the amount of deformation-induced grain size reduction and the proportion of fine-grained matrix to porphyroclasts (Sibson, 1977; Scholz, 2002). Generally, foliated rocks are interpreted to be a result of ductile deformation processes, while brittle deformation often does not result in the formation of a rock fabric, however, it is necessary to consider that the rheology of the host rock also highly affects the formation of foliation in rocks (Sibson, 1977; Scholz, 2002).

Table 3.1 - Textural classification of fault rocks based on fabrics, percentage of matrix and rock cohesiveness (after Scholz, 2002; Sibson, 1977).

	Random (non-foliated) fabric			Foliated			
Incohesive	Fault breccia (visible fragments > 30% of rock mass)			?			
	Fault gouge (visible fragments < 30% of rock mass)			Foliated gouge			
Cohesive	Nature of matrix	Glass / devitrified glass	Pseudotachylyte	?			
		Tectonic reduction in grain size dominates growth	Crush breccia (fragments > 0.5 cm)			0-10	Percent of matrix
			Fine crush breccia (0.1 <fragments <0.5 cm)				
			Crush microbreccia (fragments <0.1 cm)				
			Cataclasite series: Protocataclasite	Mylonite series: Protomylonite		10-50	
			Cataclasite	Mylonite	Phyllonite series	50-90	
			Ultracataclasite	Ultramylonite		90-100	
		Grain growth pronounced	?	Blastomylonite			

4. Regional Geology

The study area falls within the Malmesbury Group, which forms the basement of the Cape Fold Belt (Gresse and Theron, 1992). The Malmesbury Group is part of the Pan-African Saldania Belt, an orogenic belt with a north-trending western branch and an east trending southern branch. The stratigraphy and tectonic evolution of the Malmesbury Group are largely disputed (Rozendaal et al., 1999; Frimmel et al., 2013; Kisters and Belcher, 2018), with a common consensus that parts of the Malmesbury Group were thrust westwards onto the Kalahari Craton, forming accretionary terrane(s). West to east, these are the Tygerberg, Swartland and Boland terranes (Figure 4.1), separated by NNW trending faults.

Worcester is located in the Boland Terrane, or Boland Group, (Figure 4.1) which is believed to either be an accretionary terrane (Rozendaal et al., 1999) or a foreland basin similar to the Vanrhynsdorp Group to the north (Frimmel et al., 2013), which was deformed in a later pulse of the Saldanian Orogeny (Gresse et al., 1988). The Boland Subgroup is the youngest of the Malmesbury Group in the Western Cape Fold Belt and consists predominantly of phyllite, meta-greywacke, quartzite and minor conglomerate from the Noree and Brandwacht Formations (Frimmel et al., 2001). During the Saldanian Orogeny, peak metamorphism is estimated at ~545 Ma, by analogy with the Gariep Belt and by minimum ages given by granitic plutons (Frimmel and Frank, 1998). Greenschist facies metamorphism was generally not exceeded, except where contact metamorphism occurred near syn-tectonic granitic plutons (Frimmel and van Achterbergh, 1995).

After the Saldania Orogeny, rifting followed by regional basin subsidence resulted in the formation of the Cape Supergroup (Tankard et al., 2009) which stratigraphically overlies the rocks of the study area. The Cape Supergroup records fault-controlled rifting, documented in interlayered basal mudstones, siltstones and sandstones of the ~470 Ma Graafwater Formation. This was followed by gradual, regional subsidence, resulting in the formation of the thickly bedded, mountain forming sandstone formations. The ~465 Ma – ~445 Ma old, 2000 m thick Peninsula Formation sandstones occur adjacent to the study area. After deposition, the Cape Supergroup was deformed during mostly Triassic crustal shortening as a result of the Cape Orogeny. The age of deformation is dated to be 280-260 Ma with metamorphic temperatures of 280°C - 300°C (Hansma et al., 2016). This deformation of the CFB is considered to be the result of subduction and accretion along the southern margin of Gondwana, responsible for the development of extensive foreland basins north of the associated fold and thrust belts (de Wit and Ransome, 1992; Frimmel et al., 2001). The resulting 1300 km long Cape Fold Belt follows the coastline, forming a western, northwest trending branch and a southern, east-trending branch, which meet near the Worcester area at the Cape Syntaxis (de Beer, 1995). The branches and structures of the Cape Fold Belt and the underlying Saldania Belt are largely coaxial.

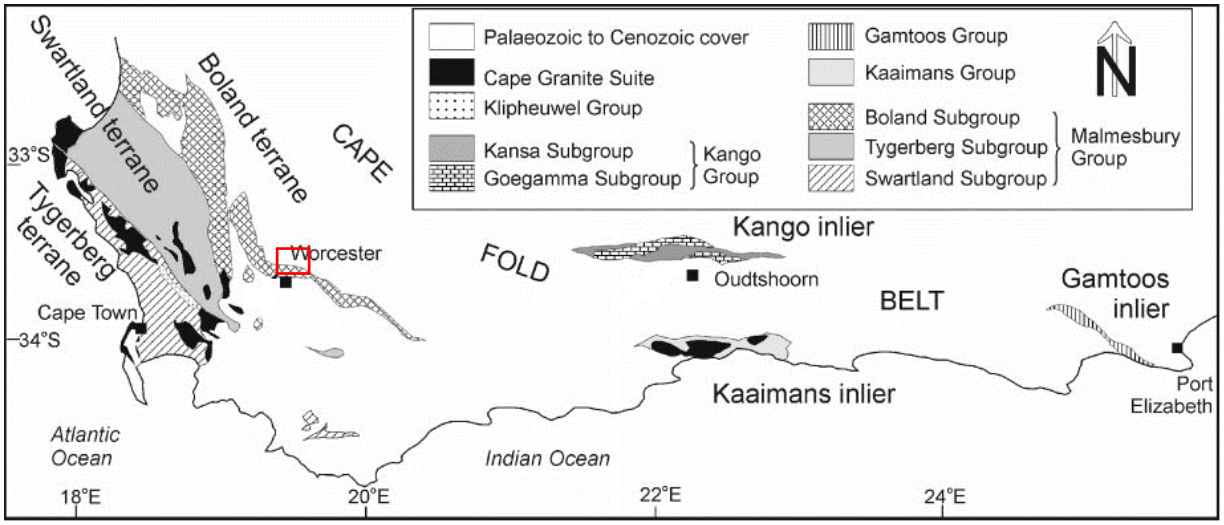

Figure 4.1 Map of locations of the major tectonostratigraphic units of the Saldania Belt within the Cape Fold Belt (modified from Frimmel et al. (2001), after Rozendaal *et al.* (1999). Red box shows the position of the study area in Figure 4.2.

4.1. Tectonism and Metamorphism in the Worcester Area

In the Worcester area, the deformation of the Malmesbury Group is attributed to the following tectonic events (Frimmel et al., 2001):

1 - Accretion, collision and juxtaposition of Tygerberg, Swartland and Boland Terranes (continent-continent collision), regional peak metamorphism and associated compressional deformation (eastward thrusting) during 545Ma tectonism (Frimmel and Frank, 1998), as result of south east directed collisional deformation during closure of the Adamastor Ocean between South America and Southern Africa (Grunow et al., 1996).

2 - Younger deformation phases between 483 - 506Ma (Gresse and Theron, 1992) with an overall northeaster wards transport, which superimposed the Pan-African lithological units and had an effect on post-orogenic molasse sediments (Frimmel and Frank, 1998). This correlates with timing and regional stress of the Ross Orogeny in adjacent Antarctica.

3 - Cape Orogeny tectonic pulses between 230 - 290 Ma (Gresse and Theron, 1992), thrusting and folding and the local formation of discrete foliations as result of concurrent angled northwest- and northeast compression of different magnitudes.

Two main low-grade metamorphic overprints are recognised in the Malmesbury rocks of the Saldania Belt in the Cape Fold Belt: the Pan-African metamorphism (~500Ma) and the Cape orogen metamorphism (~250Ma). The latter deformation episode reactivated structures in the basement rocks to some degree and produced strong overprinting of structures in areas of intense Cape orogenic activity (compression followed by extension during exhumation).

Frimmel et al. (2001) determined a marked difference between the pre- and syn-Cape orogeny metamorphic overprint in the Worcester area, where the presence of chlorite in Malmesbury is interpreted to predate the Cape orogeny; and the presence of chloritoid in schist is attributed to infiltration of an oxidizing fluid between the Malmesbury and the overlying Table Mountain Group during Cape Orogeny. Based on chlorite and chlorite-chloritoid thermometry (Frimmel et al., 2001), the temperature during Pan African metamorphism was estimated to 325±12 °C and during the Cape Orogeny to 320°C.

The field area is crosscut by the Worcester fault which strikes W-SE (Figure 4.2), with a displacement of more than 6000m in the Worcester area (Gresse and Theron, 1992) and which formed during rifting of Gondwana between 135 – 130 Ma ago along the Agulhas-Falkland Fracture Zone (Tankard et al., 2009). The remnants of the Cape Supergroup and Malmesbury basement rocks are exposed north of the fault line, whereas south of the fault line, the stratigraphically higher the Enon Formation from the Uitenhage Group (Figure 4.2) and Quaternary deposits are preserved. The fault plane of the Worcester Fault is not visible in the study area, but the change in topography and lithology is evident.

4.2. Study Area

The object of this project is a series of outcrops of the Malmesbury Group exposed near Nuy Valley, approximately 15 km East-Northeast of Worcester, in the western part of the southern branch of the Cape Fold Belt. Three main outcrops were selected for analysis within the study area, along strike of the major northwest-trending thrust faults and shear zones. The locality of these outcrops and the analysed thrusts is outlined in Figure 4.2. The outcrops are part of the hanging wall of the Worcester Fault, north of the fault line and show similar deformation features and fault kinetics thus might contain the same fault or individual faults. The Malmesbury outcrops in the study area are superficially weathered (sericitic or chloritic) phyllites covered by vegetation, as can be seen in the aerial photograph (Figure 4.2 b).

The three main selected localities are roughly within a 12 km radius from each other, along the major NW trending thrust fault, subparallel to the Worcester Fault (Figure 4.2.a). The Cross locality is on the western margin of the study area, about 11 and 9 km WNW from Boesmanskloof and Hill510 respectively. Boesmanskloof is situated approximately 1 km NW-SE from Hill510, on the immediate side of an erosional valley. The three localities, Cross, Boesmanskloof and Hill510, register a topographic elevation (maximum height) of 360m, 390m and 510m respectively, and are systematically cross cut by thrust faults striking WNW - ESE (Figure 4.1). The mapped thrust fault cuts across these three localities striking from Hill510, to Boesmanskloof across from it and further towards the Cross. The faults are not visible in aerial photographs and poorly exposed in the field in a regional scale but observable at outcrop (macro) scale. At all three localities, the analysed fault zone lies within the Brandwacht Formation from the Malmesbury Group. The Brandwacht Formation forms both the footwall and the hangingwall of the studied localities. This formation has been described as consisting of grewacke and pelite with interbedded conglomerates composed of poorly sorted, irregular lenses containing quartz, greywacke and phyllite clasts (Rozendaal et al., 1999).

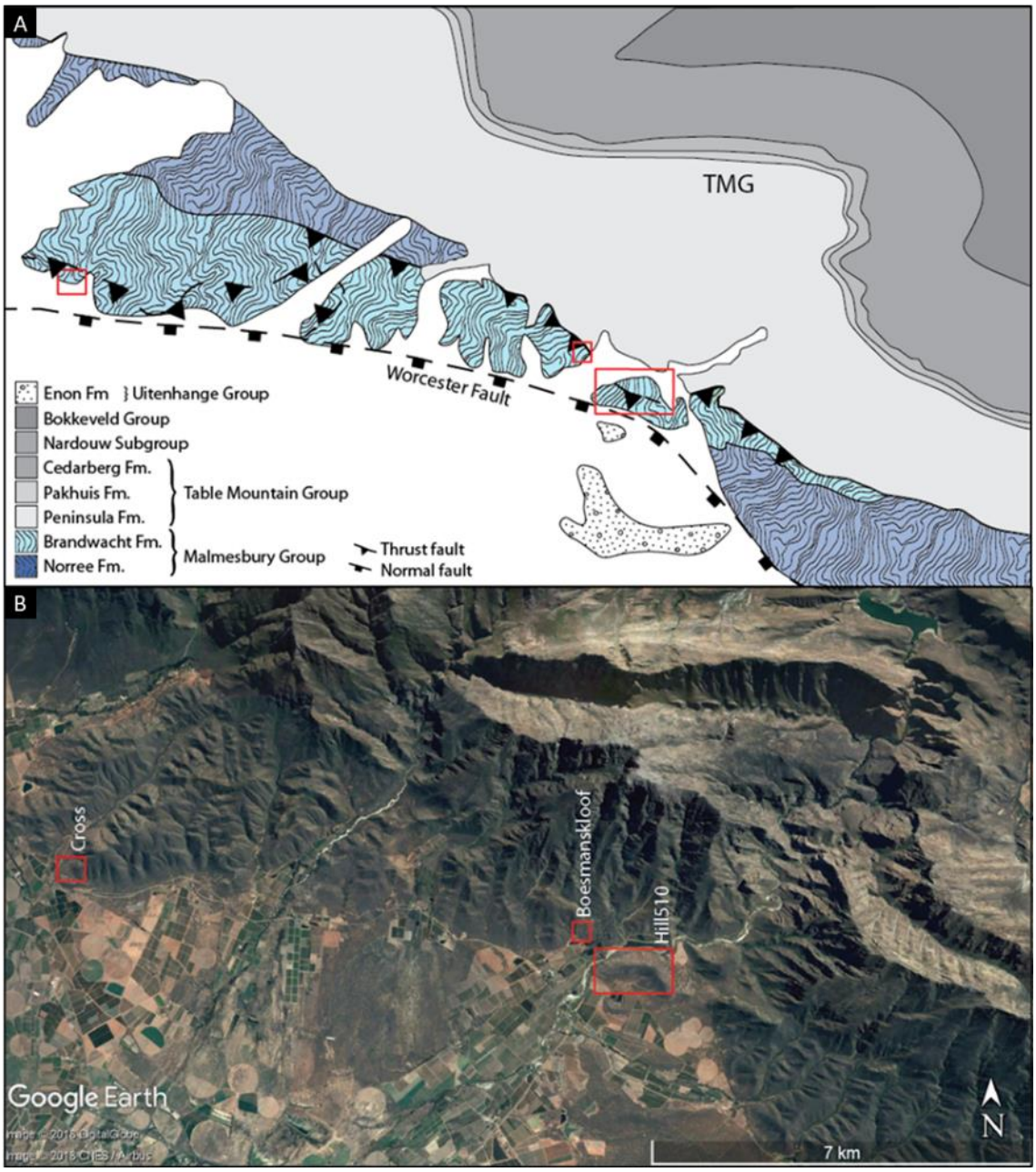

Figure 4.2 Geological map simplified (a) from 1:50 000 and 1:250 000 Worcester geological map sheet 3319da showing main WNW-ESE regional thrust faults and posterior Normal Worcester Fault; and (b) corresponding aerial photograph of area NE of Nuy Valley. Red boxes show studied outcrops and sample localities: Cross, Boesmanskloof and Hill510.

5. Field Observations

This Chapter presents the field observations. Field analysis of faults zones mainly consisted of mapping and documenting at the local scale the distribution of the different fault rocks, fault orientation (strike-dip direction) and style of faulting, thickness and geometry of fault rock elements within selected outcrops. Samples of various fault-rocks throughout the study area were collected for further analysis.

From a petrographic point of view, Boesmanskloof and Cross are fairly homogeneous consisting mostly of quartzites, and schists associated with minor limestones and quartzites respectively. Hill510 has been mapped in detail as it has significantly better fault zone exposures and shows the most variation in lithology and rheology in the area, containing all fault rock types described in this chapter.

5.1. Deformation Zone Lithology

Three main lithological units are recognized within the Malmesbury Group, in Nuy Valley and surroundings: greenschist facies metapelites (chloritoid schist and muscovite chlorite schist), marbles and metasandstone units. All these rocks types are overprinted by various degrees of deformation and the contacts between these main lithological units vary and are seldom exposed.

5.1.1. Metapelites

Metapelites from the Malmesbury Group compose the main lithology in the area and form both hanging wall and footwall of the faults. The major phases in the mineral assemblage are chlorite, muscovite and quartz and minor chloritoid in some samples; classifying the metapelites into chlori-muscovite schist and chloritoid schist. These rocks are fine grained and have a green lustre, preserved even post-silicification (Figure 5.1.a). The chloritoid schists contain porphyroblasts of chloritoid (average 1–2 mm long laths) (Figure 5.1.b). These metapelites display a strong schistosity and quartz veins are often present and abundant in this unit. Close to the studied fault zone, this lithology is foliated and deformed, and generally contains a moderate to high silica content.

5.1.2. Metasandstone lenses

Metasandstone is present in the study area in the form of lenses of various sizes, ranging from meter to several meters long and wide. These greywacke bodies are widespread along the faults damage zone, usually as lenses wedged in the fault core or as part of the footwall, underlying high strain zones. The greywacke is composed of predominately poorly sorted, medium to coarse, angular quartz grains, feldspar and small lithic fragments in a clay rich matrix (Figure 5.1.c). The contact between the metasandstone lenses and the metapelites varies, but it is predominantly sharp and often characterized by high strain zones, deformed schist bands or fault gouges.

5.1.3. Marble (Mylonite)

The (limestone) marble unit is present in both Hill510 and Boesmanskloof. In the former location, it lies as an approximately 10m thick, semi horizontal horizon in the footwall of the middle fault (MSZ). It is typically surrounded by schist and underlies the metasandstone fault rocks, where the fault is almost barren of quartz veining. This unit contains a high percentage of calcite, is very fine grained and strongly deformed (Figure 5.1.d) and typically surrounded by brecciated or mylonitic rocks. The contact between

the limestone and other lithological units could not be established due to extensive weathering and high coverage by vegetation and scree. It is likely that the deformation associated to the fault thrust this project focuses on, was not necessarily what deformed the original limestone to mylonite, and that rather, during thrusting, the already mylonitized limestone just became further deformed (but did not go from limestone to mylonite. Thus, these are not necessarily host rocks, but more like deformation zone rocks.

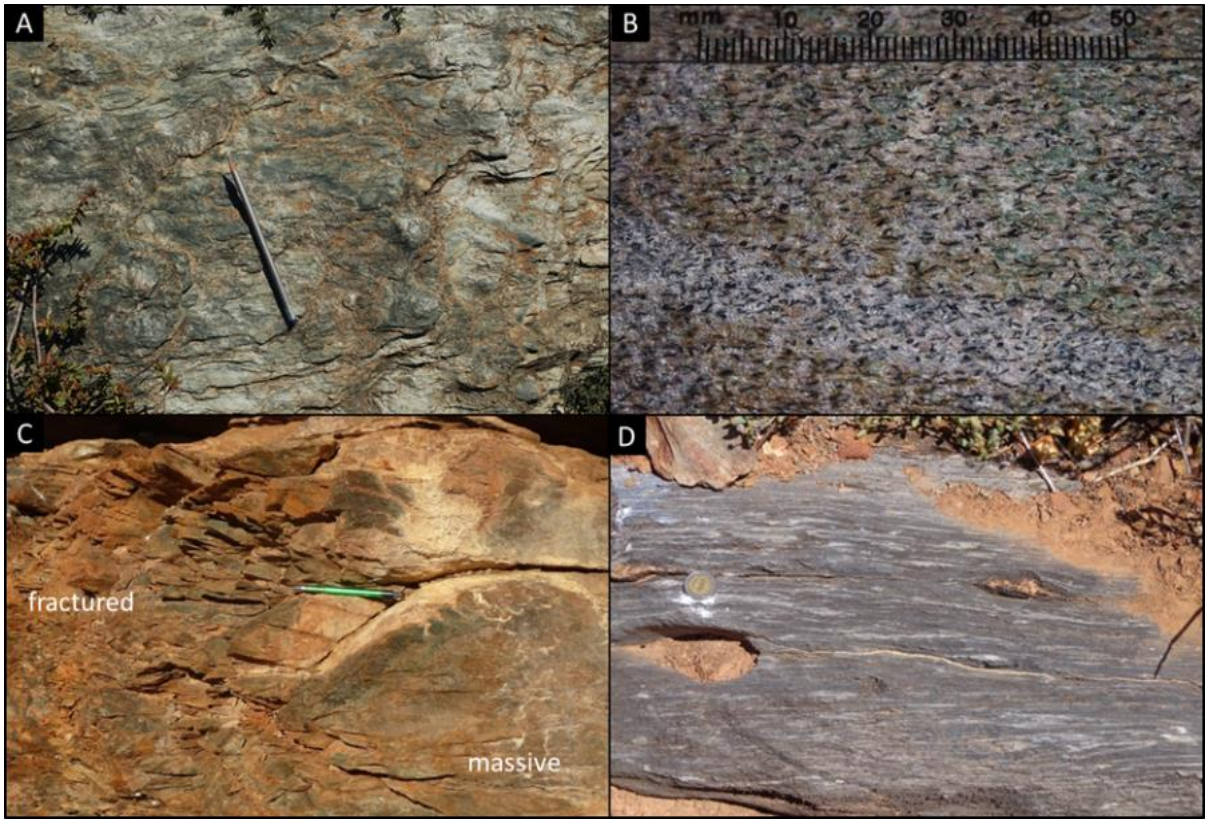

Figure 5.1 Main lithological units in studied area. A) Representative metapelite; B) Chloritoid schist with chloritoid porphyroblasts, from outcrop between Hill510 and Boesmanskloof; C) Metasandstone lens: fractured (left) and massive (right); D) Mylonitic limestone with ~0.5 - 1 cm wide shear bands.

5.2. Faulting

As mentioned before, Hill510 has been analysed in greater detail. This locality consists of a hill within the Leipzig Farm, allowing for visible cross sections to be drawn and clear exposure of the different rock assemblages displaying both brittle and ductile deformation fabrics. Here, the thrust fault consists of three quasi distinct, semi parallel striking approximately WNW (~285°) (Figure 5.2) and dipping preferentially southwards. The fault zones are generally semi planar and their thickness ranges from several to tens of metres.

As both shearing and faulting occur somehow intermittently along and across the profiles in Hill510, the high strain planes in the study zone are referred to as both faults and shear zones, depending on the scale of description. When referring to the map and to the full outcrop on the scale of Hill510 (Fig. 5.1), the high strain planes are referred to as thrust faults, whereas on a smaller scale (profiles) the complexity and combination of brittle-ductile structures rather classifies these faults as heterogeneous shear zone.

The three thrust faults can be identified in Hill510 and their position has been mapped and extrapolated based on the position of the fault planes, high strain zones and position and prevalence of the fault rocks, in two cross sections (Figure 5.2). The degree of deformation within the fault zone varies with distance from individual fault cores and relative position to lithostratigraphic heterogeneities. The fault zones contain brecciated areas, limestone mylonites, abundant quartz veining, cataclasites, and intensely deformed fault gouges, cohesive and incohesive. The hanging wall is often characterized by a higher degree of silicification in the schist and abundance of quartz veins. The footwall is generally composed of deformed and foliated schist and in some sections, mylonitic limestone. The latter is present in the form of a discontinuous horizon in the footwall of the Middle Fault (MSZ) in Hill510 and in portions along the fault plane cutting through Boesmanskloof locality. The faults are not visible in aerial photographs and are typically poorly exposed in the field at a regional scale but can be observed at the scale of the outcrop.

On Hill510, along strike, the three traced faults show variable damage zone thicknesses and continue discretely for hundreds of meters, spaced 10 – 30 m apart within the exposed outcrop of this hill. The faults contain isolated lithologies and structures in a variably silicified wall rock. The observed sense of shear along the faults is NNW – SSE, locally determined by mineral lineations in the schist, the geometry of the conjugate fracture sets, fault plane measurements and SC fabrics in high strain zones, described in Chapter 6. In the following chapters, these faults will be referred to as Upper, Middle and Lower Faults (also referred to shear zones when referring to smaller scale), corresponding to their respective position in Hill510 (Figure 5.2). The assemblages within fault zones vary both along faults and between the three mapped areas, and the contacts between hanging wall and footwall are either sharp (discrete fault planes) or gradual (shear zones of variable thickness). Two wallrock profiles were taken across the same fault to depict lithological heterogeneities, approximately 110 m from each other, along the Lower Fault (location pointed put in Figure 5.2 a and b) and are presented in following chapter.

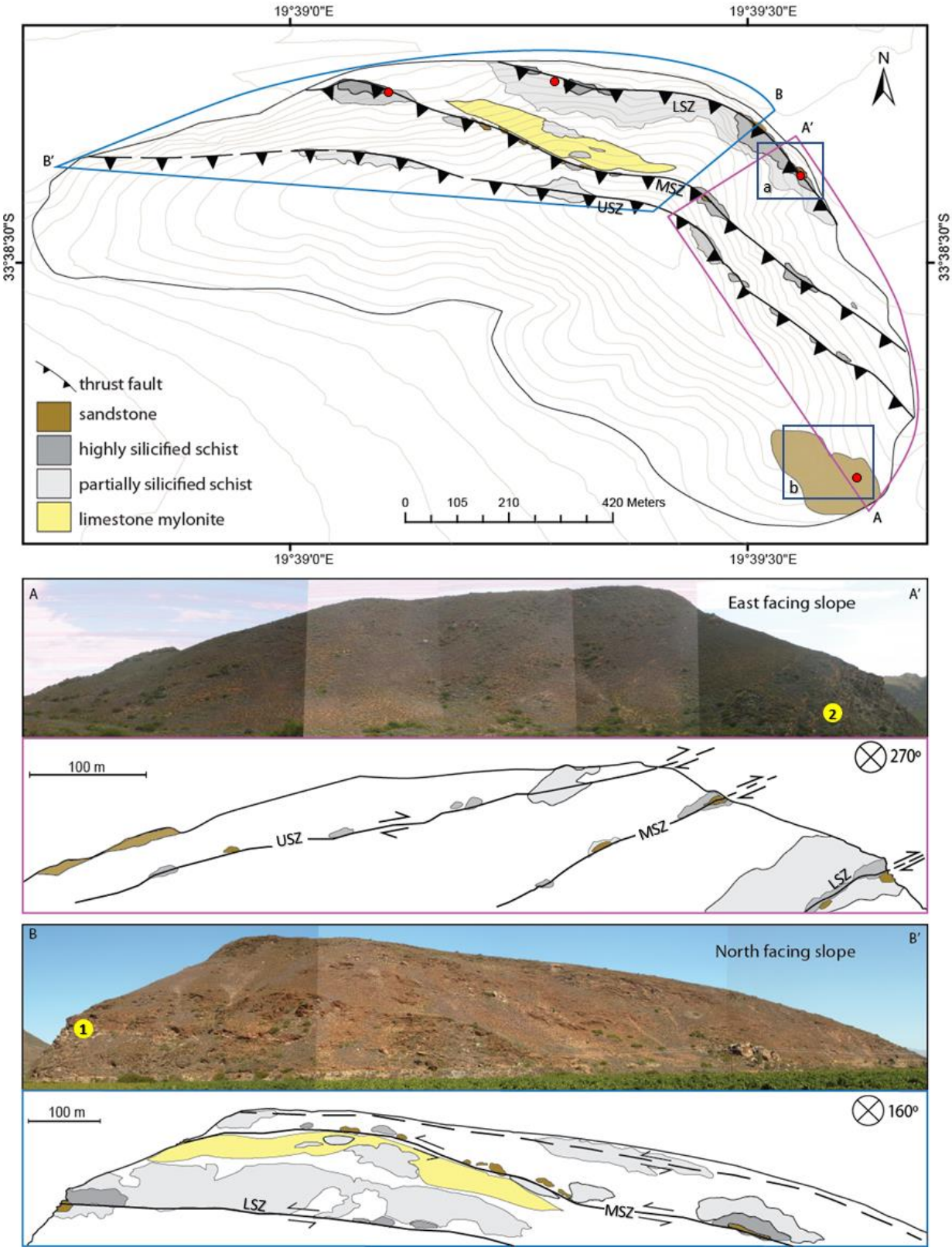

Figure 5.2 Compiled geological map of Hill510, showing position of the three main high strain zones which are formed by a combination of fault planes and shear zones (USZ: Upper Shear Zone, MSZ: Middle Shear Zone, LSZ: Lower Shear Zone) and distribution of mappable lithological units. Annotated panoramic photos of Hill510 showing East facing (A) and North facing (B) slopes, fault core trace outlines and main lithological changes. The areas where the lithology is not specified represent lack of in situ sampling (most likely schist). The solid lines represent observable fault cores, and dashed lines are the extrapolated position of the fault core based on the relative position of the fault rock outcrops. Yellow labels show position of representative wallrock profiles (1 and 2); red dots represent main locations of structural measurements in Hill510. The boxes (a, b) point out the position of the fracture sets data, corresponding to stereonets in Figure 8.1.

5.3. Wallrock Representative Profiles (Hill510)

This Chapter will present two wallrock profiles taken across and along the Lower Fault (LSZ) in Hill510 (Figure 5.2 for position of profiles). The fault zone outside of the presented profiles either consists of sharp and discrete planes or does not have outcrop exposure. In both profiles, the hanging wall is composed of highly deformed, silicified schist and the footwall is composed of partially silicified schist.

Profile 1. North Lower Fault Zone

This profile represents a fault zone characterized by three semi-planar continuous high strain zones marked by shear planes of variable thickness (HSZ1 and HSZ2) and a discrete fault contact (HSZ3), which accommodated most strain and movement along its margins. The XRF and oxygen isotope values from samples across this profile are presented in Chapter 8.4.

High Strain Zone 1 (HSZ1) is a ~30 cm thick planar contact within hanging wall silicified schist. It contains a thin (mm-cm scale) cemented and foliated fault gouge and forms the contact between the subdivided silicified sheared schist (bottom) and silicified less sheared schist (top). HSZ1 hanging wall displays intense network veining.

High Strain Zone 2 (HSZ2) is a ~1,5 m relatively gradual high strain zone, containing isolated lenticular massive metasandstone bodies (max. 2 m long) surrounded by sheared foliated fault gouge (Figure 5.3.b). It is positioned approximately 5-6 m vertically below HSZ1. The adjacent wallrock within 2-4 m from HSZ2 is composed of silicified schist with negligible amounts of macro-veining.

High Strain Zone 3 (HSZ3) is represented by a discrete planar fault plane, 4-5 m vertically below HSZ2. It forms the contact between sheared silicified schist and the underlying poorly sheared-to-unsheared schist footwall (Figure 5.3.c).

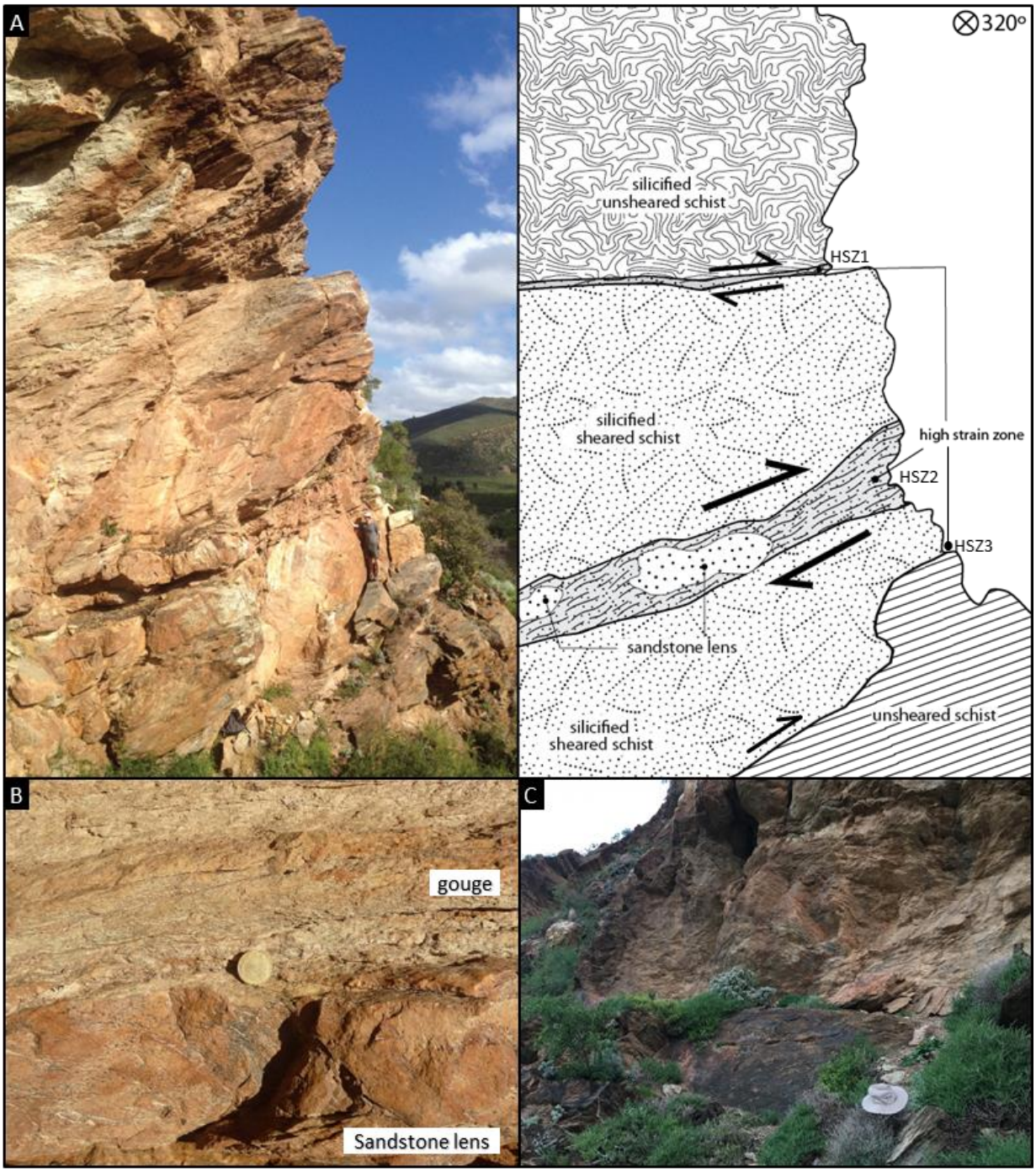

Figure 5.3 Profile 1 Simplified representative fault rock rheology: A) Photograph of outcrop at bottom fault and corresponding annotated cross section profile and fault rock lithology of Profile 1 along Hill510 LSZ; B) High Strain Zone 2, sheared and foliated fault gouge displaying SC fabrics, wrapping around massive metasandstone lens; C) High Strain Zone 3 (HSZ3), discrete fault plane between unsheared schist and silicified schist. Refer to mark (1) on East facing slope and map in Figure 5.2 for location of outcrop on Hill510 LSZ, coordinate 33°38'18.96"S 19°39'28.15"E.

Profile 2. East Lower Fault Zone

This profile represents a distributed fault zone characterized by cataclasite layers and a fracture metasandstone lens within fault core and a densely veined hanging wall.

The hanging wall comprising Malmesbury schist has a lineated and foliated fabric (L>S tectonite) and is strongly silicified, containing a high density vein system which dissipates over approximately 5-10m from the principal slip zone. The fault core is marked by a high strain zone defined by 2 cataclastic horizons that form adjacent to a metasandstone lens. The metasandstone lens is absolutely devoid of quartz veins and intensely fractured, with a maximum thickness of 1.5m and thins out to 20cm close to its edges (Figure 5.4.c). The footwall Malmesbury schist is only slightly silicified in comparison to the hanging wall and is generally devoid of quartz veins or quartz clasts.

The top cataclatise to ultracataclasite horizon is 10-15cm thick and underlies a ~30cm layer of sheared fault gouge contining SC fabrics (Figure 5.4.b), bounded by highly silicified and and sheared schist. The basal cataclasite horizon in ~20cm thick and is in contact with a secondary metasandstone lens, also tapered towards the edges. The layers of cataclasite to ultracataclasite define the principal slip zone within the damage zone (Faulkner et al., 2010; Fagereng and Toy, 2011). The thick high strain fault core thins out along the side of the shear zone (northwards in the direction of location of Profile1), becoming a sharp planar contact, contained between silicified schist blocks (Figure 5.4.c).

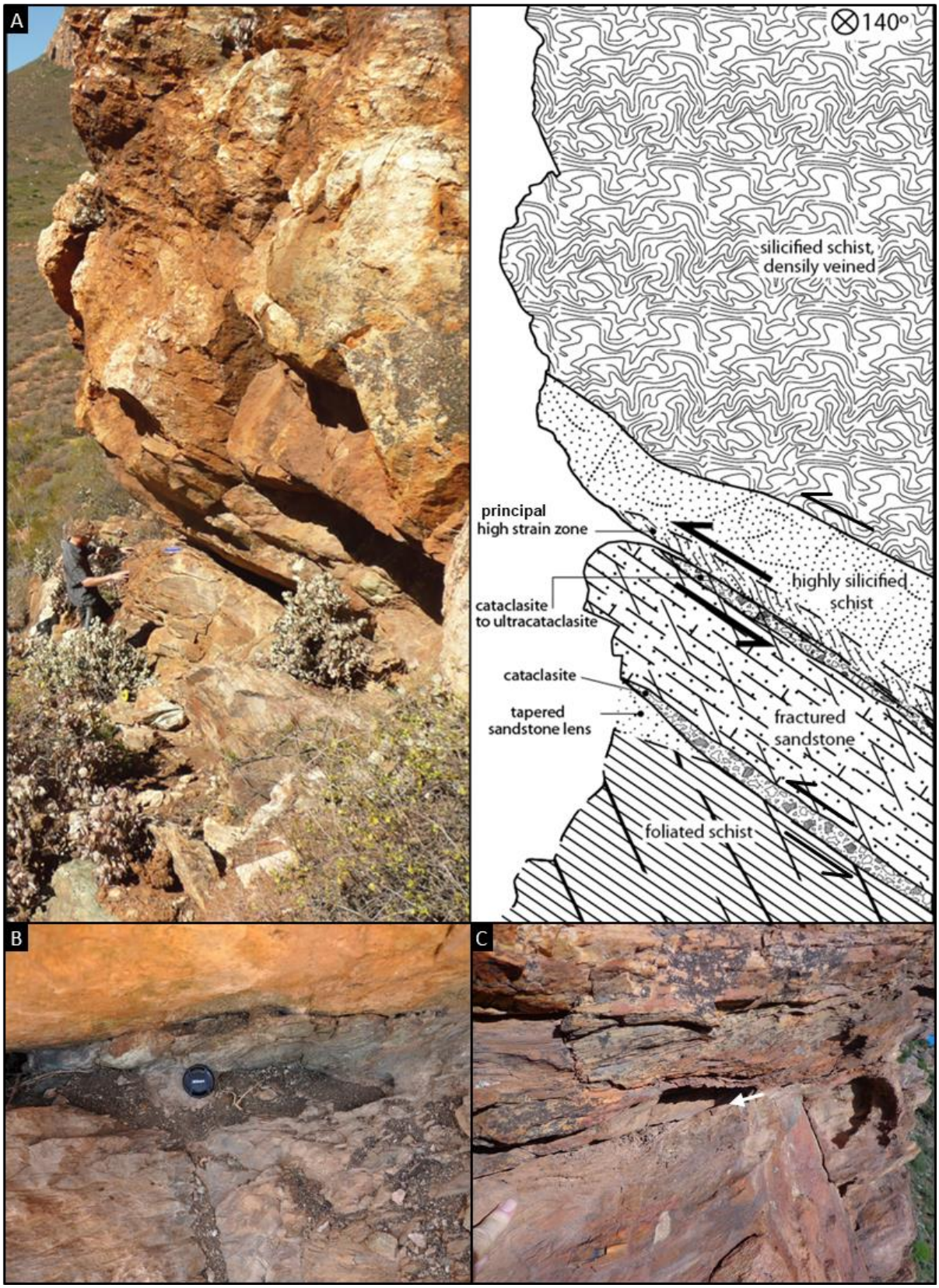

Figure 5.4 Profile 2 Simplified representative fault rock rheology: A) Photograph of outcrop at lower fault and corresponding annotated cross section profile and fault rock lithology of Profile 2 along Hill510 LSZ. B) sheared fault gouge overlying cataclastic metasandstone in high strain zone; C) tapering fault gouge alongside high strain zone, sharp fault plane between profile 2 and 1. Refer to map in Figure 5.2 for location on Hill510 LSZ coordinate 33°38'23.50"S 19°39'31.30"E, (2) north facing slop of 510.

5.4. Fault Rock Assemblages

This Chapter focuses on the macroscale description of the rock units in the fault zones mapped and presented in Chapter 5.2. The fault rocks vary from moderately to highly silicified schists often intensely veined, to cataclasites, hydraulic and quartzitic breccias, fault gouges and mylonitic limestones. The dominant fault wallrock in the study area consists of silicified schist, meatsandstone lenses, quartzites, and the fault rock breccias, cataclasites and mylonites are found within high strain zones in fault cores of shear zones.

5.4.1. Silicified Schist

Silicified schists form the predominant fault-rock and are ubiquitous throughtout the study area, present in all three main study localities (Hill510, Boesmanskloof and Cross). Overall, the degree of silicification in the schist visibly varies within the faullt zone and the hanging wall is generally more silicified than the footwall. Silicified schists are subdivided into two classes, based on apparent cohesion of the rock, distribution of veins and competent quartz clasts:

- Partially to Moderately silicified schist: foliated schist displaying slightly different hues, green, brown and grey and containing a variable but well spread/gradual amount of quartz (dissolution) and little to no veining (Figure 5.5 a).
- Highly silicified schist: metapelitic schist containing an elevated and visible amount of crystallized quartz (Figure 5.5 c) and abundant veining and fractures.

5.4.2. Quartzites

Quartzites are formed by coarse and equigranular grains, composed mainly of quartz (>90%). Visible sedimentary features such as sand grains (round, 1-2mm diameter clasts) can be observed within quartzitic metasandstone lenses. Quartzites have mostly a granular texture, but some outcrops contain observable planes of foliation. Quartzitic units are found usually near other metasandstone units and in close proximity to the fault core.

5.4.3. Limestone Mylonites

Limestone mylonites are the result of deformation of limestone units in the study area. These are fine grained and composed of calcium carbonate minerals. Unlike most marbles, this unit is well foliated, displaying mylonitic layering (dark and light bands) and sheared (Figure 5.5.d).

The rock unit is strongly deformed and mylonitized and typically surrounded by mylonitic wall rock and underlies schist and quartzite, where fault is barren of quartz veins. This lithology is present below middle thrust fault on the north facing slope of Hill510 and in Boesmanskloof, below the main fault plane. Weathering and lack of exposure in between outcrops, obstruct correlations on lithological or structural grounds about this rock type.

5.4.4. Cataclasites

Cataclasites in the study area consist of angular grains (~1.5mm) in a fine matrix (Figure 5.5.f) and are found spread out within thin layers in the fault damage zone. These somewhat discontinuous thin cataclasite layers are adjacent to lenses of fractured metasandstone (protolith) of variable and considerably higher thickness. These layers of cataclasite to ultracataclasite lie within the principal slip zone within the damage zone, as seen in profile 2 (Figure 5.4). In the study area, cataclasites horizons are thin, no more than 20cm thick and form adjacent to metasandstone and quartzite bodies within fault core, or fault gouges.

5.4.5. Fault gouges

Fault gouges are clay rich, of light brown or green tinge colour and incohesive rocks, foliated and sheared and generally parallel to the fault plane, displaying parasitic folds. The gouges are fine grained and do not contain observable clasts, marked by a very high percentage of matrix. This rock type is common along the Lower Fault but not along other two fault in Hill510, where the fault planes are generally marked by sharp contacts between highly silicified schists and intensely veined schists and underlying marginally silicified schist. The appearance and cohesiveness of gouge exposures vary along the fault (Figure 5.5.i, j), from non-cohesive light brown gouges to cohesive gouges usually with a greenish tinge (silicified during or post deformation).

5.4.6. Breccias

Two types of fault breccias are recognized in the study area: hydraulic and crush breccias.

Fault crush breccias are composed of lenticular, brittle fragments of wallrock (silicified schist and metasandstone), and quartz (disaggregated veins) of variable sizes (0.5-5cm) in a silicified schist matrix. This rock type is commonly part of the hanging wall silicified schist and is usually intensely veined (Figure 5.5.b). Crush fault breccias occurring in quartzitic units are almost entirely composed of quartzite and quartz brittle fragments also of variable size (Figure 5.5.h).

Hydraulic breccia is comprised of poorly sorted angular fragments of wall-rock (schist) and quartz, cemented by hydrothermal quartz precipitates (Figure 5.5.g). This fault rock is cohesive and not widespread nor common throughout the study area and often occurs in zones of intense quartz veining.

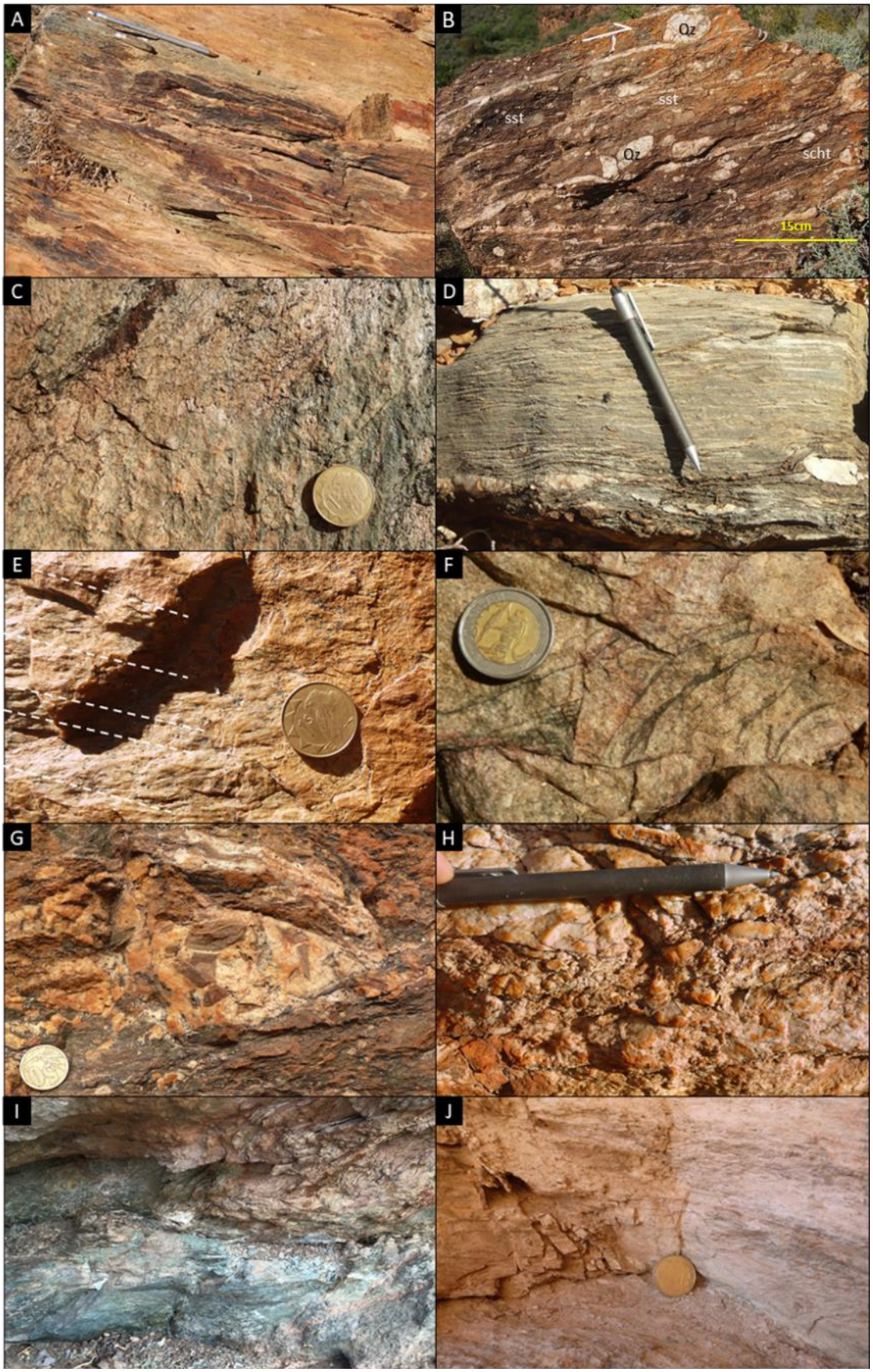

Figure 5.5 Deformation zone and fault rock units: A) partially to moderately silicified schist outcrop; B) highly silicified schist, present in the hanging wall or fault core; C) mylonitic limestone ; D) schist breccia containing quartz, metasandstone and schist clasts (breccio-conglomerate-like schist) and veins); E) quartzite displaying lineations (pointed out by white dashed lines); F) cataclasites, G) hydraulic breccia; H) quartzitic breccia; I and J) fault gouges.

6. Macrostructures and Fault Geometry

Deformation fabrics present in the study area are described in this Chapter and the sense of slip is established through shear sense indicators (both ductile and brittle). Brittle shear indicators include faults, conjugate fractures sets, fractured porphyroclasts and dilational jogs. Ductile shear indicators comprise shear bands (C' Type shear bands), folds (parasitic), lattice preferred orientation (in case of micas and chlorite alignment), asymmetric boudins and isolated asymmetric objects (porphyroclasts, sigmoids, strain shadows).

Geometry measurements of lineations, foliations, fault planes, fractures and veins were integrated using Stereonet v9.8.3 (Richard W. Allmendinger © 2011-2016). The paleo-stress orientations inferred from conjugate fracture sets were based on methodology in Bons et al.(2012).

6.1. Planar Fabrics

Bedding cannot be recognised to be pervasive in the study area due to metamorphism, intense deformation and recrystallization, and it is mostly overprinted by secondary foliation planes. The main planar fabrics distinguished in the study area include: foliation planes in metapelitic schist, metasandstone and quartzite units and fault planes

Foliation in the metapelitic schist unit is pervasive throughout the study area. It is defined by alignment of micaceous minerals (muscovite, biotite, chlorite) and, in chloritoid schist, slight preferred mineral orientation of chloritoid laths; and form planes of foliation which occur every to 0.5 - 2 cm spacing (Figure 6.1.a). Ductile flattening of grain aggregates (quartz) in silicified schist also contributed to the foliation. Other secondary foliations in schist includes schistosity and compositional and mylonitic layering (Figure 6.1.b).

Mylonitic layering occurs in limestone mylonites and in some mylonitic schist samples. In both units, this foliation is defined by semi continuous dark and light bands, <1cm spacing, and it contains down dip lineations (Figure 6.1.b, c).

Although less common, foliations are also present in metasandstone and quartzite units and are defined by planes of weakness, thin layers (~1 – 4 mm) of dark brown cataclastic material (Figure 6.1.d), likely of phyllosilicate composition.

Evident foliations in the metapelitic units, metasandstones, quartzites were measured and found to have very similar orientations and inclinations (Figure 6.1.2). The poles to foliations of these units have an average mean trend and plunge of 347/52°, where foliations in schist are slightly steeper (Fisher mean of schist = 353.4/52.5°; and of metasandstones and quartzite combined = 007.2 /63.1°; total n=101). The measured fault planes and localized foliation (defined by planes of weakness of the adjacent surrounding hanging wall and footwall are approximately parallel (Figure 6.1.1). Footwall foliations and fault planes readings have an average pole of 006/48.5°. The hanging wall is dips at the same angle, but its strike has been slightly rotated by ~10^{o} (Fisher mean 348.4/48° S). In general, the average foliation geometry in the area and fault planes measured coincide, and are closely parallel, striking E-W and dipping ~33° S (Figure 6.1.1), with a negligible rotation of hanging foliations.

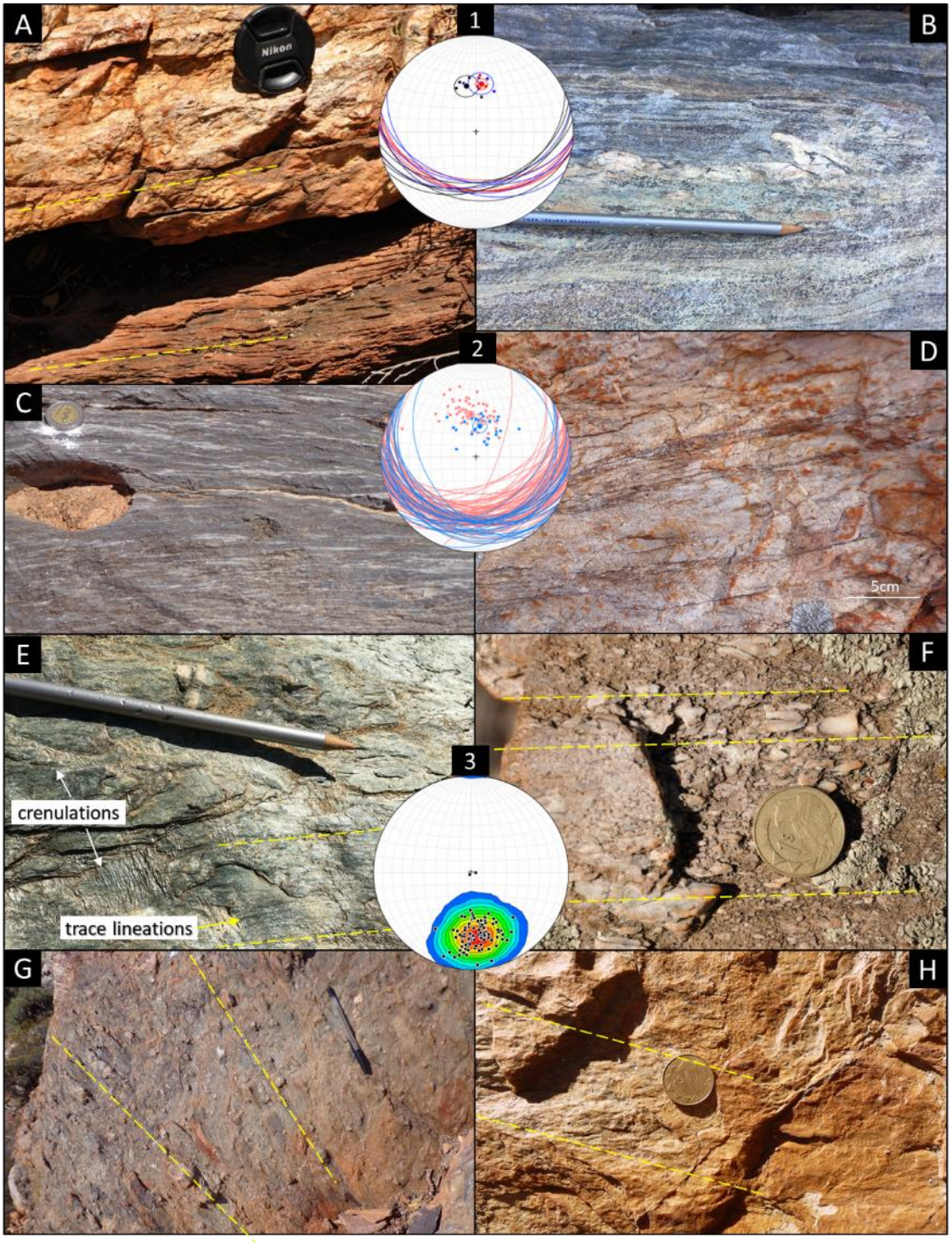

Figure 6.1 Planar and linear fabrics and lower hemisphere equal area stereonet plots: a) Foliations in highly silicified schist (top) and partially-moderately silicified schist (bottom), parallel to planar sharp contact; b) Compositional banding in schist; mylonitic layers in schist defined by elongate concentrations of quartz (top), chlorite (bottom) and chloritoid (bottom); c) mylonitic layers in mylonite; d) foliation in quartzite defined by cataclastic phyllosilicate layers; e) crenulations and slicken fibres on the foliation plane of schist; f) aligned elongated brittle quartz fragments in veined schist; g) aligned elongated semi round quartz clasts in typical silicified schist tectonite in the hanging wall; h) discrete lineations in quartzite defined by aligned recrystalized quartz grains and sparse micas. Yellow dashed lines indicate lineation orientation. 1) foliation planes in schist (n=93, pink) and foliation planes in metasandstone and quartzite outcrops (n = 26, blue); 2) lineation measurements of entire study area (n=101, contour interval = 3); and 3) closely parallel fault plane (red n=5), footwall schist foliations (blue n=5) and hanging wall foliations (black n=5) and respective poles.

6.1. Lineations

The main lineations taken into account in this project are widespread non-penetrative lineations (i.e. trace lineations, aligned minerals and reorientation of elongated clasts as result of shear deformation). These are more obvious in schist outcrops but not uncommon in other rock units.

Trace lineations form on the plane of foliation of schist and are continuous, often occurring with crenulation lineations on the same surface, perpendicular to each other (Figure 6.1. e). Elongated and aligned porphyroclasts are often of quartz composition and have variable sizes, from grains 2 mm long to elongated clasts 10 cm long in silicified schist outcrops (Figure 6.1.f, g). Other lineations are discrete and defined by preferred orientation of elongated minerals, such as chloritoid laths in the chloritoid schist which form a discrete lineation (Figure 6.1.b); alignment of recrystalized quartz grains; and sparse micas in quartzite units (Figure 6.1.h). The measured deformation lineations are combined and presented in the stereonet in Figure 6.1.1. and have a mean trend and plunge of 174.5/35.5^{o}.

6.2. Fractures and Veins

The fault damage zone contains abundant sets of fractures in more competent units, such as metasandstone lenses and outcrops of highly silicified schist. These can be grouped into three categories: conjugate joints, barren fractures (tension gashes and shear fractures) and shear fractures.

Joints are common in dehydrated metasandstone outcrops in Hill510 and have no obvious displacement along fracture planes. These form conjugate fracture sets and are grouped into 3 clear sets (Figure 6.2.a). Orientation measurements from 2 samples of conjugate joint sets from Hill510 (see map in Figure 5.2 for location of outcrops a and b) are presented in Figure 6.2 (A1 to A4) and, except for similar steep SW-NE, conjugate sets from two separate outcrops differ considerably, and kinematics considerations are ambiguous.

Observable barren fractures are generally a few centimetres long and have less than 2 cm opening thickness (Figure 6.2.b and c); and fluid filled factures (veins) widely range both in thickness and length, from a few millimetres to several of centimetres thick, and centimetre to over a metre long. The vein network is not ubiquitous but a high-density vein system (Figure 6.3.a) in the hanging wall schist is fairly widespread and common to the three selected study localities, Cross, Boesmanskloof and Hill510. The veins are quartz filled and mainly concentrated within the hanging wall but not uncommon in footwall rocks. The veins are either mutually cross-cutting or form an interconnected network and are generally semi planar on the mesoscale.

Shear veins (semi-parallel to foliation) have sharp boundaries and are associated with pressure solution selvages along the shear surface (Figure 6.3.b). These veins often contain deformation structures such as discrete foliation planes, defined by stylolitic surfaces (Figure 6.3.b), whereas similar wall rock alteration is not generally observed adjacent to semi-vertical extension veins. Most veins are deformed, folding perpendicularly to foliation (Figure 6.3.d), forming cataclastic veins (Figure 6.3.e) parallel to foliation, sheared veins (Figure 6.3.c) and rotated vuggy veins (Figure 6.3.g). Boudinage in veins is also common and outlined in the following Chapter (6.4).

Within the same area (and even same outcrops), there are barren fractures and veins with similar geometry and orientation (Figure 6.2.c), suggesting that stress field was not short lived – it remained unaltered through changes in fluid presence, and hydrothermal veins might have developed incrementally. Both veins and barren fractures display some degree of shear and rotation, often having developed a sigmoidal shape, resultant of extension and shear (combination of dilatational-shear fractures).

The crosscutting relationship is not clear in most outcrops, but it is common for veins to be crosscut by barren fractures (tension gashes from shear or dilation fractures) (Figure 6.2.c). In Hill510, apparent mutual cross cutting veins (Figure 6.3.h) are common, but at the Cross, apparent cross-cutting fabrics between differently orientated veins can be observed on some outcrops: vertical veins being cross cut by shallow dipping late veins (Figure 6.3.h).Whereas at the Cross, the vein orientation is mostly similar to the fabrics of the host silicified schist, and barren facture set has a different orientation from elsewhere (approximately 290/15^{o}) (Figure 6.2.f).

The fracture system around thrust fault zone across Boesmanskloof is a combination of flat, steep and oblique veins. Orientation measurements of veins and fracture from the studied localities are presented in stereonets in Figure 6.2 (d-f). These sets have an overall similar distribution: strong set semi parallel to foliation planes (shear veins and fractures), a semi-vertical set roughly perpendicular to lineations and striking E-W (extension veins and fractures), and more scattered dip directions of gently dipping veins and barren fractures.

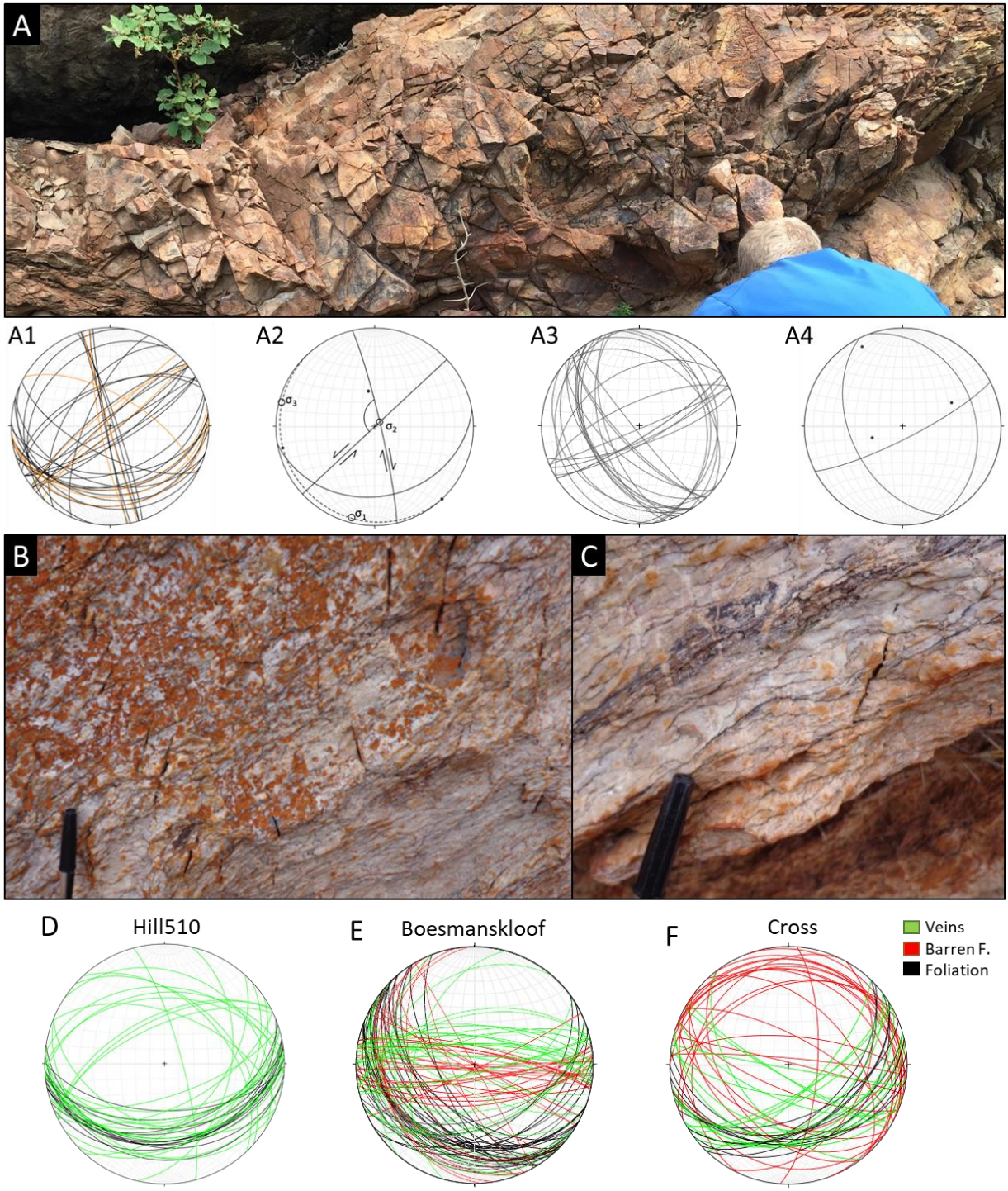

Figure 6.2 Fractures and equal area lower hemisphere stereonets: a) representative conjugate fracture sets in metasandstone lens; A1) fractured metasandstone joints (black, n=30) from damage zone of bottom fault 33 38.392S 19 39.522E and lower tapered metasandstone joints (n=9); A2) mean planes from (A1) 080/30, 227/90, 167/85 and respective poles, suggesting strike-slip fault regime; A3) core fractures in metasandstone body from south-eastern most part of Hill510 (n=28) (33 38.692S 19 39.605E) (green, n=28); and A4) mean planes from A3 340/27, 154/46 and 063/80 and respective poles; b) Barren fractures in outcrop of highly silicified schist from Boesmanskloof; c) Vein network and barren fractures at Cross locality, cataclastic layer being crosscut by vertical veins and stylolites present (note: similar geometry of some veins and barren fractures). Stereoplots of barren fractures and veins in d) Hill510, e) Boesmanskloof and f) Cross.

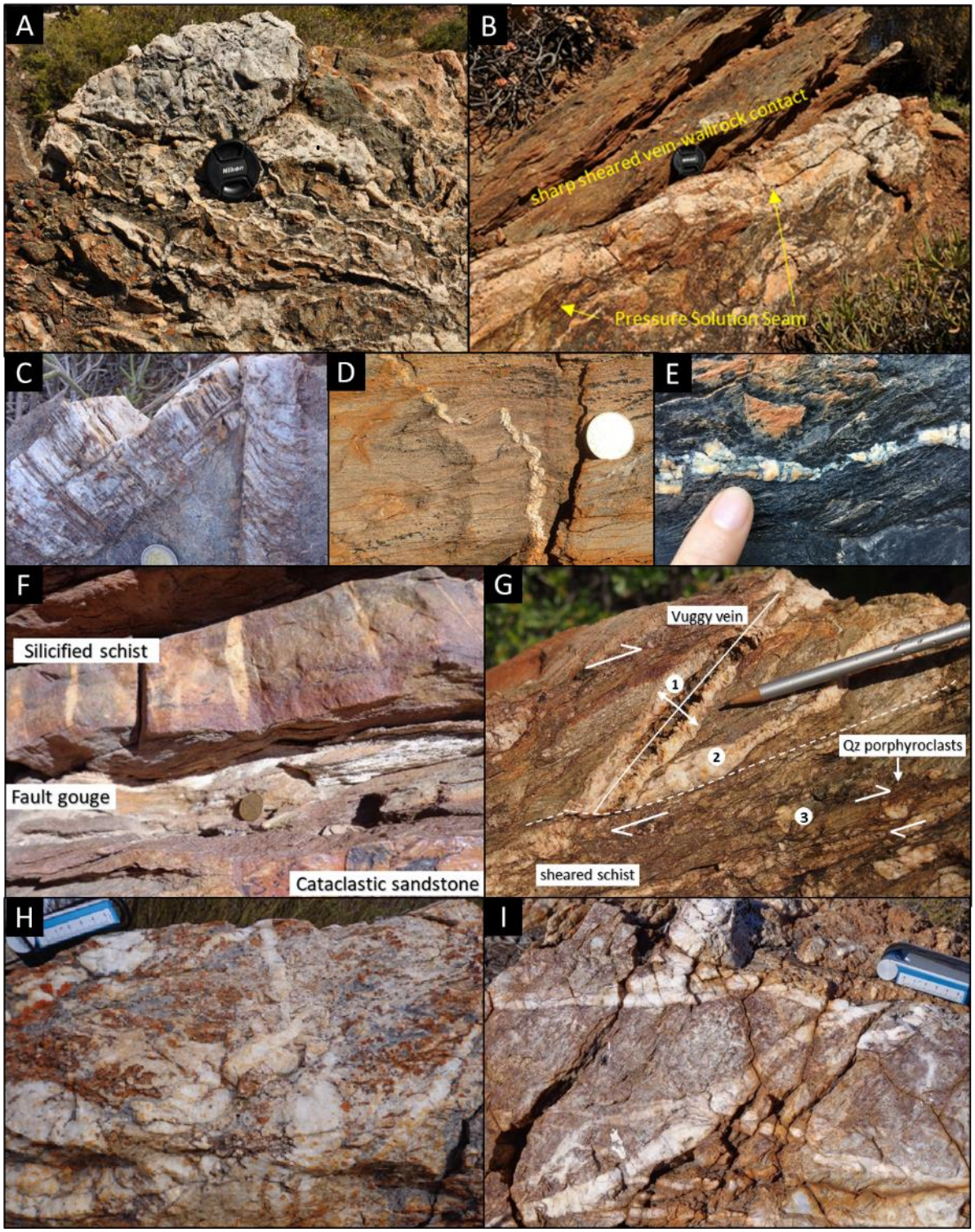

Figure 6.3 Veins: a) zone of intense development of shallow dipping anastomosing extension veins adjacent to fault; b) examples of shallow dipping fractured shear vein; c) quartz vein with crystal growth fibre lineations and crack seal surfaces, syn-tectonic recrystallization which suggests presence of fluid during deformation of rock; d) sheared vertical stylolitic vein – suggesting near horizontal σ1, corresponding to a compressional tectonic regime; e) cataclastic vein; f) subvertical extension veins in hardened silicified schist adjacent to fault gouge; g) rotated vuggy vein in sheared schist (1 fracturing, 2 fluid precipitation followed by 3 further shear deformation); h) outcrop scale vertical veins crosscut by horizontal veins from Cross; i) mutually cross cutting quartz veins in two main planes (same generation, resultant of same stress conditions).

6.3. Shear bands and porphyroclasts

Shear bands are common in partially and moderately silicified schist units, displaying C' Type shear bands and isolated asymmetric objects such as porphyroclasts and sigmoids (Figure 6.4.a). Folded quartz veins (parasitic folds) are not uncommon and are often inclined, as result of shearing (Figure 6.4.a, e).

The LS tectonites (Figure 6.4.e, f), contain both foliation and lineations (in form of elongated clasts on the plane of foliation), common throughout shear zones, easily observable in silicified schist and limestone mylonite, but also common in quartzites. In these units, the presence of rotated porphyroclats is widespread. The size of porphyroclasts is extremely variable, ranging from millimeters to tens of centimeters. The most common porphyroclasts are of quartz composition, most likely from fragmentation of previous veins, but metasandstone and schist clasts are also present in schist breccia sheared units (Figure 6.4.e). Elongated clasts are generally parallel to fault kinetics, suggesting either normal or thrust faulting, and shear sense interpretations based on these are generally ambiguous. Rigid body rotation of fractured quartz veins is also evident in the study area. Whereas rotated quartz fragments remain angular, as in the case of domino boudins, the schist matrix is sheared and foliated around quartz fragments (Figure 6.4.h). Other shear indicators present in LS tectonites are asymmetric boudins.

6.4. Boudinage

Boudins are observed in both large and small scale throughout the study areas and are easily observed in deformed quartz veins (Figure 6.4.e, f). There are two types of asymmetric boudins developed and easily observed in quartz veins: foliation parallel domino boudins (Figure 6.4.e) – few centimetres long angular boudins with millimetre wide interboudin space, typical of brittle regime deformation; and shear band boudins (Figure 6.4.f) – which have a lenticular shape with a large relative interboudin space, associated with ductile regime deformation. The observed domino boudins generally suggest top to the north sense of shear in localized areas.

The main example of large scale boudins is from the north facing section of Hill510, where metasandstone bodies outcrop along the fault plane, in the damage zone of the Middle Fault (MSZ), as a result of shearing of larger sedimentary units within the Malmesbury G roup. Quartz dilatational jogs occur along the fault plane, adjacent to the metasandstone bodies and hydraulic breccias (Figure 6.4.i).

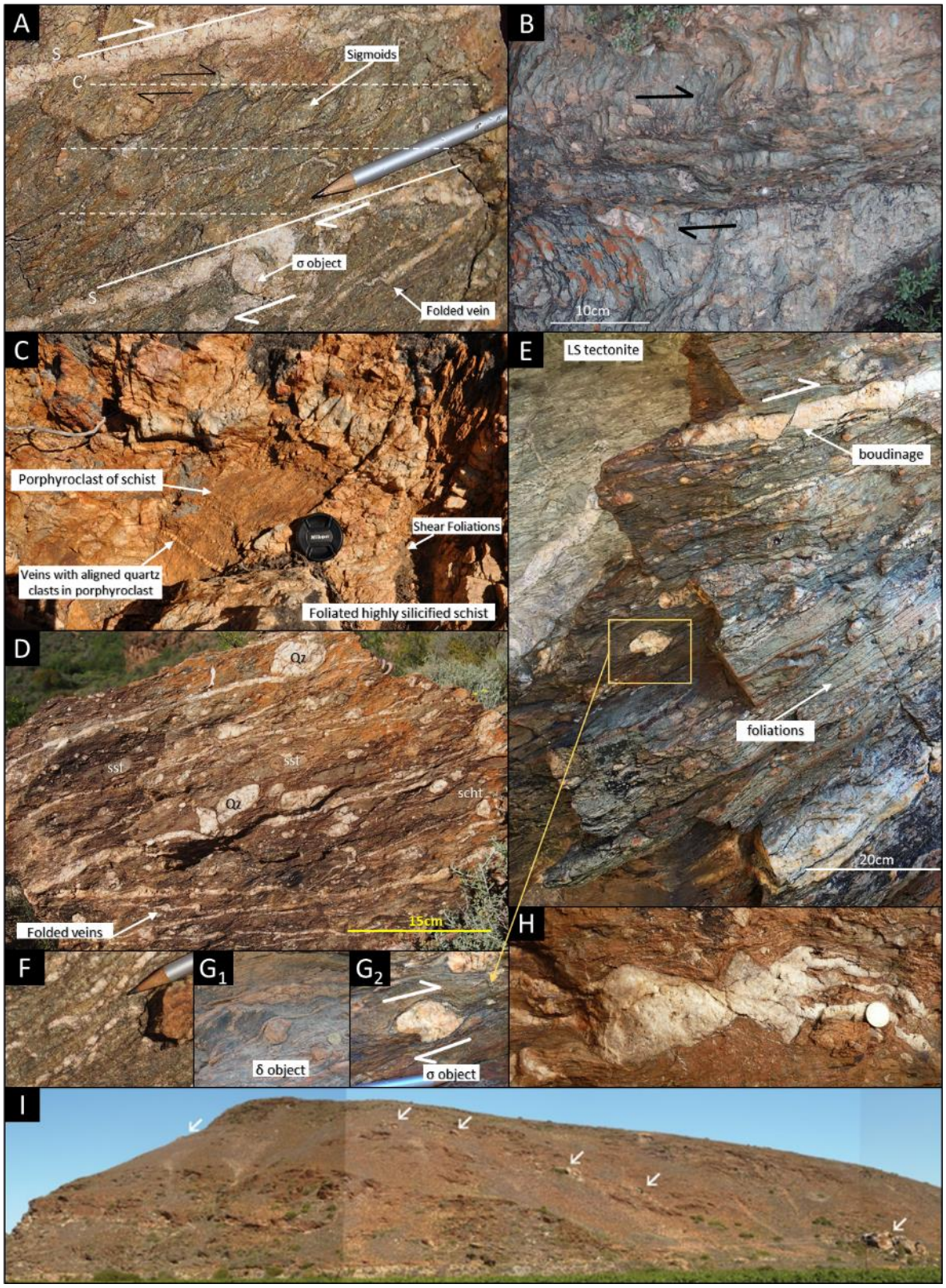

Figure 6.4 Miscellaneous shear zone macrostructures. A) SC' shear band in silicified schist outcrop displaying sigmoids, rotated clasts and parasitic folds, suggesting top to the north dextral shear sense. B) multi banded shear zone in schist crosscut by steep fabrics; c) large porphyroclast of partially silicified wallrock schist in foliated highly silicified schist (shear sense of curvature of shear foliation), ambiguous shear sense; d) sheared porphyroclasts of quartz, metasandstone and schist in veined silicified schist breccia tectonites, ambiguous shear sense; e) LS tectonites containing foliations, elongated clasts, domino boudins and porphyroclasts (note: fracture boudinage in brittle quartz layer in ductile sheared schist) suggesting top to the north dextral sense of shear; f) shear band boudins of vein quartz in silicified schist; g) quartz porphyroclasts in tectonites; h) rigid body rotation of fragmented vein quartz; i) Possible metasandstone boudins on northern face of Hill510, generally accompanied by quartz vein precipitation in dilatational jogs (Refer to Figure 5.2 for cross section).

7. Microstructures and Petrography

This Chapter describes the petrography of the different lithological units and their deformation overprint in a microscopic level, using oriented thin sections, from which deformation features were identified and deformation mechanisms inferred.

Petrographic and microstructural analysis were performed in 30μm thick thin sections cut perpendicular to macroscopic foliation plane and parallel to lineation (when visible). A total of 53 samples was collected in all 3 localities and analysed using a transmitted light microscope. This allowed recognition of mineral assemblages and microstructural properties of samples. Microstructural Analysis observations and interpretations in this Chapter are mostly based on Passchier and Trouw (2005).

All microphotographs presented in this Chapter are of 2.5x magnification (4.5mm field of view), unless otherwise specified. All samples collected lie within the fault damage zone and are classified based on Table 3.1.

Table 7.1 Classification table for rock samples collected in each locality in the study area.

Locality	**Samples**	**Fault-Rock Fabrics**	
		Microscale	**Macroscale**
Hill510	N50	schist mylonite	
	N08, N10	silicified schist	
	N37, N39	foliated fault gouge	
	N12	ultramylonitic cataclasite	ultracataclasite
	N14, N19	protomylonites	mylonitic metasandstone lens
	N20	foliated crush microbreccia	quartzite breccia
	N21	crush microbreccia	quartzite breccia
	N23	crush breccia	sheared adjacent to N12
	N16	limestone mylonite	
Boesmanskloof	N28, N02 (vein)	limestone mylonite	
	N27, N03	quartzite microbreccia	quartzite breccia
	N04	microbreccia	quartz cemented breccia
Cross	N34	hydraulic microbreccia	quartzite breccia
	N35	non-foliated crush microbreccia	cataclastic metasandstone
	N36	foliated crush microbreccia	sheared metasandstone
Representative fault host samples	N50	schist	
	N11	metasandstone	
	N28, N16	Limestone marble	
	N01, N02, N09, N35	veins	

7.1. Petrography of main (fault-host) lithological units

7.1.1. Schist

Relatively unaltered schist samples from 2 locations were collected to document the petrography of 'unaltered' schist in the surrounding area. These samples were collected from Boesmanskloof and from surroundings of Hill510, several metres (approx. 30m) below the angular unconformity between Malmesbury Group and the Table Mountain. Two mineral assemblages are identified in schist samples, defined by the presence or absence of chloritoid: muscovite chlorite schist and chloritoid schist (Samples Nuy2 and N50, Figure 7.1a and b).

The samples of schists collected from footwall are predominantly composed of quartz, fine-grained white mica, chlorite and trace amount of ilmenite and graphite (opaque minerals).

The **chlorite-muscovite schist** is composed of 50% micas (muscovite), 15% chlorite, 20% quartz and 5% feldspar (albite). Micaceous minerals form part of the very finely grained matrix, sized ~0.1mm or less, and the average quartz and feldspar grain size is ~0.2mm. The foliation in the schist samples are defined by alignment of micas and occasional mylonitic layering of quartz aggregates.

The **chloritoid schist** is composed of ~15% chloritoid, 20% quartz, 50% micas (muscovite), ~10% chlorite, and ~5% of graphite. The presence (modal proportion and crystal size) of chloritoid is variable in outcrop and in thin section scale. Chloritoid occurs as subhedral, lathic and semi-randomly oriented poikiloblastic crystals overprinting the foliation. The laths are ~ 0.3 - 1 mm long and commonly form clusters of opaque inclusions of graphite. Fibrous growth of quartz and micas is common in pressure shadows of chloritoid laths.

In both schists, chlorite occurs within the very fine-grained micaceous matrix. In the chloritoid schist, the foliations are similar to the chlorite-muscovite schist, but a sparse lineation formed by semi random alignment of chloritoid laths is present.

The schist generally contains a strong foliation with micas (chlorite, muscovite) defining the schistosity and small anhedral grains of quartz and feldspar (individual or multiple recrystallized grains) being rigidly rotated within the foliation. Secondary foliations (mylonitic fabrics and crenulations) are also common in this unit.

7.1.2. Quartzitic Metasandstone

These samples are of quartzofeldspathic composition, containing quartz (~80%), white micas (~5-15%), feldspar (albite ~10-5%) and trace of oxides (magnetite or ilmenite). Overall there is no preferred orientation of grains in the metasandstone, except for partial apparent planes caused by stylolitic cleavage surfaces.

The size of the quartz clasts in the relatively undeformed metasandstone is irregular, with clast size ranging between 0.2-4 mm and mostly well rounded (Sample N11, Figure 7.1c). The larger grains contain subgrain boundaries, transecting bands of new grains, bulging grain boundaries (grain boundary migration) and previously recrystallized grains. Thin bands of opaque minerals are present in the matrix suggesting dissolution-precipitation deformation during compaction.

7.1.3. Limestone Marble

Limestone marble samples are predominantly composed of calcite, aragonite and detrital quartz clasts (<15%). They have a mylonitic fabric overall, with some randomly orientated, fragmented and rotated clasts of variable sizes. The quartz clasts in the limestone mylonite samples display undulose extinction and serrated boundaries (Figure 7.1d and e), suggesting deformation accommodated by frictional mechanisms. These clasts are fractured (micro faults) and fragments display rigid-body rotation (cataclastic flow) in a ductile matrix (Samples N16 and N28, Figure 7.1e and Figure 7.6.b). Under microscopical analysis, calcite veins within limestone mylonite samples can be observed (Figure 7.6.a).

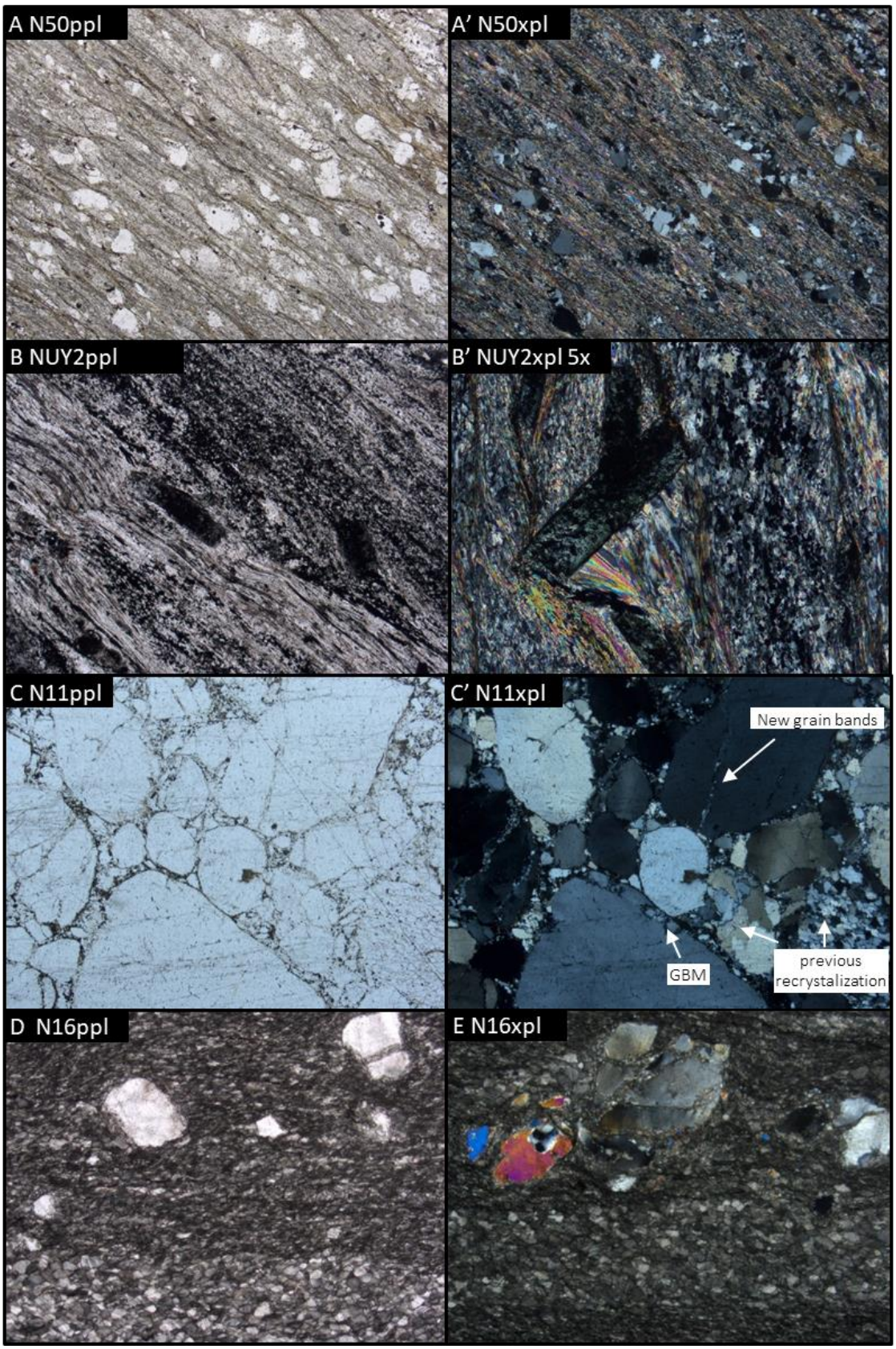

Figure 7.1 Microphotographs of representative main lithological units (lenght=4.5mm): a)N50 Chlorite-muscovite schist; b) NUY2 Chloritoid schist, sparsely oriented chloritoid laths in quartz and micas matrix and b') fibre growth of mica and quartz in chloritoid lath strain shadow (5x magnification lens); c) N11 quartzitic metasandstone; d and e) N16 limestone marble.

7.1.4. Veins

As in macroscale, the size and orientation of veins vary greatly in microscopic scale as well. Veins often have well preserved anhedral elongate-blocky quartz crystals, at high angle to the vein-wallrock margin (Sample N09, Figure 7.2.b). The vein wall rock contacts are generally sharp (Samples N01 and N09, Figure 7.2.a and b) but irregular margins are not uncommon, displaying opaque fluid precipitation (Samples N09 and N35; Figure 7.2.b and c).

N01 is a sample from a massive vein with apparent ductile fabric in mascroscale. Under the microscope, this sample is composed of irregular and truncated quartz clasts containing abundant stylolitic cleavages, crosscut by micro-veins of quartz (Figure 7.2.a).

Although less abundant, quartz veins are also present in limestone mylonite units (Sample N02, Figure 7.2.d), forming porphyroclasts (σ) of quartz with undulose extinction and irregular boundaries within a very fine grained recrystallized matrix.

Interpretation of Vein Formation:

The porphyroclasts of vein fragments in the limestone samples suggest grain boundary migration and subgrain formation, indicating continuous shearing of the vein subsequent to crystallization.

Sharp vein contacts suggest vein formation by brittle fracture formation succeeded by fluid infiltration and mineral precipitation. And portions of irregular contacts (Samples N09 and N35, Figure 7.2.b and c) suggest that the veins were affected by later deformation of rocks by diffusive mass transfer. Different degree of deformation of quartz veins within same sample, could suggest multiple events of vein formation and deformation of veins through diffusion creep and dissolution creep (intracrystalline plasticity).

Deformation of veins dependant of their orientation relatively to plane of foliation (and shear direction) and size of vein (thickness). Veins formed at high angle to foliation are folded, with axis parallel to foliation planes; and veins semi parallel to foliation experience extensional deformation, forming boudins and rotated clasts (Sample 10, Figure 7.3.a).

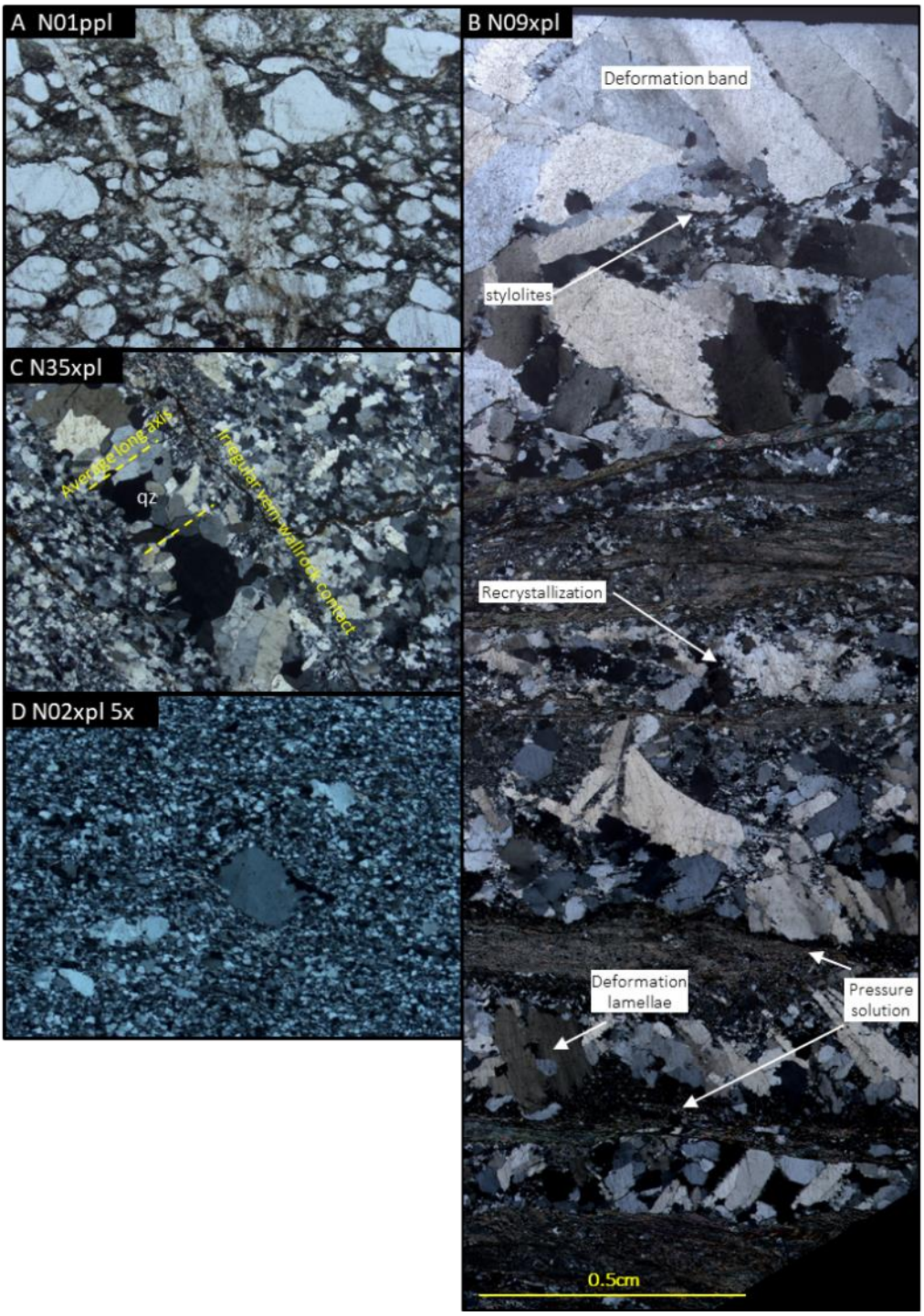

Figure 7.2 a) N01 microvein in sample from massive quartz vein is schist from Boesmankloof containing irregular sized truncated quartz grains and stylolitic cleavages (result of dissolution creep and diffusion creep); b) N09 multiple vein semi parallel to foliation planes in schist, blocky elongated grains oblique vein boundary. Grains containing deformation band (top right), deformation lamellae; and stylolitic cleavages (pressure solution) are common; c) N35 opaque fluid filled fractures and quartz veins (high angle) overprinting cataclastic quartzite. Quartz vein recrystallized and annealing from Cross 33°37.559S 19°32.410E; d) N02 mylonitic vein quartz in limestone. Very fine grained. Sheared porphyroclast of quartz with undulose extinction in fine grained recrystallized matrix (5x magnification lens)

7.2. Microstructures by locality

This Chapter presents the microstructural observations from samples analysed from each locality in the study area.

7.2.1. Hill510

Hill510 has the most variety of both deformation zone rocks and fault rock types: metasandstone, schist (silicified and highly silicified), limestone mylonite (marble), cataclasites, gouges and breccias.

Limestone mylonites contain fractured and rotated quartz grains (<1.5mm) in ductile foliated calcite matrix (Figure 7.1e). The quartz fragments contain fluid sealed microfractures (cataclasis and diffusive mass transfer), undulose extinction (intracrystalline plasticity) and are semi rotated (intergranular flow) (Figure 7.1 d and e).

Silicified schist samples in this locality have mylonitic fabrics, cataclastic fabrics or both.

The mylonitic fabric in schist samples are formed by a continuous alignment of micas (matrix) and aligned lenses of quartzofeldspathic aggregates <0.3mm wide (Figure 7.1.a). Subhedral porphyroclasts of quartz (<0.03mm diameter) with pressure shadows and undulose extinction are wrapped around by the aligned mica in the matrix. Crenulations (CS) in mica rich layers are common, whereas quartz is generally microfractured and recrystallized within quartz veins or larger quartzitic clasts (Samples N50 and N10, Figure 7.1.a, Figure 7.3.a).

Highly silicified schist samples (Sample N08, Figure 7.3.b) are saturated with quartz microveins and fragmented quartz porphyroclasts. Large well-rounded clasts of wallrock schist which are apparently more competent, can be observed within these samples. The matrix contains a high percentage of fine grained newly crystallized quartz grains with little undulose extinction. Stylolites and fluid healed microfractures are abundant in these samples.

The analysed **cohesive gouge** samples from main high strain zone 1 in profile 1 (Chapter 5.3.0) consist of frictionally reduced very fine grains and have a high percentage of quartz. This samples display multiple semi parallel slip surfaces and chloritoid laths (~2mm) usually concentrated along fluid healed slip surfaces (Samples N39 and N37, Figure 7.3c and d).

Deformed quartzitic metasandstone samples present in Hill510 vary from protomylonite to protocataclasites, microbreccias and crush breccias.

Sample from top **cataclasite to ultracataclasite** horizon from high strain zone in profile 2 (Chapter 5.3) has very reduced grain size (<0.05mm), predominantly composed of quartz and trace amounts of micaceous minerals. This sample is microscopically partly mylonitized and contains foliations defined by ~0.05mm thick layers of fine-grained material and a pronounced linear fabric defined by elongate newly recrystalized quartz grains and micas (Sample N12, Figure 7.3e and f), creating a ultramylonitc fabric. Quartz rich mylonitic layers are formed by elongated aggregates of quartz containing abundant subgrains, recognized by discrete, sharp and low relief boundaries (Passchier and Trouw, 2005).

Brecciated samples are generally composed of angular to subangular quartz clasts with wide range of sizes (0.05 – 0.5mm) and low to moderate undulose extinction, forming **crush microbreccias** (Samples N20, N21, Figure 7.4.a, b). Fractured angular quartz grains with sharp truncated boundaries and stylolitic cleavage surfaces are abundantly present (Figure 7.4.a, b). SC fabrics are present on grain scale, defined by flattening of elongated quartz grains and abundant intergranular pressure solution surfaces (dark seams in sample N20 Figure 7.4.a), forming both S- and C-surfaces, classified as **a foliated crush microbreccia**.

In contrast, a **non-foliated crush breccia** sample adjacent to cataclasite horizon in profile 2 consists of rounded quartz grains, and pressure solution is only present in grain interspaces within bulging subgrain boundaries in quartz grains, within microfractures and planes of undulose extinction subgrain boundaries (Sample N23, Figure 7.4.c). The grains display weak undulose extinction and subgrain formation is concentrated around grain boundary contacts, associated with bulging recrystallization (regime 1).

Protomylonites are also present in Hill510 and contain both fractured quartz clasts with varying degrees of recrystallization and anastomosing shear slip surfaces (SC fabric). Shear slip surfaces are rich in micas and opaque minerals and enhanced by intergranular flow of mica around quartz porphyroclasts. Microstructures such as deformation bands, annealing within fractures, and subgrains are common in both samples of sheared metasandstone lenses, N19 and N14 (Figure 7.4.d and e). N19 contains equant porphyroclasts with deformation bands and strong undulatory extinction, anastomosing zones of extremely fine recrystallized grains along grain boundaries, with lenticular clasts forming a disjunctive foliation, and zones of recrystallized grains defining extensional shear bands (Figure 7.4.d)(characteristics typical of regime 1 formed by subgrain boundary bulging). Whereas N14 displays sigmoids composed entirely of recrystallized quartz subgrains (augen), with serrated boundaries (Figure 7.4.e), anastomosing shear bands rich in micaceous minerals, and newly recrystallized grains which are larger in comparison to those in sample N19 (Figure 7.4.d) (thus containing microstructures associated to regime 2 to 3, formed by a combination of subgrain boundary rotation and migration).

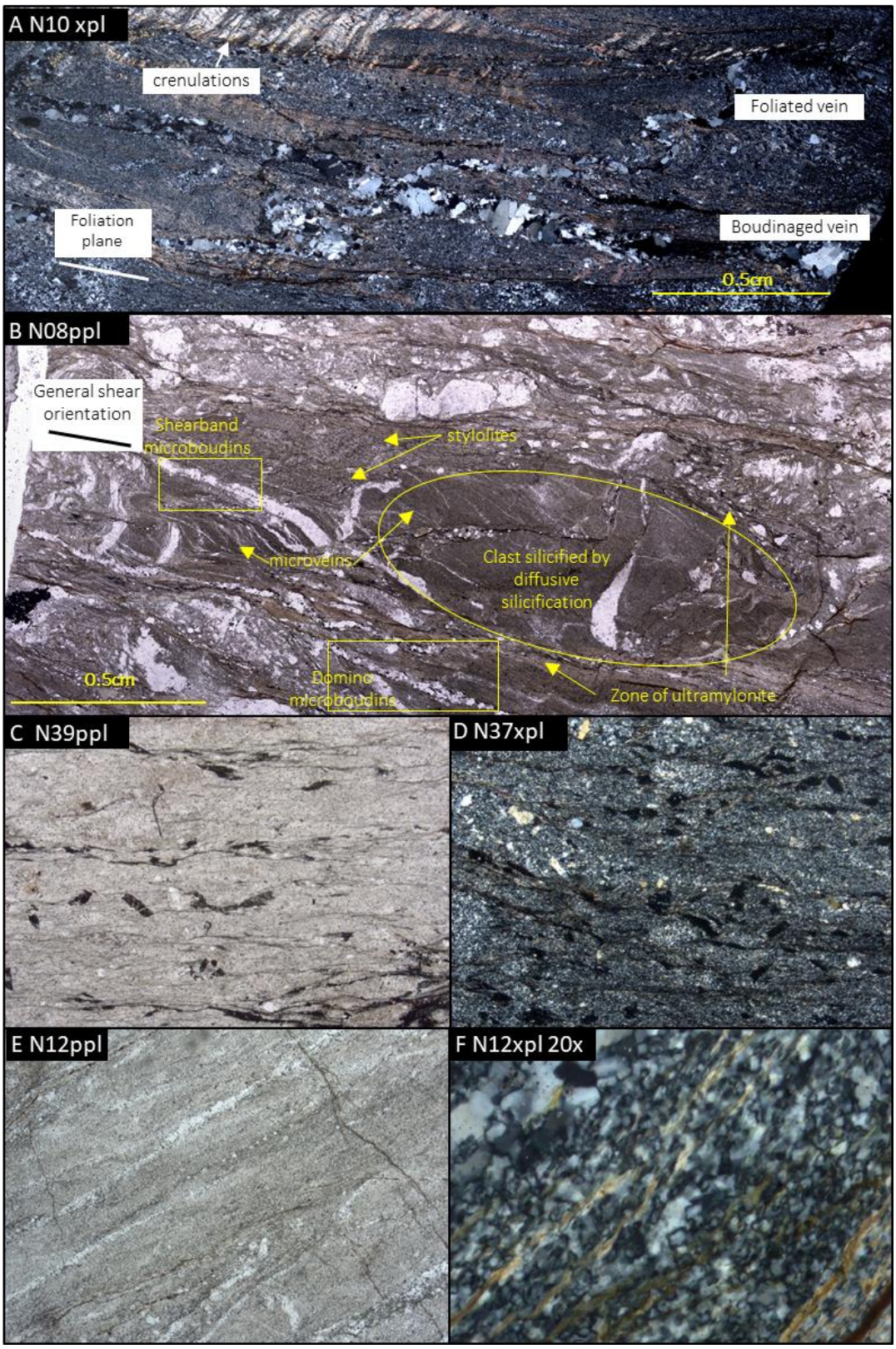

Figure 7.3 Microphotographs from samples from Hill510: a) N10 foliated moderately silicified schist with mica crenulations and recrystallized quartz matrix, crosscut by differently orientated quartz veins; b) N08 highly silicified schist with abundant quartz microveins, fractured and rotated quartz clasts and vein fragments, abundant stylolites and microfractures; c) N39 and d)N37 are cohesive gouge samples with chloritoid laths; e) N12 ultramylonitic sample of cataclasite horizon; f) N12 recrystallized very fine grained quartz grains and aligned mica forming ultramylonite layers (field view = 0.56mm).

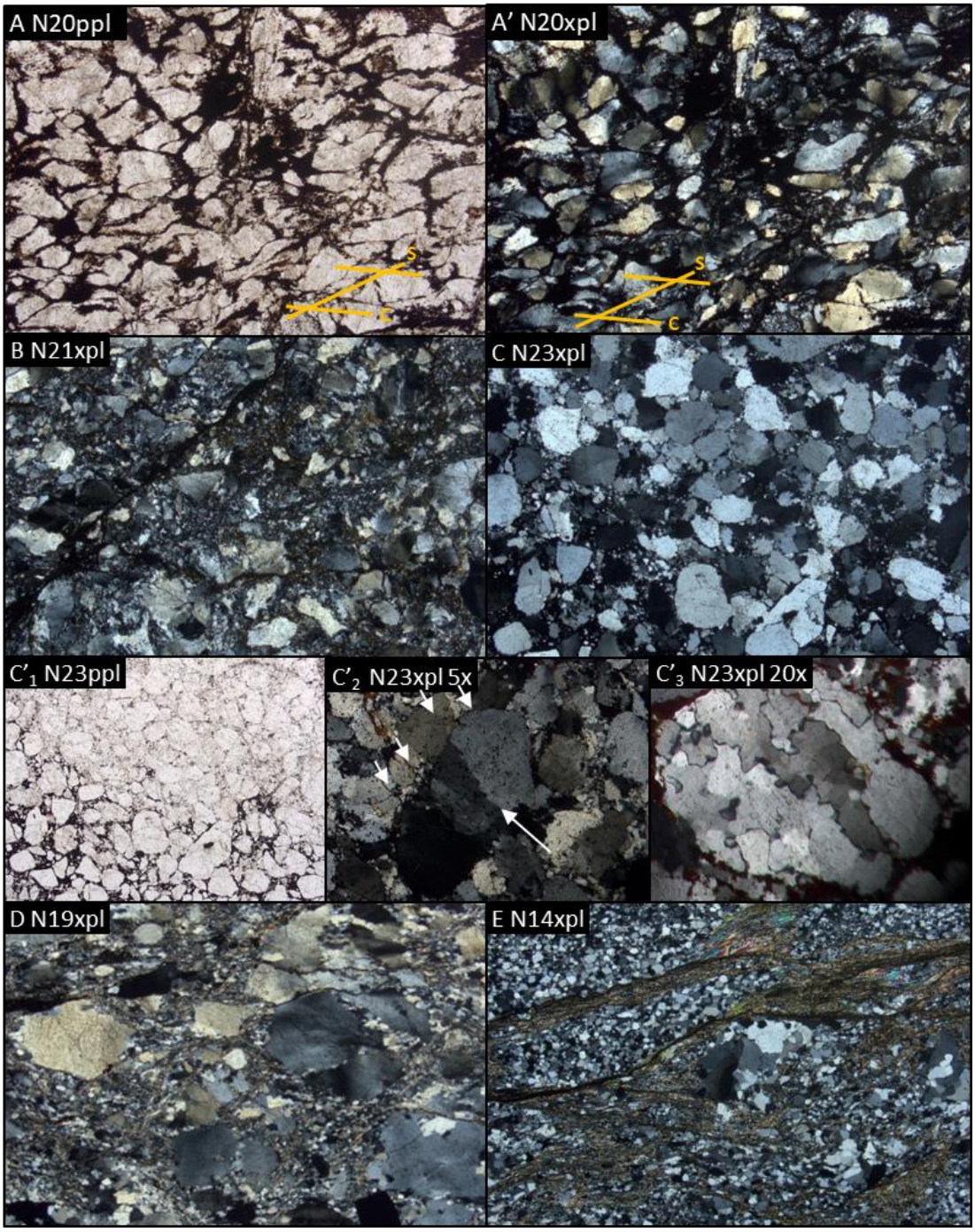

Figure 7.4 Microphotos from samples from hill510 (cont.): a) N20 crush microbreccia ; b) N21 crush microbreccia with angular quartz grains and stylolites; c) N23 metasandstone with subangular to round low undulose extinction grains; c'$_1$) ppl microphotograph showing intergranular fluid solution (bottom right); c'$_2$) microfractures (arrows) within planes of undulose extinction subgrain boundaries (field of view=2.25mm); c'$_3$) pressure solution stylolites formed within bulging subgrain boundaries of quartz grain (field of view=0.56mm); d) N19 protomylonite sample displaying equant porphyroclasts, deformation bands and strong undulatory extinction, anastomosing zones of bulging recrystallization and lenticular clasts forming a disjunctive foliation; e) N14 protomylonite displaying optically visible subgrains surrounding recrystallized porphyroclasts and SC fabric, forming sigmoids.

7.2.2. Cross

The Cross locality has a relatively homogenous lithology consisting predominantly of quartzite. Three representative **quartzitic samples** from this area display different deformation fabrics:

Non-foliated microbreccia, Sample N35, is composed of fine-grained bimodal recrystallized grains (0.1-0.3mm) that although recrystallized (containing bulging and irregular boundaries), does not contain a mylonitic fabric (Figure 7.5.a). The bimodal grain size and the elongated blocky shape of the grains suggest these grains are disaggregated from a recrystallized quartz vein. **Foliated microbreccia**, sample N36 is composed of mostly very fine-grained recrystallized quartz grains (~0.15mm) and partially elongated creating a faint foliation (Figure 7.5.b). Stylolitic solution seams are common in both these samples.

Hydraulic microbreccia, sample N34 (Figure 7.5.c), is composed of irregular angular fragments of strongly recrystalised quartzite clasts (0.2 -2 mm), with sharp and straight boundaries and fluid healed fractures (micro-brecciated). Grain fragments in this sample have little evidence for rotation and frictional sliding.

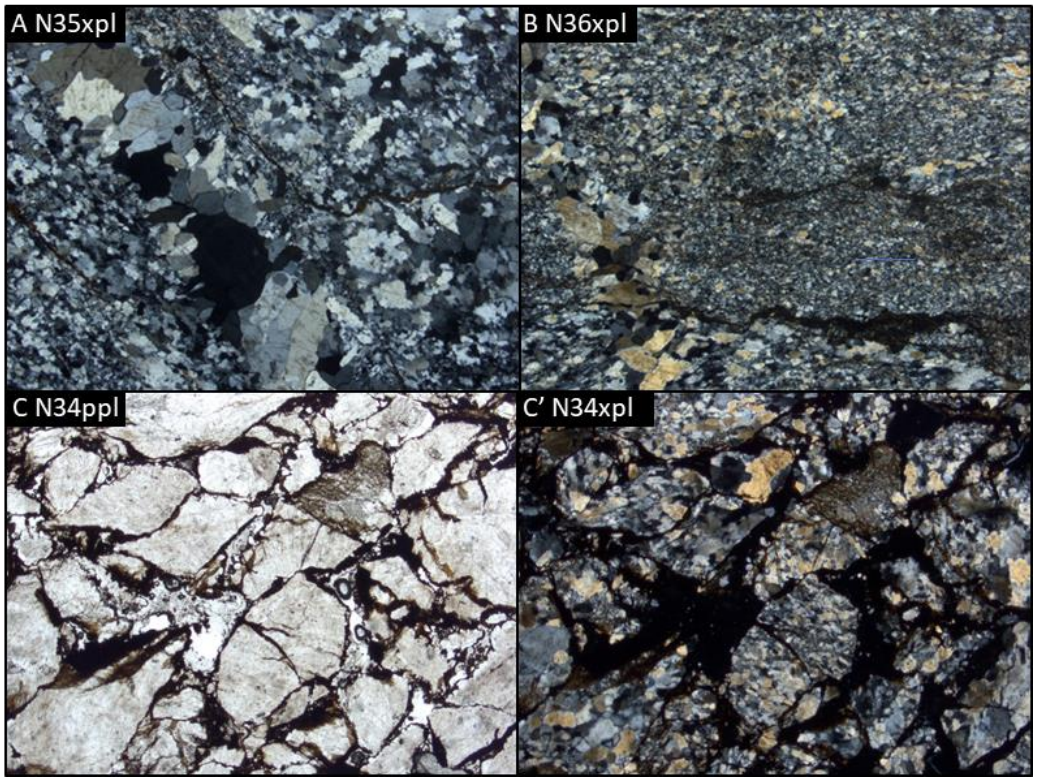

Figure 7.5 Microphotographs from quartzite samples from Cross locality: a) N35 non-foliated microbreccia; b) N36 semi foliated fine grained microbreccia, c) N34 hydraulic microbreccia.

7.2.3. Boesmanskloof

This area's lithology mainly consists of schist and minor limestone mylonite horizon and quartzites. Silicified schist and limestone mylonite samples from this area are macroscopically similar to samples from Hill510. Schist was not sampled at this locality and it is assumed to have undergone same deformation microscopically as samples from Hill510 (see Chapter 7.2.1).

Some **limestone mylonite** samples (N28) from this locality contain a higher amount of quartz grains in matrix than those of Hill510 (N16). The quartz grains (0.1-0.2mm) are fairly unimodal, not elongated and regularly distributed throughout matrix (Figure 7.6 a). The foliation in this sample is disrupted and semi-discontinuous calcite veins with irregular and discontinuous margins are present (suggesting vein formation by dissolution-precipitation). Larger quartz porphyroclasts are frequently transected by microfaults at a high angle to the foliation suggesting rigid-rotation (Figure 7.6 b) and contain with calcite pressure shadows (Figure 7.6 a and b).

Quartzite microbreccias under the microscope are either massive and composed of very finely grained quartz, without a clear alignment nor clear boundaries (Sample N27, Figure 7.6 c); or contain quartz porphyroclasts (~1mm clasts and vein fragments) in recrystallized quartz matrix with anastomosing thin fluid seams (Sample N03, Figure 7.6 d)(typical of regime 2 deformation).

Quartz cemented microbreccias (Sample N04) are present in this locality and consist of poorly sorted truncated subangular to rounded quartz grains. Grain size ranges between 0.1 - 0.5mm and have negligible undulose extinction, sharp boundaries and microfaults within grains. Stylolitic surfaces in samples are also abundant (Figure 7.6 e).

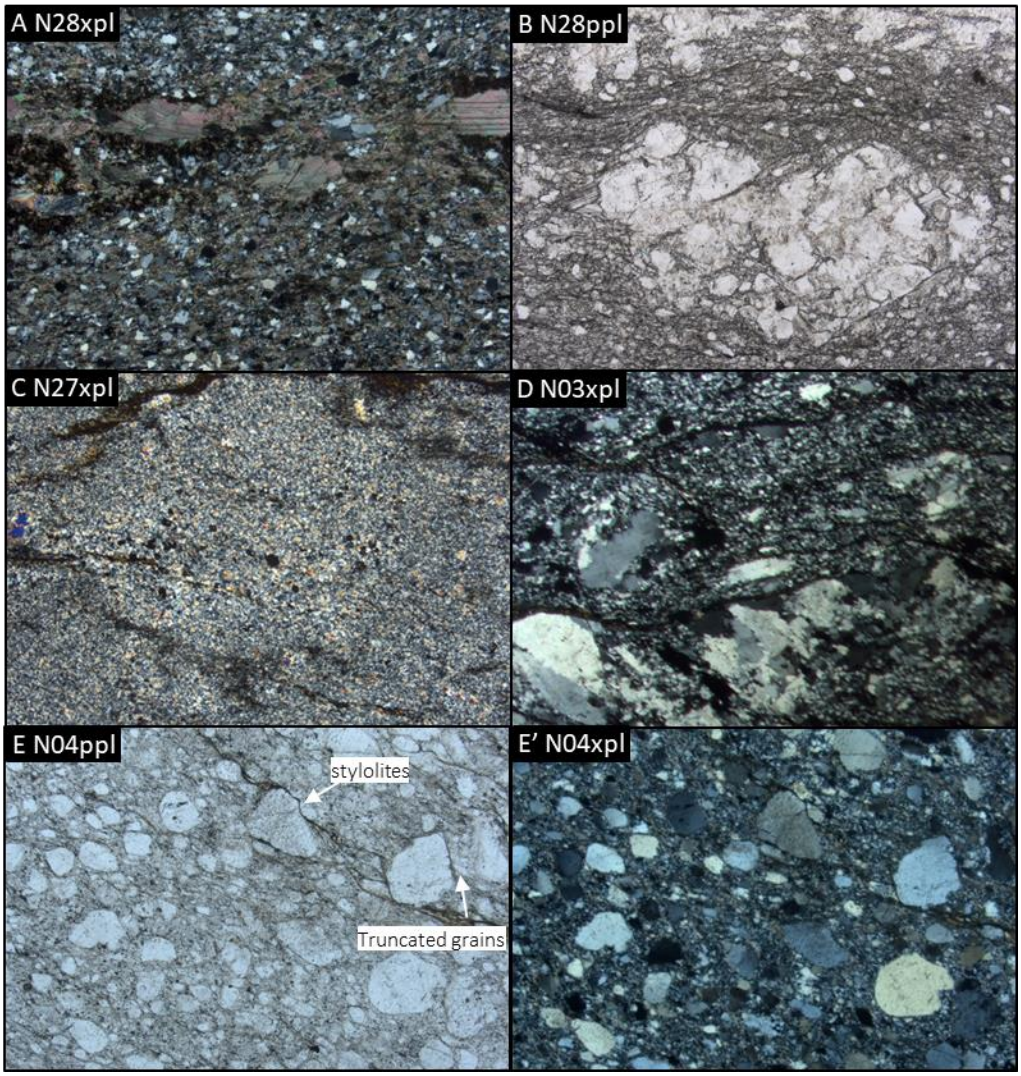

Figure 7.6 Microphotographs from samples from Boesmanskloof a) N28 limestone mylonite with calcite veins and abundant quartz fragments; b) fractured quartz clasts rigidly rotated in limestone mylonite; c) N27 microbreccia with very finely reduced quartz grains (by cataclasis) from cataclastic quartzite; d) N03 microbreccia with quartz clasts and veins recrystallizing (subgrain boundaries and undulose extinction), contain thin irregular anastomosing fluid healed slip surfaces; e) N04 quartz cemented cataclasite with abundant truncated grains (no undulose extinction) and stylolitic surfaces.

7.2.4. Summary of Microstructures

Samples from Hill510, Boesmanskloof and Cross locality contain similar textures with multiple features preserved in same samples. Truncated grains, stylolitic surfaces and fluid filled seems are almost ubiquitous in all samples of competent and incompetent rock types, suggesting deformation by dissolution precipitation which indicates presence of fluid in samples.

Metasandstone samples contain most of the observed cataclastic fabrics in the study area, however ductile fabrics are also present in these units. Cataclasis is evidenced by fractured quartz grains displaying little to no undulose extinction and transected by microfractures containing observable displacement parallel to microfractures boundaries (rigid body rotation); hydraulic cataclastic samples contain clear fragments with sharp boundaries and fluid healed fractures, suggesting cataclasis and dissolution precipitation were the dominant deformation mechanisms. Microstructures resultant from viscous mechanisms are not uncommon in this lithology however (e.g. Samples N14, N19, N03, etc). Quartz grains and aggregates display strong subgrain recrystallization and anastomosing shear cleavages are present. These display fabrics typical of regime 1, 2 and 3, thus deformed by dislocation creep mechanisms associated with different relative temperatures or strain rates (Chapter 2.1.1.3).

The limestone and schist samples mostly display mylonitic textures, and cataclastic fabrics are mostly related to the quartz porphyroclasts. These incompetent units' matrix usually displays a continuous fabric and more closely-spaced foliations. An increase in the quartz ratio in these units is associated to a more disruptive foliation, as quartz clasts and vein fragments in this samples are generally fractured and rigidly rotated with poor subgrain recrystallization.

8. Geochemistry and Fluid-Rock Interactions

X-ray fluorescence (XRF) and Oxygen Isotope analysis were conducted on samples across fault zones in study area in an attempt of determining the origin of fluid and to quantify the PT conditions experienced by the wall rock during deformation.

8.1. Analytical Methods

A vertical profile across a section of the fault core and damage zone was taken. Samples were collected and their location relatively to the fault core were registered.

Oxygen isotope analysis was undertaken in order to study changes in composition throughout said fault zone and determine fluid origin.

Clean quartz vein material was handpicked from coarsely crushed vein samples from the three study localities. The quartz crystals were then powdered and used to calculate oxygen isotope ratios. This procedure was performed in the stable isotope laboratory in the Department of Geological Sciences of the University of Cape Town. The methodology outlined in Fagereng and Harris (2014) was followed. The detailed analytical methodology and facilities at the University of Cape Town can be found in Harris and Ashwal (2002), and details on the laser fluorination technique in Harris and Vogeli (2010).

Samples were dried for over 24h at 50°C and processing followed methodology outlined in Fagereng and Harris (2014), where for whole-rock powders, approximately 10 mg samples were loaded into nickel reaction tubes and degassed for 2 h under vacuum at 200 °C. The samples were then reacted with ClF_3 for at least 3 h at 550 °C to facilitate release of oxygen, which was converted to CO gas by reaction with a hot carbon rod and collected in glass “break seal” tubes. The isotope ratio in the extracted gas was measured with a Finnegan Mat DeltaXP mass spectrometer in the Department of Archaeology at the University of Cape Town. Two quartz standards (an internal standard MQ) were analysed with every 8 unknowns, and the standard data were used to normalise the raw data to the SMOW (Standard Mean Ocean Water) scale. The data collected is reported in standard d-notation, relative to SMOW (Table 8.2).

X-Ray Fluorescence (XRF) analysis was used to determine the major elemental composition of the fault rock minerals (bulk rock composition) in powdered samples, which is necessary for determining the physical conditions under which faulting occurred and to calculate the water content and fluid production history. The data used to construct Isocon Diagram and the mineral equilibria model. The methodology followed is outlined in Diener et al (2017):

Mineral compositions were determined using a JEOL JXA-8100 **electron microprobe** housed at the University of Cape Town. Analyses were carried out using a 15 kV acceleration voltage, 20 nA probe current and 2–3 µm spot size. Counting times were 5s for both backgrounds and 10s for peaks on all elements. Data was processed with ZAF matrix corrections and quantified using natural mineral standards. The representative compositions of minerals in the schists are presented in Table 12.1 in Appendix 12.

Major oxides (values reported as wt.% except for H_2O^- and LOI) were measured on fused disks prepared from ignited powders. The samples weight lost upon heating the sample powder at 110°C overnight is represented by H_2O^-. "loss on ignition" (LOI), represents the weight change (positive if weight lost) upon

heating the sample to 800°C for 4 hours. Samples can gain weight during ignition if they have little water and abundant ferrous iron (which oxidizes to ferric iron oxide, Fe_2O_3), thus uptaking oxygen. Sulphur reported as wt% SO_3 is measured on fused disks. If otherwise unstated, the lower limit of detection for major oxides is 0.01 wt.%.

The **Mineral equilibria modelling** (MnNCKFMASHTO) was used to determine the pressure and temperature conditions under which faulting occurred, and to identify possible mineral breakdown reactions that might have led to periods of elevated fluid pressure in the faults.

The metamorphic conditions experienced by the Malmesbury schist during faulting was quantified through calculated pseudosections. These diagrams show all the stable multivariant phase assemblages in a chosen chemical system for a specific rock composition and can be used to constrain metamorphic conditions and P–T paths. Pseudosections were calculated in the model system MnO–Na2O–CaO–K2O–FeO–MgO–Al2O3–SiO2–H2O–TiO2–Fe2O3 (MnNCKFMASHTO) using THERMOCALC 3.45 (Powell and Holland, 1988 updated September 2015) with an updated version of the internally consistent dataset of (Holland and Powell, 2011 dataset file tc-ds63.txt, created 05/01/2015). The activity–composition models used in the calculations are those of White et al. (2014). The aluminosilicates, quartz and aqueous fluid (H2O) are pure end-member phases. Bulk rock compositions were determined by X-ray fluorescence analysis using a Philips X'Unique II wavelength-dispersive spectrometer housed at the University of Cape Town. These analyses were converted to the MnNCKFMASHTO model system by disregarding the small amount of Cr2O3 present (~ 0:01 wt.%) and accounting for P2O5 by assuming that it occurs in apatite and subtracting a stoichiometric amount of Ca from total CaO. The amount of O added to the bulk composition was chosen to allow ~10 % of total Fe to be Fe3+. The bulk compositions used to construct the pseudosections are presented in Table 12.1, and the calculated diagrams are presented in Figure 8.1.

8.2. Mineral Equilibria Modelling

Three samples of pelitic schists were used for the mineral equilibria modelling in order to investigate its metamorphic pressure and temperature conditions, and the conditions of likely fluid production which could lead to periods of high fluid pressure.

Sample NUY2 and sample NUY3 have the same mineral chemistry and contain chloritoid, chlorite, muscovite and quartz as major phases in the mineral assemblage. Sample NUY50 is of similar composition to other two samples but does not contain chloritoid. The analysed samples are characterized by a low-grade assemblage and therefore the models have been calculated over a temperature and pressure interval spanning from 150 to 500°C and 1 kbar to 10 kbar.

Both diagrams are overall dominated by muscovite (mu), chlorite (chl) and ilmenite (ilm), in excess in all variance fields.

At the lower temperature end, over the entire investigated pressure interval, the assemblage is dominated by kaolinite. At intermediate temperatures and pressures above 5 kbar, lies the stability field of chloitoid (ctd). At higher pressures and low temperature conditions, biotite comes in and at the highest PT conditions, above 430°C, garnet (g) and epidote (ep) become stable.

The inferred equilibrium assemblage for sample NUY2 and NUY3 is muscovite (mu), chlorite (chl), ilmenite (ilm), sphene (sph) and water (H_2O); and chloritoid (ctd) for sample NUY50.

Since the system is highly hydrated and the fluid movement through the fault is being investigated, it is likely that the schist samples investigated have been saturated in water, and as such it has been calculated and fluid content is shown in diagrams (dashed lines in Figure 8.1).

The water lines (dashed lines in Figure 8.1) represent the percentage of total amount of water present in mineral assemblage (14 mol % in total used in calculations for fluid saturated rock, 14mol % H_2O = 100). According to the calculated model, the inferred mineral assemblage of the samples analysed have the same water content field, between 0.97 and 0.98. These contours represent lines through which the rocks would have undergone dehydration, thus estimated that rocks released 2-3 mol % of fluid (out of 14mol % total) through dehydration during deformation over the PT interval calculated (150 to 500°C and 1 kbar to 10 kbar). This indicates minor dewatering of the footwall and almost insignificant dehydration of both muscovite chlorite schist and chloritoid schist during faulting.

Table 8.1 XRF major elements mineral composition data used to calculate pseudosections in Figure 8.1.

Sample (wt.%)	SiO_2	TiO_2	Al_2O_3	Fe_2O_3	MnO	MgO	CaO	Na_2O	K_2O	P_2O_5	SO_3	Cr_2O_3	NiO	H_2O^-	LOI	Sum
Nuy2	72.54	0.69	13.66	5.71	0.08	0.45	0.36	0.28	3.31	0.30	b.d.	0.01	0.01	0.06	2.04	99.52
Nuy3	73.55	0.77	13.10	5.47	0.06	0.49	0.32	0.29	3.14	0.31	b.d.	0.01	0.01	0.08	1.83	99.41
N50 MG	70.94	0.60	12.95	5.62	0.03	2.37	0.13	0.23	2.83	0.15	0.01	0.01	0.01	0.12	3.28	99.28

Assuming the samples experienced the same metamorphic history and stabilized at similar conditions, superimposing both pseudosections and overlapping the conditions estimated from each sample provides a constricted estimate of metamorphic conditions, highlighted in yellow in Figure 8.1. The

overlap of the constructed pseudosection sample conditions lies at intermediate pressures and temperatures, at 5 - 8 kbar and 250 - 400 °C.

This PT interval is not crosscut by water contours, indicating that water content in samples remained unchanged within the calculated PT conditions, ie. water has not been released through dehydration during deformation.

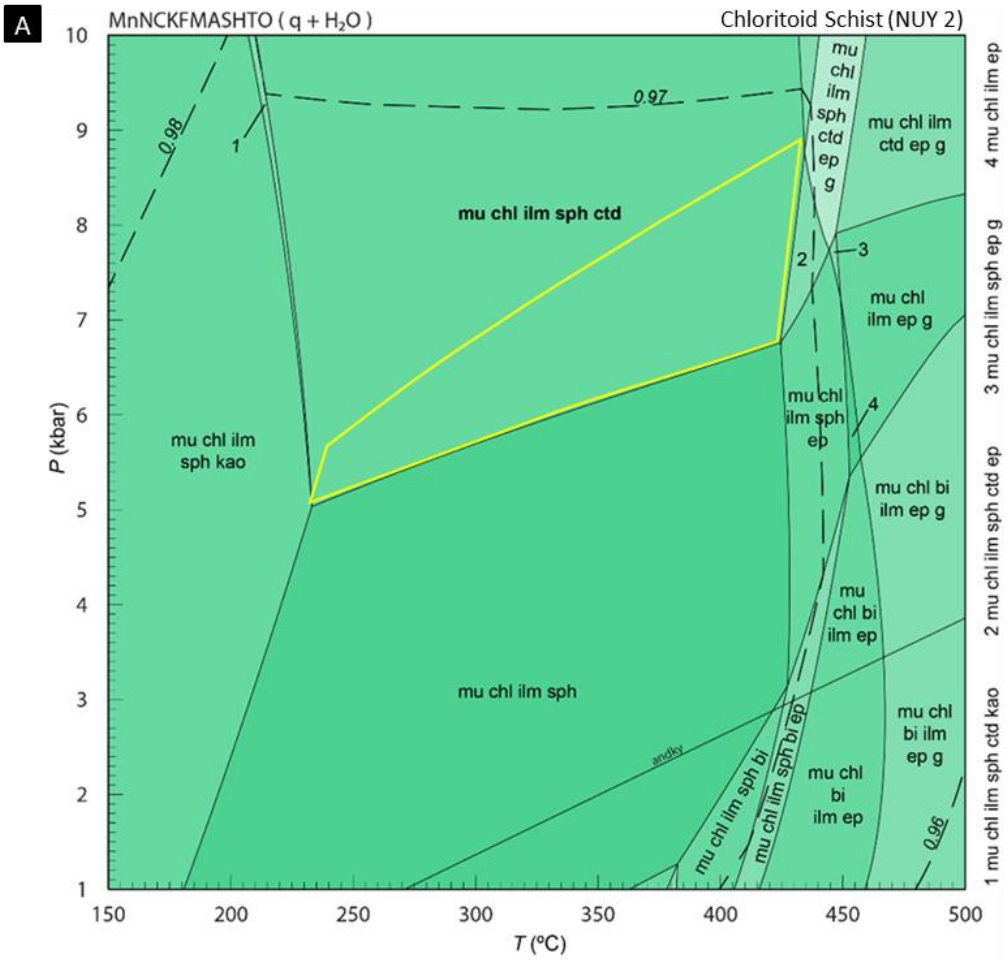

Figure 8.1 Calculated P-T pseudosections for samples (a) Chloritoid Schist – NUY 2 and (b) Muscovite- Chlorite Schist – NUY50. Mineral assemblage observed in each sample is in bold font. Yellow area denotes overlapping conditions for both samples.

8.3. Oxygen Isotope Analysis

Oxygen Isotope analysis included whole rock samples of silicified schist (samples N37 to N49); and clean quartz vein material handpicked from coarsely crushed vein samples. The samples were then powdered to be used to calculate oxygen isotope ratios in the stable isotope laboratory at the Department of geological Sciences of the University of Cape Town.

The $\delta^{18}O$ values obtained are listed in the table below (Table 8.2), separated by the rock type of the analysed material and range from 11.2 to 15.3. Whole rock sample of silicified schist samples have an average $\delta^{18}O$ of 12.6, whereas the vein material $\delta^{18}O$ values have a relatively higher average of 14.1.

Table 8.2 Oxygen isotope values of vein material and whole rock samples

	Vein Material						Quartzite
Sample	N05	N09	N24	N25	N29	N33	N37
$\delta^{18}O$	14.3	13.4	13.9	13.7	15.3	11.2	13.3
	Whole Rock - Silicified Wallrock Profile						
Sample	N37	N38	N39	N40	N41	N42	N43	N44	N45	N46	N47	N48	N49
$\delta^{18}O$	13.3	12.6	12.6	13.7	12.6	12.7	12.6	12.8	12.1	13.1	12.2	12.7	13.3

The histogram below plots $\delta^{18}O$ values of both whole rock and vein material samples. The values distribution indicated that overall, fluid constituting vein material has higher $\delta^{18}O$ composition than that of wallrock schist and quartzites.

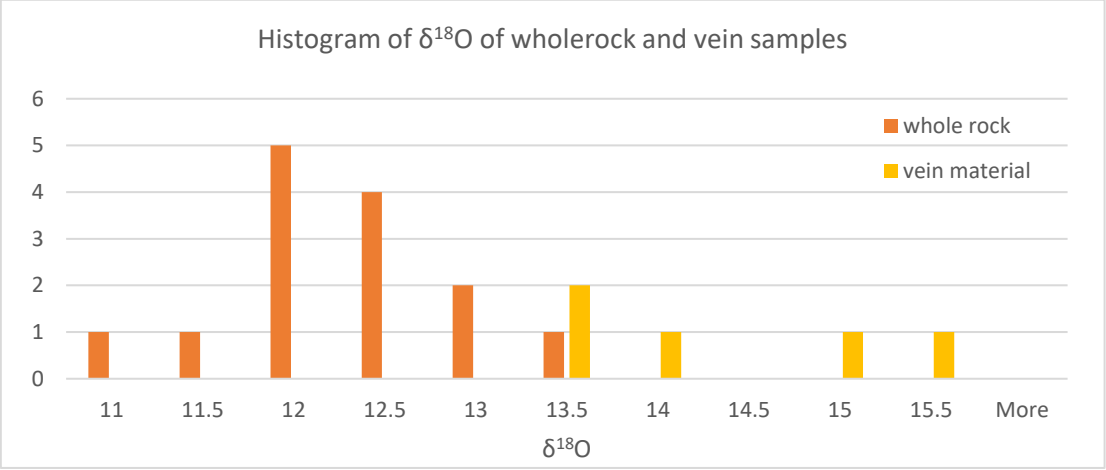

A plot of silicified schist whole-rock $\delta^{18}O$ values and samples' location across the shear zone vertical profile is presented in Chapter 8.4.

8.4. Geochemical and Isotope Profile

XRF and oxygen isotope data collected vertically across the fault zone reveal that the fluid-rock ratio and therefore the degree of silicification of the wall rock varies across profile. The footwall has the lowest values of silica relative to the alumina content (~10). The highest values (42.4 - 49) occur on the hanging wall in immediate proximity to the fault core (within 1m from the fault core). Thus, there is an obvious addition (~35 SiO_2/Al_2O_3) of silica in the fault core and the hanging wall.

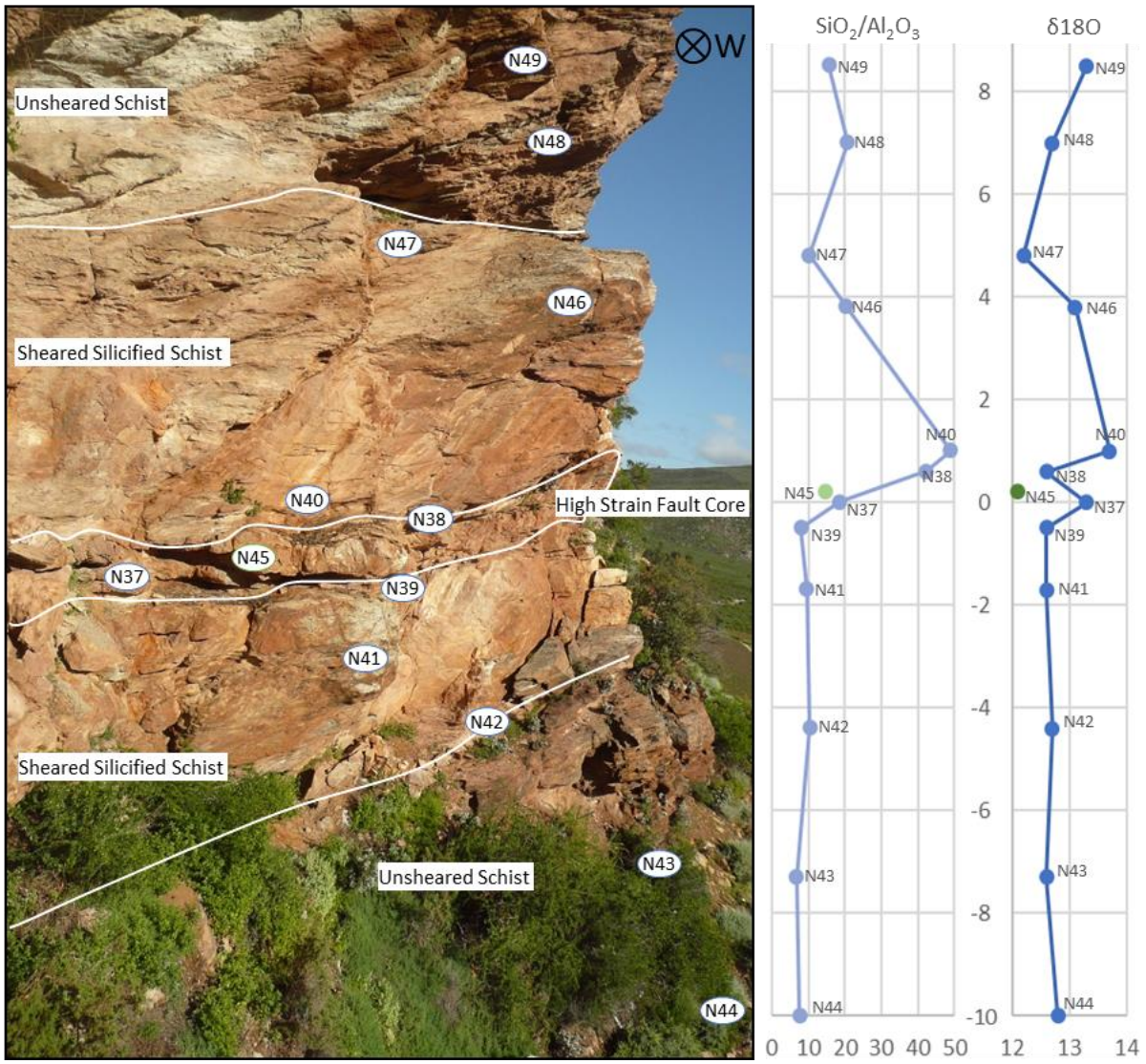

Figure 8.2 Vertical Profile across Representative Profile 1. a) Simplified lithology; Plot of plot of b) wall rock silica content relative to wall rock alumina concentration, and c) oxygen isotope values as a function of distance (metres) away from the fault gouge (x = 0). Circular labels show position of samples.

The fault core contains both finely sheared gouge (N37) and highly strained quartzite lenses (N45), which have the lowest silica to aluminium ratio relatively surrounding fault core. The hanging wall is highly silicified with the occurrence of quartz veins (position N46 and immediate surroundings). Silica content in the hanging wall schist increases sharply closest to fault core, from ~ 10 to a maximum of 49, and gradually decreases to 10.2 with vertical distance away from it, towards the secondary high strain zone. Veined schist contains slightly lower silica alumina ratio as quartz is mainly precipitated

within macroscopic veins. The footwall silica values are low in comparison to those of the hanging wall and show insignificant variation throughout the footwall, irrespectively of the samples' distance from the fault core.

There is a general directly proportional trend between the SiO_2/Al_2O_3 and $\delta^{18}O$ measurements, ie. High $\delta^{18}O$ values correspond to high silica alumina ratios, thus fluid has higher $\delta^{18}O$ than fault host rocks.

8.5. Isocon Diagram

XRF measurements of hanging wall rock and fault core were used to create the below isocon diagram (Figure 8.3). The Isocon Diagram presented in this Chapter is based on the methodology outlined in Grant (1986). In the diagram, the altered rock is represented by a highly silicified and deformed metapelitic schist sample, collected from the fault core (sample N38, x = 0). Whereas the unaltered wall rock is represented by sample N49 collect from hanging wall (x ~ 8.5m from fault core) with the least degree of silicification (as shown in Figure 8.2, SiO_2/Al_2O_3 Graph).

Two lines of equal concentration (isocons) are displayed in the diagram in Figure 8.3:

1: Constant mass line, assuming no mass change (gradient = 1)

2: The best fit line passing through the origin (0), Ti and Al, as these elements are commonly immobile in low grade metamorphic conditions (ie. Fagereng and Harris, 2014 and references therein).

The equation to the isocon is:

$C^A = (M^O/M^A)\, C^O$ (Grant, 1986)

Where: C^A = concentration of an element in the altered rock; C^O = concentration of an element in unaltered rock (rock with the lowest degree of alteration); and M^O/M^A = constant, ratio of masses prior and post alteration, equivalent to the slope of the isocon.

The calculated gradient of best fit line going through the origin, Ti and Al, is 0.40 (before scaling elements by a factor of k).

The diagram reflects a substantial increase in SiO_2 near the fault core relatively to unaltered wall rock.

The Si content lies above both the constant mass isocon and the immobile Ti and Al isocon, suggesting a significant increase in the silica content of the wall rock during deformation, as apparent in the field.

There is no apparent selected depletion of components in altered rock, all components deplete at the same rate, roughly following best immobile Ti and Al isocon.

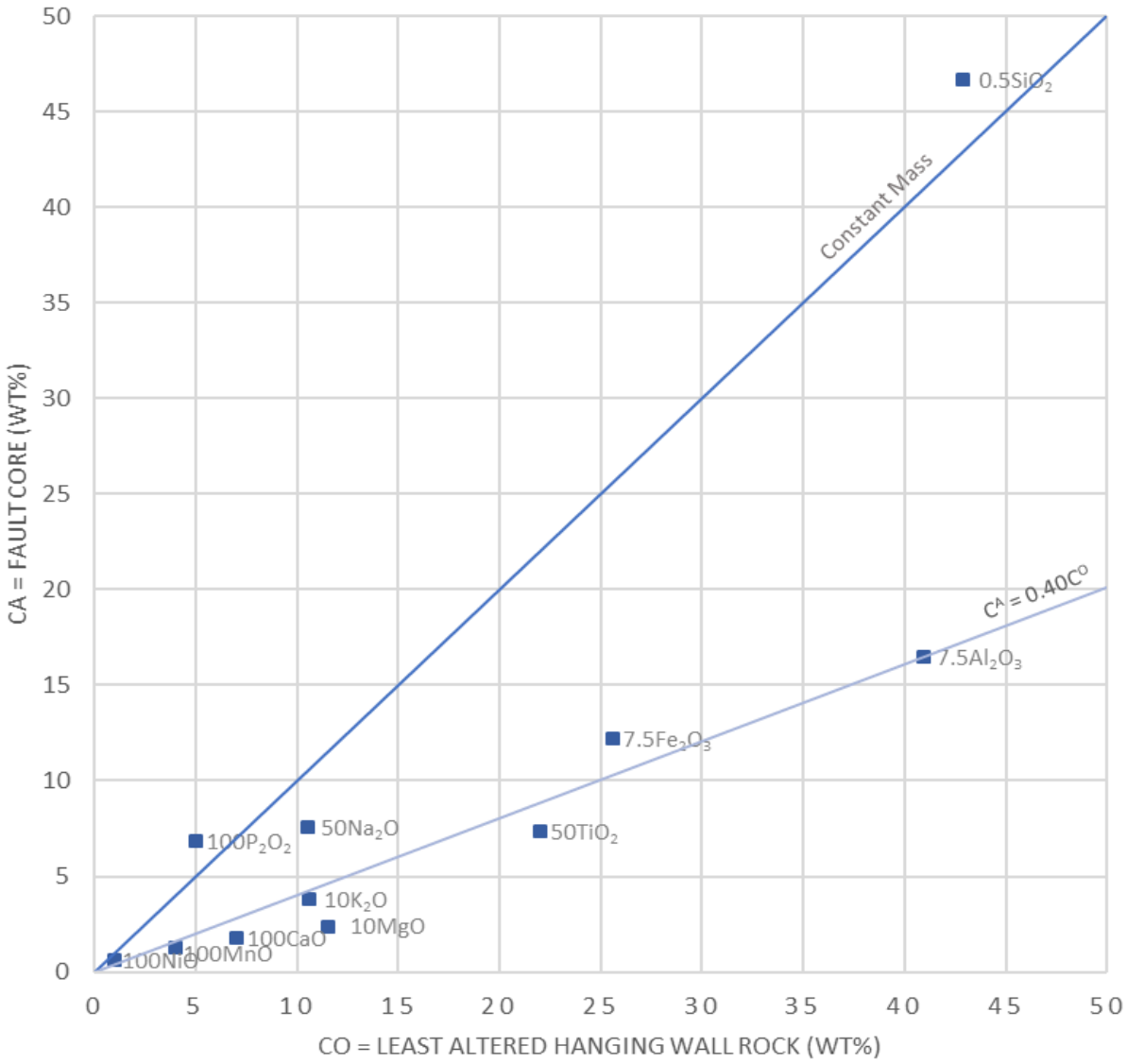

Figure 8.3 Scaled element concentrations in hanging wall least altered rock sample and fault core sample. A mass loss of ~60% is estimated for the fault core relatively to the hanging wall rock assuming immobile Ti and Al. Si significant increase in core sample.

9. Discussion

Field observations of fault geometries combined with macro- and micro- structure analyses indicate overprinting deformation fabrics, resultant from a combination of deformation mechanisms (cataclasis, dislocation creep, dissolution-precipitation). The response of the fault rocks to shear stress is expected to vary with composition, the presence and abundance of fluids, strain rate, environmental conditions etc. all of which are preserved in particular textural characteristics. The contribution of these factors in creating overprinting deformation fabrics and styles will be discussed in detail in the following chapters.

9.1. Deformation Fabrics Overprint

In a broad sense, the ductile regime is characterized by mylonitic fabrics and is predominantly a result of aseismic plastic shearing (Hickman et al., 1995), whereas the brittle regime is characterized by fracturing, and it is discontinuous by definition. Brittle deformation in the studied area was mainly accommodated in the form of fault gouges, cataclasites, hydraulic breccias, cohesive fault crush breccias, and anastomosing quartz shear and extension veins. Ductile deformation was mainly accommodated in the form of lower greenschist mylonites and limestone mylonites. The bulk rheology of fault rocks has been determined based on the ratio of its constituents with different viscosity, low- to high-viscosity minerals, and its phase distribution in the rock (Handy, 1990).

Lineations, foliations, shear bands and SC fabrics are classified as viscous deformation features, whereas fractures, veins, tension gashes and fracture boudins result from frictional deformation processes and are classified as brittle features. Macroscale evidence for the overprint of ductile fabrics by brittle deformation includes veining and fracture formation in schist units, which are initially deformed by viscous shear and foliated (e.g. Figure 6.3). Macroscale evidence for the overprint of brittle features by ductile deformation includes shear of brittle regime associated rock types and structures such as ductilely sheared cataclastic rocks (e.g. foliated fault gouge containing SC fabrics)(Figure 5.3.b) and lineations formed by the alignment of brittle quartz fragments in competent rocks (Figure 6.1.f).

As presented in Chapter 6, the study area exhibits a combination of these macrostructures, brittle and ductile. The coexisting structures could be a product of rheological anisotropies (e.g. Druguet et al., 2009); or reflect the evolution from brittle to ductile regimes through time, during prograde metamorphism (e.g. Fusseis et al., 2006) and from ductile to brittle during exhumation. This will be discussed further in Chapters 9.2 and 9.3.

Overall, the deformation style in the three studied localities is mixed continuous-discontinuous. Hill510 fault zone is heterogeneous, containing at least three different lithological fault host rocks. The fault deformation is mainly focused in the schist, and potentially in the limestone horizon (relatively incompetent units) and along lithological boundaries, surrounding metasandstone lenses. The heterogeneous nature of the shear zone in Hill510 is observed in Chapter 5.3 in the wall-rock profiles (Figure 5.3 andFigure 5.4). The Boesmanskloof and Cross localities have fewer lithological heterogeneities than Hill510, but the fault slip styles are, nonetheless, variable and fault rocks display both brittle and ductile fabrics, as evidenced by the presence of schist and limestone mylonites and

quartz cemented breccias in Boesmanskloof and both semi mylonitic and cataclastic quartzites at the Cross locality.

9.2. Deformation mechanisms

Cataclasis is interpreted as a frictional deformation mechanism, whereas solution-precipitation and dislocation creep are considered viscous deformation mechanisms (Passchier and Trouw, 2005). Based on microscopical observations (Chapter 7), dislocation creep is dominant in small grain size units such as ultracataclasite (N12) and in samples that have a higher ratio of incompetent to competent minerals, enhancing viscous regime fabrics. This is best exemplified in metasandstone samples containing a higher amount of micaceous minerals (greywacke) which form anastomosing shears bands (N14 vs N19). Cataclasis was the most crucial deformation mechanism during silicification of the wall-rock schist, through the development of micro-veins followed by dissolution-precipitation. Quartzitic fault rocks and quartz components within mylonitic rock types generally display abundant fracturing and rigid body rotation at the macroscale, as well as at the microscale. Some cataclastic fault rocks may also have formed in the presence of dissolution-precipitation creep, as evidenced by abundant pressure solution selvage seams in microbreccias (e.g. N20) (also described elsewhere by Fagereng and Toy, 2011; Rowe et al., 2012; Gratier and Gamond 1990).

Overall, both cataclasis and dislocation creep deformation mechanisms occur in highly deformed fault core rocks, occasionally overprinting each other. However, evidence for dissolution-precipitation is present in most rock samples from the fault core in the form of stylolitic surfaces, pressure shadows, fluid healed fractures and truncated grain boundaries. The ubiquity of dissolution-precipitation is expected according to the conceptual model as this mechanism occurs in both brittle and ductile regimes of the brittle-ductile transition (Chapters 3 and 2.1.1). Ubiquitous evidence for this mechanism throughout the study area could also be resultant from significant fluid presence during deformation and could suggest that fluid pressure and strain rates were determining factors of deformation styles (e.g. Fagereng, 2012). Fluid dissolution-precipitation is likely very important in determining the rheology of fault-rocks, the duration of interseismic strength recovery and potentially the establishment of impermeable barriers along fault zones. This mainly manifests through fracture healing and sealing, followed by episodic fracturing and permeability enhancement. This mechanism could lead to repeated transient fluid overpressures, connected to the seismic cycle (Gratier and Gueydan, 2007; Hickman, 1955 and references therein). A summary of the primary field and lab observations and deductions is presented in Table 9.1 below.

Table 9.1 Summary of field and lab observations per lithological units.

lithology		limestone	schist (low silicification)	schist (high silicification)	metasandstone/quartzite
mineralogy		calcite, aragonite, detrital quartz	mica, chlorite, quartz, (chloritoid)	quartz, micas and chlorite (chloritoid)	quartz, minor feldspar and trace micas
typical fault rocks		limestone mylonite	mylonitic schist and gouges	breccias	cataclasites and breccias
position relative to high strain zones		footwall	mostly footwall and localised hanging wall	hanging wall	high strain zone core
common macrostructures		lineations and banding	foliations, lineations, shear bands, sc fabrics	lineations, fractures, shear bands, fracture boudins, intense veining	fractures, tension gashes, veins, lineations to a lesser extent
common microstructures		foliated matrix containing fractured and rotated quartz grains with fluid sealed microfractures	continuous fabric, closely-spaced foliations and crenulations	microfaults, stylolites, abundant microveins	angular fragments, random fabrics or anastomosing, disjunctive fracture fabrics and sigmoids (recrystallised grains)
deformation mechanisms in order of dominance	**in matrix**	intracrystalline plasticity	intracrystalline plasticity and dissolution-precipitation	dissolution-precipitation and intracrystalline plasticity	cataclasis, dissolution-precipitation and intracrystalline plasticity
	in quartz	cataclasis and intracrystalline plasticity	intracrystalline deformation, dissolution precipitation and cataclasis	cataclasis and dissolution precipitation	
overall rock deformation fabric		mostly ductile	ductile and brittle	brittle and ductile	brittle and ductile
ratio of competent/incompetent material		low	→	→	high
shear strain rate		likely fairly uniform strain rates	fluctuating shear strain rate		likely localised peaks in shear strain rate
dominant associated shear zone seismic styles		mixed, but mostly continuous	mixed	mixed	mixed, but mostly discontinuous

9.1. Fault geometry and kinematics

Based on the fault plane and shear foliation geometries (Chapter 6), the shear zone in the study area strikes E-W and dips ~33°S. The trace lineations lie on the plane of foliation and have an average orientation of 174.5/35.5°, inferred to coincide with the overall shear orientation. Thus, the faults strike almost perpendicularly to the determined transport direction (as deduced from lineations) and are well oriented for N-S shortening and perhaps N-S extensional stress during exhumation. Shear indicators in the field mostly suggest top to north displacement along the shear zones, indicating thrust fault kinematics (~N-S compression).

Conjugate fracture sets in metasandstone lenses from Hill510 (Figure 6.2, a and b) suggest fracture sets formed under variable stress conditions (strike-slip and normal fault regime) and do not match general N-S compression. Barren and fluid filled fractures have an overall similar distribution: strong set semi-parallel to foliation planes (shear veins and fractures), a semi-vertical set roughly perpendicular to lineations and striking E-W (extension veins and fractures), and more scattered dip directions of gently dipping veins and barren fractures. Thus, veins and fractures are likely to have formed over time (mostly during compressive stress) and could suggest localized strain within the fault, fluctuations in fluid pressure and strain rate, or rotation after formation. Furthermore, they are inferred to likely represent a time-integrated population over multiple earthquake cycles, with associated co-seismic and post-seismic stress changes, in addition to potential overprint of multiple deformation phases.

9.2. Environment constraints: Temperature and Pressure

Based on mineral equilibrium modelling determination of the likely P–T conditions experienced by the metapelitic schists during deformation, the Malmesbury Group in the study area did not experience conditions above those of greenschist facies and fault rocks record sub-greenschist to lower greenschist facies conditions. Peak pressure conditions range between 5 – 8 kbar and temperature has an interval between 250°C and 400°C (Figure 8.1), perhaps closer to 250°C lower end based on the presence of chloritoid and temperatures calculated by Frimmel et al. (2001) (~320°C).

Common collisional environments have average geothermal gradients between 20 - 30°C.km^{-1} (Brown, 1993). Assuming an average geothermal gradient of 25°C.km^{-1} during deformation, the studied fault has been exhumed from 10 – 15 km depth. In thrust faults, the general transportation of material is from deeper to shallower depths in the crust. Therefore, theoretically, a variety of fault rocks formed in different conditions may coexist, and earlier high temperature ductile fabrics might be overprinted by lower temperature brittle fabrics during thrusting and exhumation. This overprint is not apparent throughout the study area, as mineral assemblages are similar above and below observed shear zones suggesting that the PT conditions are similar across the studied thrust fault.

Faults in the study area were favourably oriented for reactivation during deformation under N-S orientated stress fields, such as that of the Pan-African deformational phases (–~500 Ma) and the Cape orogeny (~250 Ma) which are semi coaxial (Chapter 4.1). It is possible that the observed overprinting structures represent temporal variances and multiple deformation episodes. However, based on chlorite and chlorite-chloritoid thermometry (Frimmel et al., 2001), the temperature during these orogenies closely coincides, the Pan African metamorphism was estimated at 325±12 °C and during the Cape Orogeny at 320°C. Thus, peak temperature remained relatively constant throughout both deformation episodes that had a significant impact on the metamorphic assemblage and regional geology deformation. This is interpreted to diminish the likelihood of the observed coexisting brittle and ductile structures being primarily a result of temperature changes.

As determined by mineral equilibria modelling, peak metamorphic pressure ranged between 5 – 8 kbar (~ 9 km range). During thrust fault development, the metamorphic pressure is mainly a result of burial and exhumation processes. Based on the geological history of the area, deformation in the Worcester area is ascribed to the compressive tectonic events mentioned above (and in Chapter 2.1) suggesting that the studied shear zone did not experience regional extension stress in between deformation events. Furthermore, there is no apparent gradual change in pressure as a change in the mineral assemblage is not observed. Thus, ambient pressure likely remained reasonably constant (with no drastic erratic oscillations) during thrusting, as strain was taken up by deformation in the fault zones. Pressure is inferred to have only decreased as the principal compressive stress axis magnitude and orientation changed from compressional to lithostatic regime, along with exhumation from depths of approximately 10–15 km to the surface. This may have been associated to a late extensional regime of the Worcester Fault.

The observed coexisting brittle and ductile structures in the study area would require multiple significant burial and exhumation events to justify considerable pressure and temperature changes. However, these would probably erase evidence of deformation styles overprint, suggesting that it is unlikely that changes in temperature and pressure are the driving factor of the oscillations in deformation styles observed in the field area.

9.3. Composition

Metasandstones, quartzites, highly silicified units and veins form competent lenses and layers and are generally associated with brittle deformation features, such as fractures, tension gashes and fracture boudinage, as well as adjacent cataclasite layers and fault gouges. The schist layers contain the most ductile fabrics relatively to other units, and it is likely they have accommodated the most strain in the study area. It is inferred that the incompetent units acted as shear zones surrounding other more competent units such as metasandstone and quartzite. Therefore, composition plays a crucial role in determining brittle and ductile rheology of fault rocks, particularly at a macroscale.

Profiles 1 and 2 (Figure 5.3 and 5.4) represent heterogeneous fault zones, several meters thick (~10 m) displaying mixed mode continuous-discontinuous deformation and multiple high strain zones. Within a relatively incompetent schist matrix, wrapping around competent units (relatively competent fractured or massive metasandstone lenses), asperities are inferred to have formed along the fault. The dynamics between competent and incompetent units in the study area can be represented by this relatively viscous flow of schist around more competent metasandstone bodies. A similar behaviour is retraced at microscale as micaceous minerals flow around quartz porphyroclasts. Conversely, the more competent units such as metasandstone and silicified schist generally show pervasive discontinuous deformation and localized brittle deformation (cataclasis). Thus, heterogeneities in rock composition provide constraints for the distribution of fault zones with higher seismogenic potential in the study area (Bons et al., 2012; Druguet et al., 2009; Fagereng and Sibson, 2010).

The most apparent microscopic observation in samples with compositional heterogeneities is that the relative dominance of deformation mechanisms is governed by the mineralogy. For example, large quartz porphyroclasts generally remain relatively brittle in comparison to micas (in schist) and calcite (in limestone); often deforming by rotation, fracturing or recrystallization (as observed in samples N50, N19 and N16, N28) (Chapter 7). Some quartz clasts are preferentially deformed, probably due to favourable lattice preferred orientation and individual mineral resistance. Samples with similar protolith and grain size might contain ductile fabrics (e.g. N19) or brittle fabrics (e.g. N21 and N23), and samples with reduced grain size might be favourably deformed by recrystallisation (e.g. ultracataclasite Sample N12). Thus, although grain size contributes to the partitioning of deformation mechanisms, it is likely not responsible for deformation partitioning in studied rocks.

There is evidence for overprint of deformation mechanisms within samples of similar composition and grain size, for example in quartzitic samples N34 and N36, both from the Cross locality, displaying a high degree of recrystallisation, suggesting dislocation creep was an important deformation mechanism, at least during initial deformation. However, sample N36 developed a semi mylonitic fabric through dislocation creep and dissolution-precipitation, whereas sample N34 was discontinuously deformed through cataclasis and dissolution-precipitation. Since the composition is similar, this suggests local variations in strain rate, temperature or fluid pressure controlled the active deformation mechanisms.

The schist generally deforms by ductile mechanisms such as intracrystalline plasticity and intergranular flow (which involves frictional sliding and rigid rotation of grains without intragranular deformation). However, field and microscopic evidence, such as hydraulic breccias with schist fragments and vein filled microfractures, indicate localised brittle fracturing of otherwise ductile schist. The wall rock contains varying degrees of silicification which changes its composition and

increases shear resistance of schist, creating a more heterogeneous wall rock with sections of more competent rocks, irregularly distributed. This is ascribed to the fluid effect and discussed in Chapter 9.4. However, taking into account solely compositional alterations due to cementation and fluid precipitation, such effect can only justify brittle overprint as rocks become silicified and more competent, but not the reverse overprint. Therefore, although composition is a first order factor controlling the rheology of the fault rocks, it cannot justify by itself the diversity in the style of faulting.

To summarize, temperature, ambient pressure, grain size and lithotype discussed above cannot explain deformation style oscillations in schist; thus, such variations might be dictated by an increase in pressure fluid and strain rates.

9.4. Fluid

9.4.1. Long term fluid effect on rheology

The presence of abundant fluid during active deformation is evidenced by the occurrence of hydraulic breccias, intense veining networks in the hanging wall of multiple faults, and syn-tectonic recrystallisation in veins. Furthermore, fluids contributed to chemical compaction of fault gouges, to fine-grained vein-filling material and silicification of wallrock by dissolution-precipitation processes, as evidenced by stylolites and truncated grains in veins (e.g. N01) in silicified schist (e.g. N08) and metasandstone (e.g. N20, N21) samples.

The interaction between deformation and fluid presence controls the bulk properties of rocks as the increase in silica content in otherwise incompetent wallrock leads to its strengthening and enhances embrittlement. The presence of fluid in metamorphic rocks results in the compositional alteration from metasomatic fluid-rock interaction due to large volumes of fluid, or through fracturing, followed by fluid precipitation (crack and seal). Macro- and microstructures, particularly in silicified schist samples, indicate that episodic fracturing and brecciation are often followed by cementation and crack-sealing by fluid precipitation. Such structures suggest a considerable variance of fluid amounts through time. Post silicification deformation would result in brittle structures forming in the silicified bodies. The simplified structural evolution of quartz veins and host rocks below (Figure 9.1) demonstrates the effect of silicification in rock rheology and vein orientations through time, whereby fracturing occurs preferentially in silicified rocks and multiple fracturing events, even under the same kinematics, result in differently oriented veins.

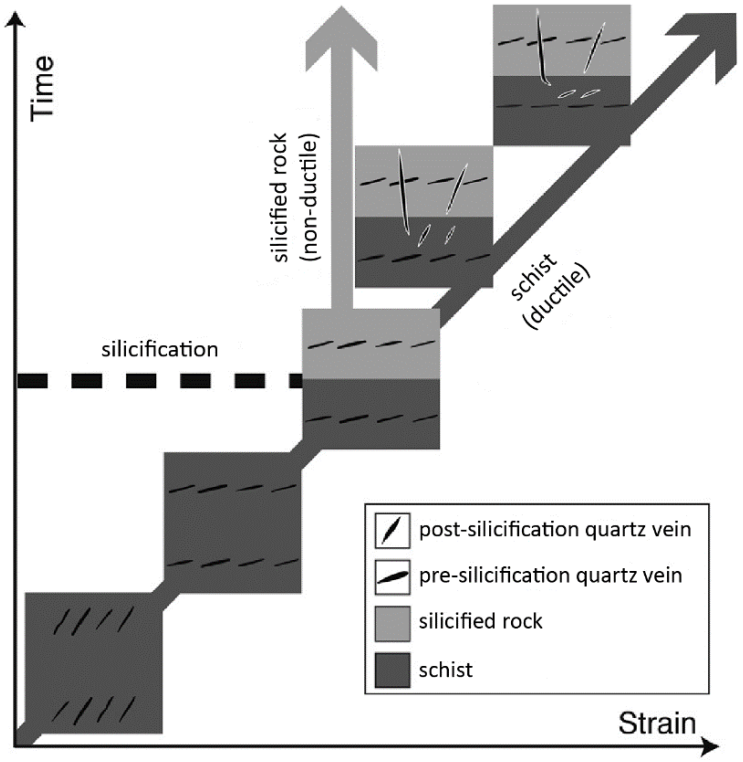

Figure 9.1 Simplified conceptual structural evolution of quartz veins and host rocks, showing relative strain vs relative time; demonstrating progressive events and a silicification event separating two veining episodes (based and modified after Mateen et al., 2015) (diagram not to scale and study area suggests likely multiple fluid injection events).

The development of a grain-scale micro-fracture network as observed in hanging wall silicified schist samples leads to an increase in permeability during viscous deformation, as was also described in Bons (2010), and sealing of such fractures would then lead to a decrease in permeability. In this manner, precipitation of fluid within fractures and microfractures and deformation by dissolution-precipitation in fine-grained fault rocks could contribute to the post-seismic or interseismic sealing of the rock, decrease in permeability of fault rocks by filling in intergranular spaces (as observed in sample N23, Figure 7.4) and consequently to stress build-up between seismic ruptures (e.g. Boullier et al, 2011), allowing slip even at slow shear stress (Blenkinsop and Sibson, 1992).

9.4.2. Fluid Source

Hydraulic breccias are associated with areas of high fluid concentration and intense veining in the study area. These features indicate movement of a significant fluid volume through the fault to account for fluid-rock ratios (Fagereng and Harris, 2014). Dehydration of the wallrock schist is unlikely to be the source of abundant fluid present in the study area, as mineral equilibria fluid calculations indicate that there was no dewatering of the analysed samples within the calculated PT conditions, in the 5 - 8 kbar at 250 - 400 °C interval (Figure 8.1). However, the muscovite chlorite schist could have released a considerable amount of water during prograde metamorphism, representing 1 - 2% loss of fluid through dehydration from 150 to 250°C and 1 to 8 kbar. Considering that muscovite-chlorite schist comprises the main lithology in the study area, 2% loss of water can result in a high fluid abundance in places where there is a channelised flow.

Information about the fluid content in fault rocks and its origin can be constrained through geological, geochemical and isotopic studies of shear zones. The most common sources of fluid in shear zones are meteoric fluids carried downward by circulation; and metamorphic fluids generated by dehydration of mineral constituents during prograde metamorphism (Hickman, 1995). The composition of fault fluids varies depending on factors such as the source and the amount of water-rock interaction along the flow path (Hickman, 1995). The isotopic composition of metamorphic fluids is highly variable, with $\delta^{18}O$-values ranging from 5 to 25‰, whereas low-grade metamorphic pelites generally have $\delta^{18}O$-values ranging from 15 to 18‰ (Fagereng and Harris, 2014 based on references therein). Pelitic schists and shales, representing the main lithology in Nuy Valley, typically have whole rock $\delta^{18}O$ ranging from 14 to 19‰. The secondary lithologic units in the study area are limestones with typical $\delta^{18}O$ of 20 to 32‰; and metasandstones, which have a range of $\delta^{18}O$ between 10 and 20‰ (Figure 9.2).

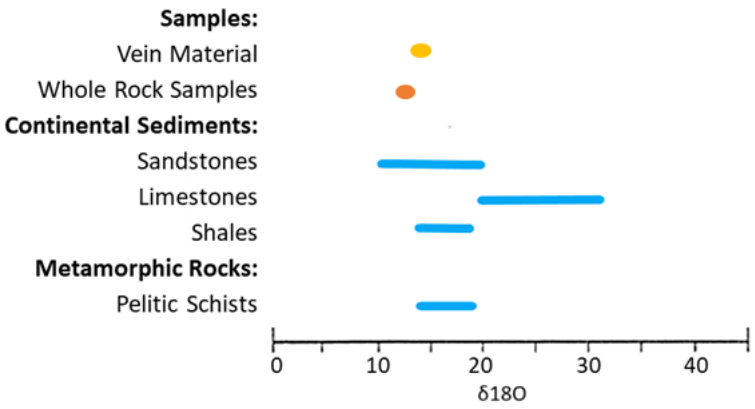

Figure 9.2 Average $\delta^{18}O$ of analysed samples (yellow: vein material; orange: whole rock) and of various major crustal rock types (blue). The ranges marked by blue correspond to typical, representative values and purposefully exclude extreme examples of many rock types. Adapted from Eiler (2001), data sources referenced therein.

The $\delta^{18}O$ values of the vein samples range from 11.2 to 15.3 ‰, and whole rock samples' $\delta^{18}O$ values are between 12.1 and 13.3 ‰. Thus, it is inferred that both sample groups likely share a common source of fluid. In general, vein quartz $\delta^{18}O$ variation with temperature can be categorized into two end-members: the rock-buffered end-member in which the minerals in the host-rock determine the isotope ratio in the fluid; and the fluid-buffered model in which the $\delta^{18}O$ value is determined by the isotope signature of a large reservoir and the temperature sensitive fractionation factor between the reservoir's fluid and quartz (Fagereng and Harris, 2014). Given the small range in $\delta^{18}O$ values of the host rocks and vein material, the system is inferred to be rock buffered and the most probable source of fluid in these samples is metamorphic water from muscovite-chlorite schist (dehydration during prograde metamorphism) or from rocks not in the immediate vicinity of the studied faults. It is unlikely that there was fluid exchange with carbonates from limestone horizons present both in Hill510 and Boesmanskloof, as $\delta^{18}O$ values of vein material are significantly lower than those of limestone, which inherently have much higher $\delta^{18}O$ values than those of siliciclastic rocks (Figure 9.2).

Based on the Isocon Diagram (Figure 8.3), the calculated gradient of the best fit line going through the origin, Ti and Al, is 0.40 (before scaling elements by a factor of k). This gradient is interpreted to correspond to a ~60% average mass loss in the highly-deformed schist adjacent to the fault core, relatively to the unaltered samples. The most significant observations are: the substantial increase in SiO_2 near the fault core relative to the wall rock, and the lack of a preferential depletion of components in the altered rock. All components are depleted at a similar rate, roughly following the immobile Ti and Al isocon. These observations suggest that the silica injection is probably secondary, as a result of fluid migration through the fault; and that the decrease in element concentrations in the altered rock is a product of dilution by a silica-rich fluid injection of ~60% rather than of reaction alteration.

Based on the mineral equilibrium model (Chapter 8.2), the fluid is not the result of dehydration of the wallrock as these do not release a large amount of fluid during deformation (1 - 2% during prograde and 0% during peak metamorphism). Furthermore, the positive correlation between $\delta^{18}O$ and SiO_2/Al_2O_3 in samples of the fault core (Chapter 8.4) indicates a high-T fluid source. Assuming that the source rock had similar $\delta^{18}O$ to the wallrock before alteration, the increasing isotopic values at the fault core might be due to an increase in the fractionation factor between quartz and water caused by

a higher thermal contrast. A fluid released at high PT conditions, would be expected to be enriched in Si, due to the increased Si solubility at supracritical conditions. Therefore, the large concentration of fluid most likely originated from rock dehydration from other areas such as from the deeper parts of the fault zone footwall. This fluid could have been transported either along-strike or up-dip for more than tens of metres.

9.4.3. Fluid Pressure

As previously mentioned, brittle deformation in the study zone was mainly accommodated in the form of fault gouges, cataclasites, hydraulic and quartzitic breccias and veins. These fault features, however, are associated with different fluid regimes during active deformation:

High-density vein system in the hanging wall of fault zones indicates sites of local extension fracture or dilational shear zones, formed by development of brittle fractures followed by fluid infiltration and precipitation. This is supported by the sharp nature of the vein-wallrock contacts (as previously observed by Fagereng and Harris (2014) and references therein). Fault rocks such as hydraulic breccias require fluid pressure (P_f) to be higher than the least principal compressive stress (σ_3); and cementation indicates a considerable amount of fluid present. Extension fractures likely contain minerals precipitated from a fluid transported from external sources after hydrofracturing occurred at relative fast slips (potentially seismic), and fluid influx from surrounding fluid channels such as fracture and fault conduits. Cycles of vein precipitation and fracture formation are inferred to correspond to cycles of an incremental increase in fluid overpressure. This would result in fluid pressures higher than σ3 and collateral hydrofracturing leading to progressive fault–fracture intense vein network (e.g. Fagereng and Harris, 2014). Conversely, based on field and lab observations, the formation of fault gouges is the result of cataclastic detritus on a fault surface associated with steady state frictional shear along rock masses (as in Sibson, 1977). This requires mechanical deformation in an environment with little or no fluid present within the fault plane during deformation, and cementation of this fault rock occurring post its formation.

Thus, the presence of both dry fractured metasandstone, fault crush breccias which are fluid-poor and intense vein systems which are fluid-rich in close proximity (within <10 m) in Hill510 (Figure 5.4), and high-density veins systems and tension gashes in the same outcrop in Boesmankloof (Figure 6.2.b), suggest variability in the fluid flow and thus different fluid regimes, locally and/or temporally. Furthermore, it is inferred that frictional deformation occurred (at least locally) in the presence and absence of immediate large quantities of fluid. This could mean that fluid was only available for discrete intervals during deformation and imply changes in fluid pressure throughout the deformation life of the thrust fault, and that the fault slip styles are not driven solely by fluid pressure changes. Alternatively, given the relatively ubiquitous presence of fluid and multiple overprint of fluid injection events, fluid was rather abundant throughout various deformation events. It is likely that seismic slips were driven by confining pressure variances associated to fluid pressure changes in adjacent areas (i.e. initiating in fluid overpressured areas and propagating through the adjacent wallrock).

In summary, fluids appear to silicify and strengthen the observed faults, with fluids from an external source. The advective fluids imply fault dilation (through seismic slip), which may be driven by fluid overpressure, followed by fluid flow and healing, creating a more competent fault along the previous

failure. This may then occur cyclically and is generally tightly related to seismic/interseismic cycles (Gratier and Gueydan, 2007; Sibson, 2014; Sibson et al., 1988) as fault behaviour changes with changes in fluid pressure (and vice versa if a fluid is present). Alternatively, complex the fault rock distribution occurs because the fault rheology evolves and the position of weakness planes within fault zone, therefore, changes with time.

9.5. Strain Rates

In Chapter 9.3, the compositional heterogeneity has been determined to be a first order factor in the strain partitioning in the study area. The resulting heterogeneous shear zone comprising mixed-mode continuous and discontinuous deformation, indicates that variable shear strain rates accumulated within the shear zone (Figure 3.1) which could lead to a localised slow-slip in incompetent rocks and likely fast-slip in competent rocks (e.g. Fagereng et al., 2014). The rheological heterogeneities in the primary shear zones are likely natural areas of conditional seismic stability (Figure 9.3Figure 9.3).

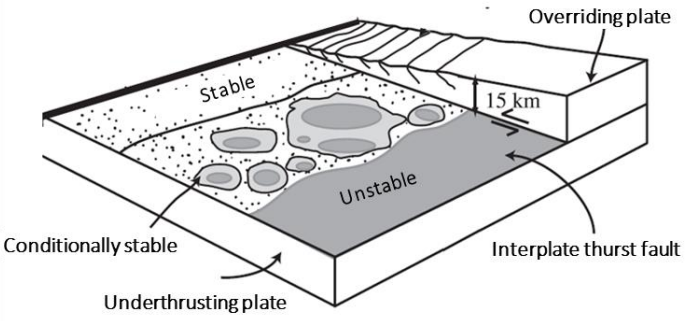

Figure 9.3 Schematic illustration of frictional conditions of thrust fault planes and position of their typically stable, conditionally stable and unstable areas (modified from Bilek and Lay, 2002).

The presence of discrete discontinuous fault planes and incrementally developed hydrothermal veins in the study area is associated with seismic slip (Fagereng and Toy, 2011), whereas ductile fabrics are usually resultant from aseismic creep. Different mechanisms or dynamic recrystallization (dislocation creep) are also considered to have formed at relatively different strain rates (i.e. regime 1, 2 and 3) at constant temperature (Chapter 2.1). Pseudotachylite, which is considered to form exclusively during seismic slip (Sibson, 1977; Passchier and Throuw, 2005), is absent in the study area. However, this does not exclude the possibility of drastic peaks in strain rate as strain is released through brittle faulting. Variation in strain rate is thus likely to have been cyclic (associated to seismic cycle) given the mutually cross-cutting relationships of slip styles observed in the field and the periodic fracture (vein) formation (perhaps associated co-seismic and post-seismic stress changes). Foliated cataclastic rocks (sample N20, Figure 7.4.a) with well-formed SC fabric and containing high amounts of pressure solution seams, could indicate deformation under low strain rates and high fluid (Figure 9.4). Whereas foliated cataclastic rocks are associated to interseismic deformation, the presence of non-foliated and unsorted cataclastic textures would indicate that either deformation occurred in a dry environment with slow strain rates, or in a fluid-rich environment at fast strain rates (e.g. Rowe et al., 2012, Niemeijer and Spiers, 2005, 2006), which for this study is probably the latter.

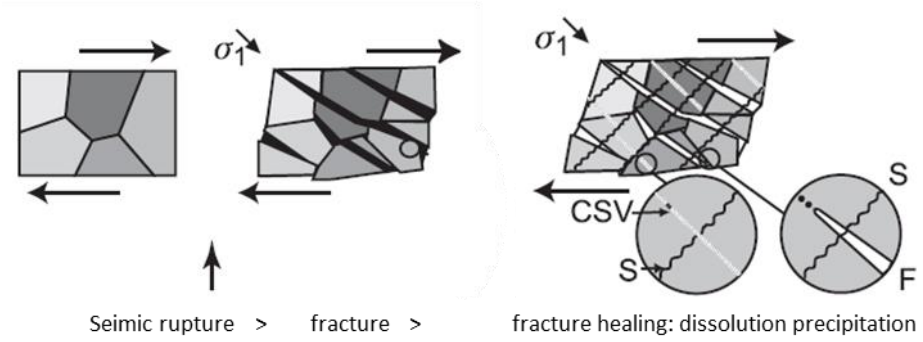

Figure 9.4 Schematic evolution of postseismic (or interseismic) sealing of a fault zone. The porosity (black) linked to the fracturing process is progressively sealed by a mineral deposit (white). Dissolution along stylolites or solution cleavage (S) is triggered by fracturing (F) and is associated with aseismic, postseismic, or interseismic deformation that releases stress. Solution cleavage (S) and associated postseismic crack-sealed veins (CSV) also accommodate part of the strain aseismically for the duration of the interseismic period (after Gratier and Gueydan, 2007).

Throughout the seismic cycle, slow strain rates occur within the interseismic interval, leading to viscous deformation of fault rock, whereas short-lived high strain rates occur during seismic ruptures resulting in frictional deformation overprint. These are subsequently overprinted by ductile deformation as rock accumulates stress (interseismic phase). This process is therefore cyclic and potentially evidenced in the study area by the mutually cross-cutting relationships of cataclastic and viscous fabrics.

Strain rate variability (seismic and interseismic periods) is probably further driven by the presence of fluid as it weakens (fluid pressure decreasing effective stress and promoting frictional sliding) and strengthens (silicification) the fault (as discussed in Chapter 9.4.1); and partitioned throughout rheological heterogeneities (Chapter 9.3) and may vary locally and temporally.

10. Conclusion

The strain recorded in Nuy Valley is mainly resultant from a horizontal compressional stress environment, and the faults are favourably oriented for reactivation under N-S compression and possibly extension, which allows for potential temporal overprint of deformation mechanisms along previously formed planes of weakness. The ambient pressure and temperature conditions under which deformation in the study area occurred are confined to 250 – 400^{o}C and 5 – 8 kbar, based on mineral equilibria modelling. These conditions appear to have remained relatively constant throughout the multiple compressional deformation events and thus are inferred to not constitute a determining factor leading to slip style cyclicity.

The compositional heterogeneity is a first order determining factor of the rheology of the fault rocks and therefore dictates the preferential deformation partitioning in the wallrocks. Concurrently, the presence of fluids increased the fault rock cohesion (through silicification), strengthening the shear zone, which could result in the observed fault rheology evolution and dictated the position of fault slip development with time.

Geochemical and isotopical analyses suggest that the fault zones acted as a fluid conduit for metamorphic fluids derived from a higher temperature source in deeper parts of the fault zone footwall that could have been channelized and transported either along-strike or up-dip; they may also imply fault dilation (through seismic ruptures), possibly driven by fluid overpressure, followed by fluid flow and healing.

Deformation of rocks in macro-, micro- and regional level as described in this project indicate an overprint and cyclicity in deformation styles throughout the Nuy Valley, evidenced by the various structures occurring from a combination or overprint of multiple deformation mechanisms: cataclasis, dislocation creep and dissolution-precipitation. Dissolution-precipitation is ubiquitous throughout the fault zone and could signify the presence of fluid during deformation and suggest the dominance of fluid pressure and strain rates on determining the deformation and fault-slip styles. Fluid dissolution-precipitation is likely very important in determining the rheology of fault-rocks, the duration of interseismic strength recovery and potentially the establishment of impermeable barriers along fault zones in Nuy Valley. This mainly manifests through fracture healing and sealing, followed by episodic fracturing and permeability enhancement. Varying strain rates, potentially recording seismic slip and aseismic creep through time, are likely enhanced by this effect of fluid, as faulting weakens the fault by decreasing effective stress with increasing fluid pressure and strengthens the fault and partitioned deformation throughout rheological heterogeneities.

In the Nuy Valley, the interplay between composition and fluid presence seem to justify heterogeneities in the style of deformation within fault, by affecting the rheology of fault rock through time and thus strain rates.

11. References

Bilek, S.L., Lay, T., 2002. Tsunami earthquakes possibly widespread manifestations of frictional conditional stability. Geophysical Research Letters 29, 18-1-18–4. https://doi.org/10.1029/2002GL015215

Blenkinsop, T.G., Sibson, R.H., 1992. Aseismic fracturing and cataclasis involving reaction softening within core material from the Cajon Pass drill hole. Journal of Geophysical Research 97, 5135–5144. https://doi.org/10.1029/90JB02285

Bons, P.D., Elburg, M.A., Gomez-Rivas, E., 2012. A review of the formation of tectonic veins and their microstructures. Journal of Structural Geology 43, 33–62. https://doi.org/10.1016/j.jsg.2012.07.005

Boullier, A.-M., 2011. Fault-zone geology: lessons from drilling through the Nojima and Chelungpu faults. Geological Society, London, Special Publications 359, 17–37. https://doi.org/10.1144/SP359.2

Brown, M., 1993. P–T–t evolution of orogenic belts and the causes of regional metamorphism. Journal of the Geological Society 150, 227 LP-241. https://doi.org/10.1144/gsjgs.150.2.0227

Collettini, C., Niemeijer, A., Viti, C., Smith, S.A.F., Marone, C., 2011. Fault structure , frictional properties and mixed-mode fault slip behavior. Earth and Planetary Science Letters 311, 316–327. https://doi.org/10.1016/j.epsl.2011.09.020

de Beer, C.H., 1995. Fold interference from simultaneous shortening in different directions: the Cape Fold Belt syntaxis. Journal of African Earth Sciences 21, 157–169.

de Wit, M.J., Ransome, I.G.D., 1992. Inversion tectonics of the Cape fold belt, Karoo and cretaceous basins of Southern Africa. Proceedings of the Conference on Inversion Tectonics of the Cape Fold Belt. 269.

Druguet, E., Alsop, G.I., Carreras, J., 2009. Coeval brittle and ductile structures associated with extreme deformation partitioning in a multilayer sequence. Journal of Structural Geology 31, 498–511. https://doi.org/10.1016/j.jsg.2009.03.004

Eiler, J.M., 2001. Oxygen isotope variations of basaltic lavas and upper mantle rocks. Reviews in Mineralogy and Geochemistry 43, 319–364.

Fagereng, Å., 2012. A Note on Folding Mechanisms in the Cape Fold Belt, South Africa. South African Journal of Geology 115, 137–144. https://doi.org/10.2113/gssajg.115.2.137

Fagereng, Å., Harris, C., 2014. Interplay between fluid flow and fault-fracture mesh generation within underthrust sediments: Geochemical evidence from the Chrystalls Beach Complex, New Zealand. Tectonophysics 612–613, 147–157. https://doi.org/10.1016/j.tecto.2013.12.002

Fagereng, Å., Hillary, G.W.B., Diener, J.F.A., 2014. Brittle-viscous deformation, slow slip, and tremor. Geophysical Research Letters 41, 4159–4167. https://doi.org/10.1002/2014GL060433

Fagereng, Å., Sibson, R.H., 2010. Mélange rheology and seismic style. Geology 38, 751–754. https://doi.org/10.1130/G30868.1

Fagereng, Å., Toy, V.G., 2011. Geology of the earthquake source: an introduction. Geological Society, London, Special Publications 359, 1–16.

Faulkner, D.R., Jackson, C.A.L., Lunn, R.J., Schlische, R.W., Shipton, Z.K., Wibberley, C.A.J., Withjack, M.O., 2010. A review of recent developments concerning the structure, mechanics and fluid flow properties of fault zones. Journal of Structural Geology 32, 1557–1575. https://doi.org/10.1016/j.jsg.2010.06.009

Frimmel, H.E., Basei, M.A.S., Correa, V.X., Mbangula, N., 2013. A new lithostratigraphic subdivision and geodynamic model for the Pan-African western Saldania Belt , South Africa. Precambrian Research 231, 218–235. https://doi.org/10.1016/j.precamres.2013.03.014

Frimmel, H.E., Fölling, P.G., Diamond, R., 2001. Metamorphism of the Permo-Triassic Cape Fold Belt and its basement , South Africa. Mineralogy and Petrology 73, 325–346.

Frimmel, H.E., Frank, W., 1998. Neoproterozoic tectono-thermal evolution of the Gariep Belt and its basement , Namibia and South Africa. Precambrian Research 90, 1–28.

Frimmel, H.E., van Achterbergh, E., 1995. Metamorphism of calc-silicate and associated rocks in the Pan-African Kaaimans Group , Saldania Belt , South Africa. Mineralogy and Petrology 53, 75–102.

Fusseis, F., Handy, M.R., Schrank, C., 2006. Networking of shear zones at the brittle-to-viscous transition (Cap de Creus , NE Spain). Journal of Structural Geology 28, 1228–1243. https://doi.org/10.1016/j.jsg.2006.03.022

Grant, J.A., 1986. The isocon diagram - A simple solution to Gresens' equation for metasomatic alteration. Economic Geology 81, 1976–1982. https://doi.org/10.2113/gsecongeo.81.8.1976

Gratier, J.-P., Gueydan, F., 2007. Deformation in the Presence of Fluids and Mineral Reactions: Effect of Fracturing and Fluid – Rock Interaction on Seismic Cycles. In: Handy, M.R., Hirth, G., Hovius, N. (Eds.), Tectonic Faults: Agents of Change on a Dynamic Earth. The MIT Press, 319–356.

Gratier, J.P., Gamond, J.F., 1990. Transition between seismic and aseismic deformation in the upper crust. Geological Society, London, Special Publications 54, 461–473.

Gresse, P.G., Fitch, F.J., Miller, J.A., 1988. 40 Ar / 39 Ar dating of the Cambro-Ordovician Vanrhynsdorp tectonite in southern Namaqualand. South African Journal of Geology 91, 257–263.

Gresse, P.G., Theron, J.N., 1992. The Geology of the Worcester Area: Explanation of Sheet 3319 Worcester.

Grunow, A., Hanson, R., Wilson, T., 1996. Were aspects of Pan-African deformation linked to Iapetus opening ? Geology 24, 1063–1066.

Handy, M.R., 1990. The solid-state flow of polymineralic rocks. Journal of Geophysical Research 95, 8647–8661.

Hansma, J., Tohver, E., Schrank, C., Jourdan, F., Adams, D., 2016. The timing of the Cape Orogeny : New 40 Ar / 39 Ar age constraints on deformation and cooling of the Cape Fold Belt , South Africa. Gondwana Research 32, 122–137. https://doi.org/10.1016/j.gr.2015.02.005

Harris, C., Ashwal, L.D., 2002. The origin of low δ18O granites and related rocks from the Seychelles.

Contributions to Mineralogy and Petrology 143, 366–376. https://doi.org/10.1007/s00410-002-0349-6

Harris, C., Vogeli, J., 2010. Oxygen isotope composition of garnet in the Peninsula Granite, Cape Granite Suite, South Africa: constraints on melting and emplacement mechanisms. South African Journal of Geology 113, 401–412. https://doi.org/10.2113/gssajg.113.4.401

Hickman, S., Sibson, R., Bruhn, R., 1995. Introduction to special section : Mechanical involvement of fluids in faulting. Journal of Geophysical Research 100, 12831–12840.

Hirth, G., Teyssier, C., Dunlap, W.J., 2001. An evaluation of quartzite flow laws based on comparisons between experimentally and naturally deformed rocks. Geologische Rundschau 90, 77–87. https://doi.org/10.1007/s005310000152

Hirth, G., Tullis, J., 1992. Dislocation creep regimes in quartz aggregates. Journal of Structural Geology 14, 145–159.

Kisters, A., Belcher, R., 2018. The Stratigraph and Structure of the Western Saldania Belt, South Africa and Geodynamic Implications. In: Siegesmund, S., Basei, M., Oyhantçabal, P., Oriolo, S. (Eds.), Geology of Southwest Gondwana, Regional Geology Reviews. Springer International Publishing, 387–410. https://doi.org/10.1007/978-3-319-68920-3

Knipe, R.J., 1989. Deformation mechanisms - recognition from natural tectonites. Journal of Structural Geology 11, 127–146.

Kohlstedt, D.L., Evans, B., Mackwell, S.J., 1995. Strength of the lithosphere: Constraints imposed by laboratory experiments. Journal of Geophysical Research 100, 17587–17602.

Mateen, T., Yamamoto, H., Rehman, H.U., Terabayashi, M., 2015. Ductility contrast induced by silicification in pelitic schist of the Ryoke metamorphic belt, Japan. Journal of Structural Geology 80, 38–46. https://doi.org/10.1016/j.jsg.2015.08.009

Niemeijer, A.R., Spiers, C.J., 2006. Velocity dependence of strength and healing behaviour in simulated phyllosilicate-bearing fault gouge. Tectonophysics 427, 231–253. https://doi.org/https://doi.org/10.1016/j.tecto.2006.03.048

Niemeijer, A.R., Spiers, C.J., 2005. Influence of phyllosilicates on fault strength in the brittle-ductile transition: insights from rock analogue experiments. Geological Society, London, Special Publications 245, 303 LP-327. https://doi.org/10.1144/GSL.SP.2005.245.01.15

Passchier, C.W., Trouw, R.A.J., 2005. Micro-tectonics, 2nd ed. Springer.

Passchier, C.W., Trouw, R.A.J., 1996. Micro-tectonics, 1st ed. Springer.

Rowe, C.D., Meneghini, F., Moore, J.C., 2011. Textural record of the seismic cycle: strain-rate variation in an ancient subduction thrust. Geological Society, London, Special Publications 359, 77–95. https://doi.org/10.1144/SP359.5

Rozendaal, A., Gresse, P.G., Scheepers, R., Le Roux, J.P., 1999. Neoproterozoic to Early Cambrian Crustal Evolution of the Pan-African Saldania Belt , South Africa. Precambrian Research 97, 303–323.

Scholz, C.H., 2002. The Mechanics of Earthquakes and Faulting, 2nd ed. Cambridge.

Scholz, C.H., 1998. Earthquakes and friction laws. Nature 391, 37–42.

Scholz, C.H., 1989. Mechanics of Faulting. Annual Review of Earth and Planetary Sciences 17, 309–334.

Scholz, C.H., 1988. The brittle-plastic transition and the depth of seismic faulting. Geologische Rundschau 77, 319–328.

Sibson, R.H., 2014. Earthquake Rupturing in Fluid-Overpressured Crust: How Common? Pure and Applied Geophysics 171, 2867–2885. https://doi.org/10.1007/s00024-014-0838-3

Sibson, R.H., 1986. Brecciation Processes in Fault Zones : Inferences from Earthquake Rupturing. PAGEOPH 124, 159–175.

Sibson, R.H., 1983. Continental fault structure and the shallow earthquake source. Journal of the Geological Society 140, 741–767.

Sibson, R.H., 1982. Fault zone models, heat flow, and the depth distribution of earthquakes in the continental crust of the United States. Bulletin of the Seismological Society of America 72, 151–163.

Sibson, R.H., 1977. Fault rocks and fault mechanisms. Journal of the Geological Society 133, 191–213.

Sibson, R.H., Robert, F., Poulsen, K.H., 1988. High-angle reverse faults, fluid-pressure cycling, and mesothermal gold-quartz deposits. Geology 16, 551–555.

Tankard, A., Welsink, H., Aukes, P., Newton, R., Stettler, E., 2009. Tectonic evolution of the Cape and Karoo basins of South Africa. Marine and Petroleum Geology 26, 1379–1412. https://doi.org/10.1016/j.marpetgeo.2009.01.022

Tesei, T., Collettini, C., Barchi, M.R., Carpenter, B.M., Di Stefano, G., 2014. Heterogeneous strength and fault zone complexity of carbonate-bearing thrusts with possible implications for seismicity. Earth and Planetary Science Letters 408, 307–318. https://doi.org/10.1016/j.epsl.2014.10.021

Tullis, J., 2002. Deformation of Granitic Rocks: Experimental Studies and Natural Examples. Reviews in Mineralogy and Geochemistry 51, 51–95.

Tullis, J., 1990. Experimental studies of deformation mechanisms and microstructures in quartzo-feldspathic rocks. Deformation Processes in Minerals, Ceramics and Rocks. 190–227.

Twiss, R.J., Moores, E.M., 1992. Structural Geology. Freeman and Company.

White, R.W., Powell, R., Johnson, T.E., 2014. The effect of Mn on mineral stability in metapelites revisited: new a–x relations for manganese-bearing minerals. Journal of Metamorphic Geology 32, 809–828. https://doi.org/10.1111/jmg.12095

White, S.H., Burrows, S.E., Carreras, J., Shaw, N.D., Humphreys, F.J., 1980. On mylonites in ductile shear zones. Journal of Geophysical Research 2, 175–187.

12. Appendix: XRF major element data (Mineral Composition)

Table 12.1 XRF Major Element Data

Sample	SiO_2	TiO_2	Al_2O_3	Fe_2O_3	MnO	MgO	CaO	Na_2O	K_2O	P_2O_5	SO_3	Cr_2O_3	NiO	H_2O^-	LOI	Sum
	wt.%	wt.%	wt.%	wt.%	wt.%	wt.%	wt.%	wt.%	wt.%	wt.%	wt.%	wt.%	wt.%	wt.%	wt.%	wt.%
Nuy2	72.54	0.69	13.66	5.71	0.08	0.45	0.36	0.28	3.31	0.30	b.d.	0.01	0.01	0.06	2.04	99.52
Nuy3	73.55	0.77	13.10	5.47	0.06	0.49	0.32	0.29	3.14	0.31	b.d.	0.01	0.01	0.08	1.83	99.41
N-37	91.19	0.13	4.89	0.85	0.01	0.14	0.02	0.17	1.19	0.05	b.d.	b.d.	0.01	0.10	0.71	99.46
N-38	93.32	0.15	2.20	1.63	0.01	0.24	0.02	0.15	0.38	0.07	b.d.	b.d.	0.01	0.08	0.53	98.79
N-39	82.34	0.59	10.29	1.58	0.02	0.15	0.13	0.23	2.49	0.17	b.d.	b.d.	0.01	0.10	1.52	99.61
N-40	94.65	0.14	1.93	1.10	0.01	0.22	b.d.	0.15	0.34	0.07	b.d.	b.d.	0.01	0.10	0.52	99.24
N-41	82.19	0.47	8.67	3.26	0.02	0.50	0.06	0.20	2.17	0.08	b.d.	b.d.	0.01	0.09	1.46	99.19
N-42	84.85	0.26	8.15	2.07	0.01	0.17	b.d.	0.21	2.35	0.07	b.d.	b.d.	0.01	0.09	1.39	99.61
N-43	75.64	0.64	11.19	5.07	0.05	1.22	0.11	0.22	2.38	0.20	b.d.	0.01	0.01	0.23	2.57	99.54
N-44	75.68	0.54	9.84	6.12	0.05	1.77	0.20	0.18	1.98	0.21	b.d.	0.01	0.01	0.11	2.29	98.99
N-45	85.58	0.37	5.87	3.37	0.04	0.97	0.24	0.20	1.31	0.19	b.d.	b.d.	0.01	0.11	1.60	99.87
N-46	89.76	0.24	4.39	2.18	0.02	0.57	0.05	0.31	0.99	0.07	b.d.	b.d.	0.01	0.08	0.96	99.64
N-47	81.27	0.45	7.92	3.54	0.01	0.67	0.11	0.38	2.12	0.16	0.05	b.d.	0.01	0.16	2.45	99.30
N-48	89.79	0.22	4.34	2.12	0.02	0.53	0.08	0.15	1.01	0.08	b.d.	b.d.	0.01	0.06	0.92	99.33
N-49	85.70	0.44	5.46	3.41	0.04	1.15	0.07	0.21	1.06	0.05	b.d.	b.d.	0.01	0.09	1.49	99.18
N-50 MG	70.94	0.60	12.95	5.62	0.03	2.37	0.13	0.23	2.83	0.15	0.01	0.01	0.01	0.12	3.28	99.28

Information:
Major oxides (values reported as wt.% except for H2O- and LOI) are measured on fused disks prepared from ignited powders,
H2O- represents the sample weight lost upon heating the sample powder at 110° overnight. If the powders submitted are moist, this value can be high.
LOI is "loss on ignition" and represents the weight change (positive if weight lost) upon heating the sample to 800°C for 4 hours.
Samples can gain weight during ignition if they have little water and abundant ferrous iron (which oxidizes to ferric iron oxide, Fe2O3), thus uptaking oxygen.
Sulphur reported as wt% SO3 is measured on fused disks
If otherwise unstated, the lower limit of detection for major oxides is 0.01 wt.%.
"b.d." is an abbreviation of "below detection" meaning that the concentration of the element was too low to quantify (generally <0.01 wt.% for major elements)